NOAA Technical Memorandum ERL WMPO-9

U.S. DEPARTMENT OF COMMERCE
NATIONAL OCEANIC AND ATMOSPHERIC ADMINISTRATION
Environmental Research Laboratories

Subsynoptic Convergence-Rainfall Relationships Based Upon 1971 South Florida Data

JOSE J. FERNANDEZ-PARTAGAS

Weather
Modification
Program Office
BOULDER,
OLORADO
November 1973

IVIRONMENTAL RESEARCH LABORATORIES

WEATHER MODIFICATION PROGRAM OFFICE

IMPORTANT NOTICE

Technical Memoranda are used to insure prompt dissemination of special studies which, though of interest to the scientific community, may not be ready for formal publication. Since these papers may later be published in a modified form to include more recent information or research results, abstracting, citing, or reproducing this paper in the open literature is not encouraged. Contact the author for additional information on the subject matter discussed in this Memorandum.

NATIONAL OCEANIC AND ATMOSPHERIC ADMINISTRATION

U.S. DEPARTMENT OF COMMERCE
National Oceanic and Atmospheric Administration
Environmental Research Laboratories

NOAA Technical Memorandum ERL WMPO-9

SUBSYNOPTIC CONVERGENCE-RAINFALL RELATIONSHIPS BASED UPON 1971 SOUTH FLORIDA DATA

Jose J. Fernandez-Partagas
Experimental Meteorology Laboratory

Weather Modification Program Office
Boulder, Colorado
November 1973

TABLE OF CONTENTS

ABSTRACT

Convergence-rainfall relationships are studied at subsynoptic scales of motion in relation to Florida convection. These relationships are based upon analyses of three selected thunderstorm cases. Analyses make use of radar and numerous surface wind and rainfall observations which were taken to the south of Lake Okeechobee, Florida, during the summer of 1971. The evolution of convergence, relative vorticity and rainfall is examined at the cloud-scale and at the meso-scale. Convergence-rainfall relationships at these two scales - together with those found for the Florida peninsula ("larger scale") - show the relation which links surface convergences and divergences at different scales with peak rainfall. Maximum surface convergence occurs first at the "larger scale" and it is followed by corresponding maxima at the meso-scale and then at the cloud-scale. After peak rainfall, maximum surface divergence occurs first at the cloud-scale and is followed by meso-scale and then by "larger scale" surface divergences. The findings of this study are discussed in relation to the parameterization and short-range forecasting of convective rainfall.

SUBSYNOPTIC CONVERGENCE-RAINFALL RELATIONSHIPS BASED UPON 1971 SOUTH FLORIDA DATA

by
Jose J. Fernandez-Partagas

1. INTRODUCTION

Convergence-rainfall relationships are described at the meso-scale and the cloud-scale as observed near the earth's surface in the vicinity of Florida thunderstorms. Motivations for convergence-rainfall studies at the subsynoptic scales are the following:

1) parameterization of the cumulus scale as a function of meso-scale and synoptic variables in modeling the tropical atmosphere,

2) short-range forecasting derived from empirical relationships,

3) test the effect of artificially induced perturbations on naturally observed convergence-rainfall relationships.

The present convergence-rainfall studies are related to afternoon thunderstorms over an observational network located to the south of Lake Okeechobee, Florida in the summer of 1971. Continuous records of meteorological parameters near the earth's surface (wind, rainfall) and of weather radar surveillance of the area are used for these studies. Three-dimensional analyses (x, y at the earth's surface; t, time) of the directly observed parameters and the derived quantities (horizontal divergence, relative vorticity) provide information for the convergence-rainfall relationships. These relationships are investigated for selected periods of July 11, 12 and 13, 1971.

Synoptic-scale conditions for these periods are characterized by a deep easterly to southeasterly flow and by a small vertical wind shear at the low and mid-troposphere over south Florida (Fernandez-Partagas and Estoque, 1972).

Analyses of observed and derived quantities are presented and convergence-rainfall relationships are discussed in the main text of this paper. A presentation in the form of individual case studies for July 11, 12 and 13, 1971 is included in Appendices A, B, and C.

2. THE NETWORK

A meso-scale meteorological network was established a few miles to the south of Lake Okeechobee in June and July 1971. This network represented a joint effort of the Florida State University and the NOAA Experimental Meteorology Laboratory (EML). The surface network was set up in relation to cloud seeding experiments conducted by EML. The network consisted of nearly 200 raingages and about 25 anemometer towers which were evenly distributed over an area of 220 sq mi. Figure 1 shows the location of the network and its observational sites.

Wind information at the 8 m level was available from most towers at all times. In contrast, only about 1/3 of the raingages were of the recording type and useful for the present study. Information from wind towers (except from those of the Dumas type) and data from recording gages (C, R types) were the source for the winds and rainfalls which were plotted and analyzed. Data from the Dumas systems were not available at the time of the analysis.

Despite these shortcomings, the density of useful data, both in terms of wind and rainfall measurements, was the best achieved in Florida since the Thunderstorm Project experiments of 1946 (Byers and Braham, 1949). This density of useful data was also greater than those of other networks in recent years (i.e. the 1970 NSSL meso-network (Operations Staff, 1972) and the 1969 Project VIMHEX network (Pacheco, 1972)). Temperature, humidity

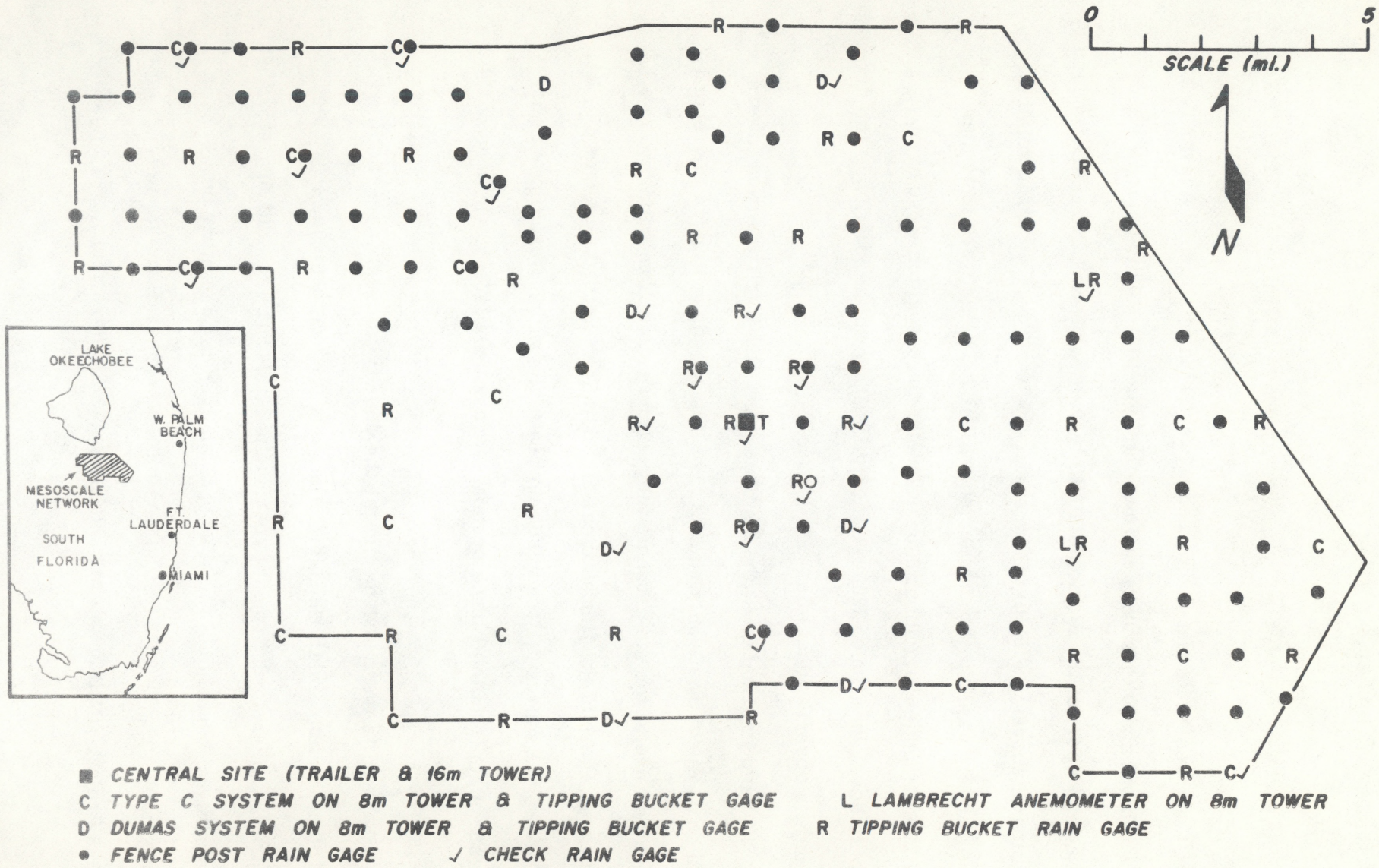

Figure 1. Location of all observational sites of the 1971 south Florida mesoscale network See text for identification of those sites which furnished useful information for the present study. The geographical location of the mesoscale network is shown in the insert.

and pressure measurements at the surface, however, were either lacking or were taken at a few isolated locations of the 1971 network. Had these types of observations been taken at numerous sites, studies on energetics and other aspects of thunderstorms would have been possible.

3. BASIC ANALYSES AND COMPUTATIONS

This section describes: a) the wind and precipitation analyses and b) the computation of wind-derived quantities (horizontal divergence, relative vorticity).

3.1 Basic Analyses

Analyses of several types were conducted for the directly-observed meteorological parameters. The types of analyses which were performed are:

1) kinematic analyses of the wind field (streamlines, isogons, isotachs),

2) rainfall analyses,

3) radar echo-depiction analyses.

These were conducted for an area of approximately 15 x 22 statute miles which enclosed the 1971 meso-network. Analyses of type 1 were carried at 5-minute intervals, while those of type 2 and type 3 were carried at 15-minute intervals. A total of 8 1/2 hours was analyzed for the periods of July 11, 12 and 13, 1971 which are indicated in table 1. This required more than 100 individual analyses of type 1, and about 35 analyses of types 2 and 3, respectively.

Table 1.

Periods of Study for Convergence-Rainfall Relationships

Dates	Times (EDT)	No. Hours
July 11, 1971	1738 - 1838	1
July 12, 1971	1500 - 2000	5
July 13, 1971	1600 - 1830	2-1/2

Type 1 analyses were the basis for derived-quantity (horizontal divergence, relative vorticity) computations, and these made use of 5-minute average winds for the wind reporting sites of the network. Streamline and isotach hand-analyses were performed by following the principles of space and time continuity, which are fundamental in such analyses. Isogons were derived from streamline patterns as the reading of accurate wind directions and wind speeds at grid points became a necessity for divergence and relative vorticity computations.

Analyses of types 2 and 3 were associated with the three-dimensional (x, y and t) rainfall description, which was used for the convergence-rainfall studies. Type 2 analyses were carried out for maps corresponding to 15-minute interval rainfalls. Isopleths were drawn by hand at 0.1 inch intervals; some effort was made in keeping continuity of rainfall patterns over the area of interest.

Analyses of type 3 consisted of assessing estimates of the area covered by radar echoes of different intensities (in percentages). Estimates were made at 15-minute intervals. Information for these estimates was taken from films of the PPI presentation of the University of Miami 10-cm meteorological radar. This radar provides contours for different levels of echo intensity, and calibration allows these iso-echo contours to correspond to prescribed rainfall rates. Simultaneously observed echoes of the same intensity level were plotted on sheets of blank paper and inked. Then, area coverages (in percentage) were determined electronically with a densitometer. Thus the time required for measuring areas was only a few seconds, compared to the many hours which might have been required had a conventional planimeter been used.

3.2 Computations and Automated Plots

Analyses of type 1 served as the basis for computations of wind-derived quantities (horizontal divergence and relative vorticity). Horizontal divergence and relative vorticity near the earth's surface were computed from the expressions

$$\nabla_H \cdot \mathbf{V} = \frac{\partial u}{\partial x} + \frac{\partial v}{\partial y} \tag{1}$$

$$\mathbf{IK} \cdot \nabla \times \mathbf{V} = \frac{\partial v}{\partial x} - \frac{\partial u}{\partial y} \tag{2}$$

where the symbols have their customary meaning. Calculations were made by using a computer program which was written by University of Miami personnel

in connection with BOMEX studies (Herrera Cantilo and Fernandez-Partagas, 1972). Horizontal divergence (to be called divergence hereafter) and relative vorticity were approximated by a finite differencing, centered-derivative scheme. Computations were carried out for a horizontal, two dimensional grid of equally spaced grid points. The grid size was variable and, in most instances (July 12 and July 13, 1971) it covered the entire area of interest. The grid covered only a portion of the area, however, in the remaining instances (July 11, 1971). Distance between adjacent grid points was set equal to 0.8 statute miles and the total number of grid points varied from 256 (partial area) to 504 (entire area). The location of the grids and the location of grid points is shown in figure 2.

Divergence and relative vorticity computations were performed at 15-minute intervals. This interval was chosen to match that of the rainfall studies. At each computation time, wind direction and wind speed were needed at every grid point for divergence and relative vorticity calculations. Wind directions were read off the isogon analyses, whereas wind speeds were read off the isotach analyses. This information was then punched on cards which were used as input for the calculations. Over 35 sets of divergence and relative vorticity calculations were performed. "Per second" was the unit used in these calculations. Divergence and relative vorticity fields were plotted by machine, but a few selected contours were added by hand. The examples of the machine plotted fields in figure 3 were chosen with the sole

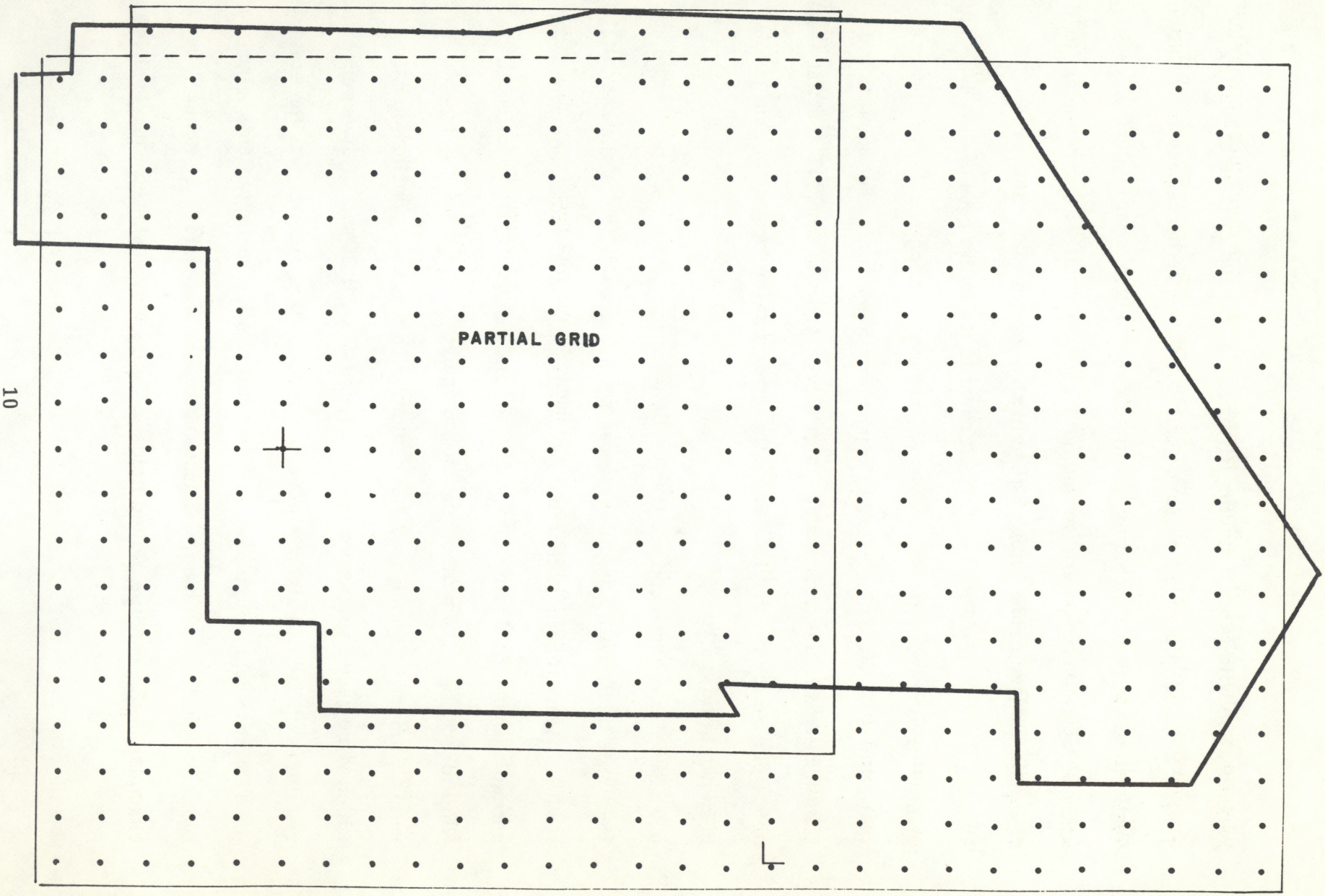

Figure 2. Total and partial grids which were used for computing wind-derived quantities.

purpose of illustrating the automated presentation of the divergence and relative vorticity fields. Thus, they do not necessarily describe events of particular significance in individual thunderstorm studies. Note that values on these graphs were arbitrarily scaled to 10^4; titles and reference points were also machine plotted.

Vectorial representations of the wind field have advantages over streamline-isotach or isogon-isotach presentations because they combine both wind direction and wind speed in the most physically realistic and graphically self-spoken manner. The same computer program which calculates and prepares plots of wind-derived quantities has the capability of preparing vectorial representations. Hence, vectorial representations of the wind field were obtained concurrently with the divergence and the relative vorticity computations and plots. An example of the wind fields is shown in figure 4.

The program is also able to compute and plot relative wind fields. For this study, no relative winds were computed on a regular basis. Some relative winds were computed and plotted, however, in relation to the case-study which is described in Appendix A.

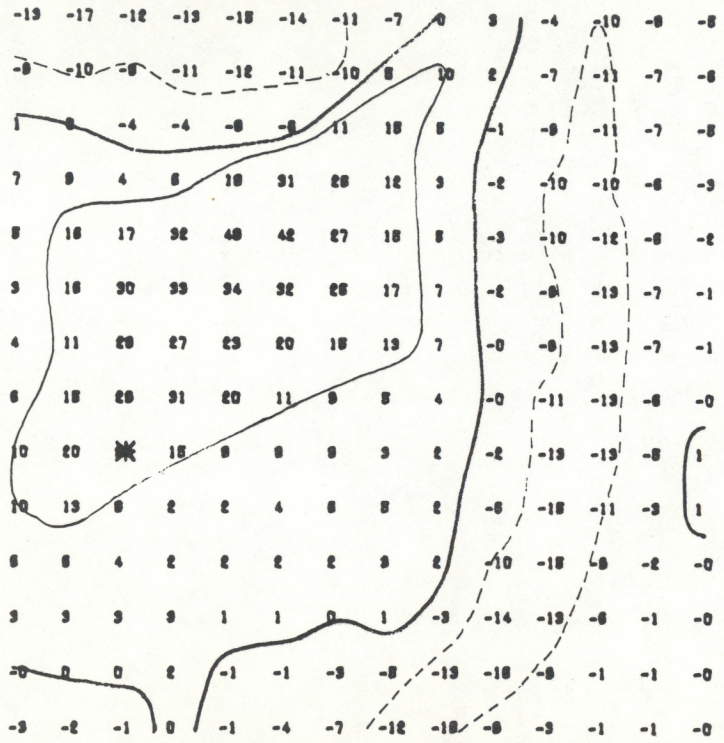

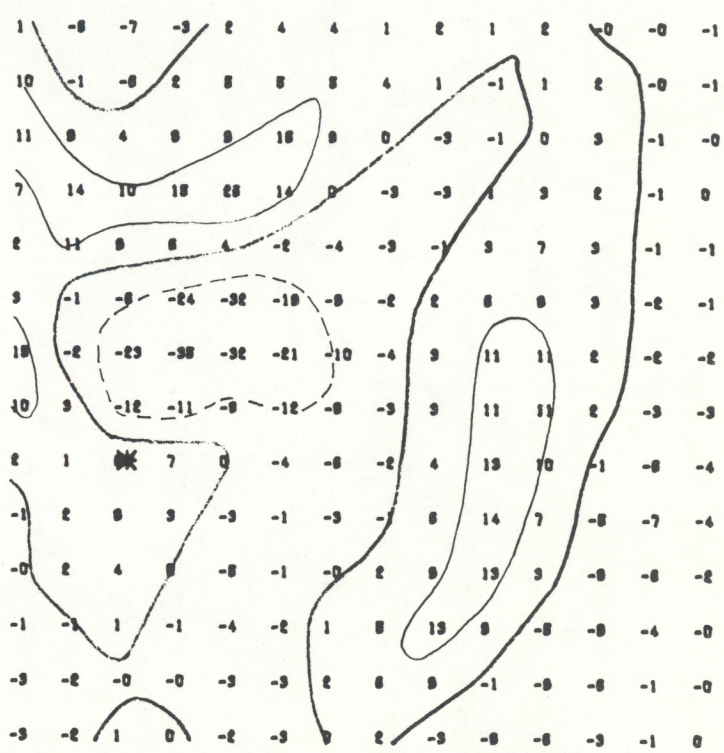

Figure 3. Examples of the machine-plotted divergence and vorticity (relative vorticity) fields. The examples shown are for the partial grid in figure 2. Computation time is 1823 EDT, July 11, 1971. Contours in heavy solid lines denoted zero values; thin solid-line contours correspond to 10^{-3} sec^{-1} divergence or positive relative vorticity values and dashed-line contours correspond to -10^{-3} sec^{-1} convergence or negative relative vorticity values.

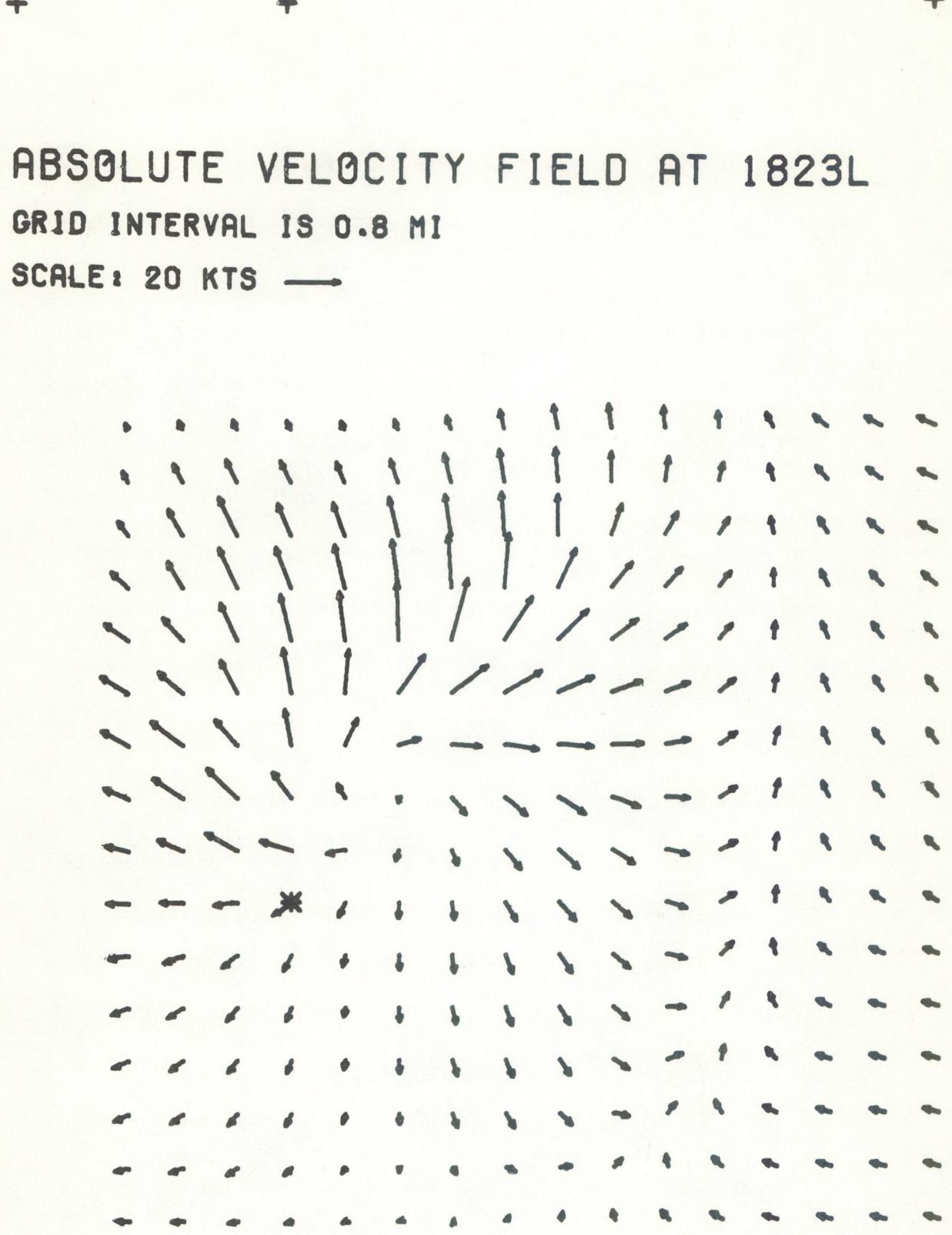

Figure 4. Example of the vectorial representation of wind fields. The example shown is for the partial grid in figure 2. Time is 1823 EDT, July 11, 1971.

4. CONVERGENCE-RAINFALL RELATIONSHIPS

This section describes the procedures that were directly applied to the convergence-rainfall investigation, and states the results that were obtained.

Correlations between different quantities (divergence, rainfall and, in addition, relative vorticity) were investigated at two different scales: the grid-point scale and the grid scale. Since the distance between grid points is very small, the grid-point scale represents the cloud-scale in nature. The so-called grid scale, whose dimension is defined at that of the grid itself (entire total grid or entire partial grid), physically represents the mesoscale as it intends to depict correlations at the scale of the network.

4.1 Procedures

The procedure for studying grid-point correlations began by a selection of the grid points to be used. Every other one of the original grid points were chosen and thus were located 1.6 statute miles apart. For most cases (7-1/2 hours on July 12, 1971 and July 13, 1971), the number of grid points used was 104. The total number of grid points was, however, 49 for the remaining cases (one hour period on July 11, 1971). The location of the grid points that were used is shown in figure 5.

Divergence and relative vorticity values at selected grid points were read off the automated graphs in units of 10^{-4} sec^{-1}. Rainfall values at the same grid points were read off the type 2 analyses in units of hundredths

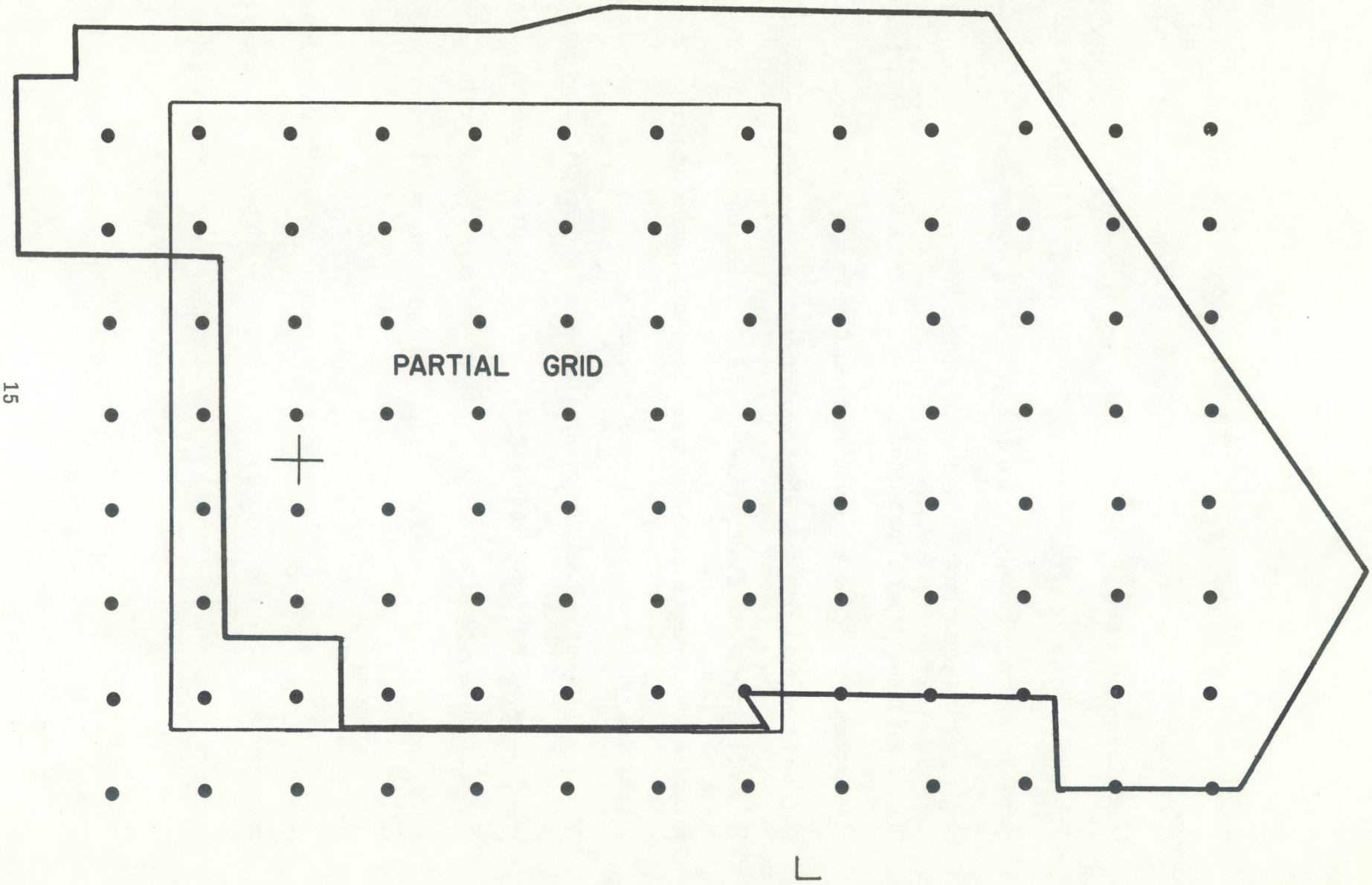

Figure 5. Locations of the grid points which were used for grid-point correlations.

of an inch/15 minutes and this procedure was applied every 15 minutes over the periods of study (see table 1). For each grid point, hand plotted graphs were prepared in order to depict time changes of divergence, relative vorticity and rainfall and then used for making correlations at the grid-point scale. In addition, scatter diagrams were made while seeking a model of convergence-rainfall relationships at the grid-point scale (cloud-scale).

The procedure for grid-scale studies involved the assessment, for the various meteorological parameters, of values which were representative of the entire grid. This was achieved by a) determining (in percent) the fraction of the total grid area which was affected by arbitrarily prescribed values of the meteorological parameters and b) averaging meteorological variables from values which were available at individual grid points. Process a) was applied to radar echoes of different intensities (from analysis of type 3). The same process was applied to regions of divergence and relative vorticity exceeding chosen values of $\pm$ 1 x 10^{-3} sec^{-1} (from automated plots). Process b) was applied to divergence, relative vorticity and rainfall values at all grid points. Processes a) and b) were repeatedly applied at 15-minute intervals throughout the study.

The evolution of the various basic parameters and/or their chosen categories was plotted in seeking meso-scale relationships. In addition, some scatter diagrams and special graphs helped in the meso-scale investigations.

4.2 Results

This sub-section illustrates: a) grid-point scale results, b) grid scale results, and c) a comparison of findings in a) and b) with previous studies on convergence-rainfall over central and south Florida (Fernandez-Partagas and Estoque, 1972).

4.2.1 Grid-Point Scale Results

Graphs of divergence, relative vorticity and rainfall evolution at grid points are shown in figure 6. Only the evolution at a few grid points for different days (July 11, 12 and 13, 1971) is presented in this figure. Some divergence and rainfall graphs are also included for a case of July 9, 1946. This latter case was originally studied by Thunderstorm Project personnel (Byers and Braham, 1949). Note that, at grid points, there is a tendency for convergence to occur right before and at the beginning of precipitation. Convergence changes to divergence as peak rainfall is approached. Maximum divergence tends to occur simultaneously with the rainfall peak or a short time thereafter. In general, this evolution is shown to be present in the 1971 and the 1946 cases and, particularly, it was most closely followed by the July 11, 1971 and the July 9, 1946 cases. Grid-point correlation studies show, however, that a large convergence value does not necessarily imply later rainfall. This was frequently the case at locations in the wake and at right angles to thunderstorm paths. This convergence-no rainfall was related to the leading edge of thunderstorm outdrafts at directions other than that of

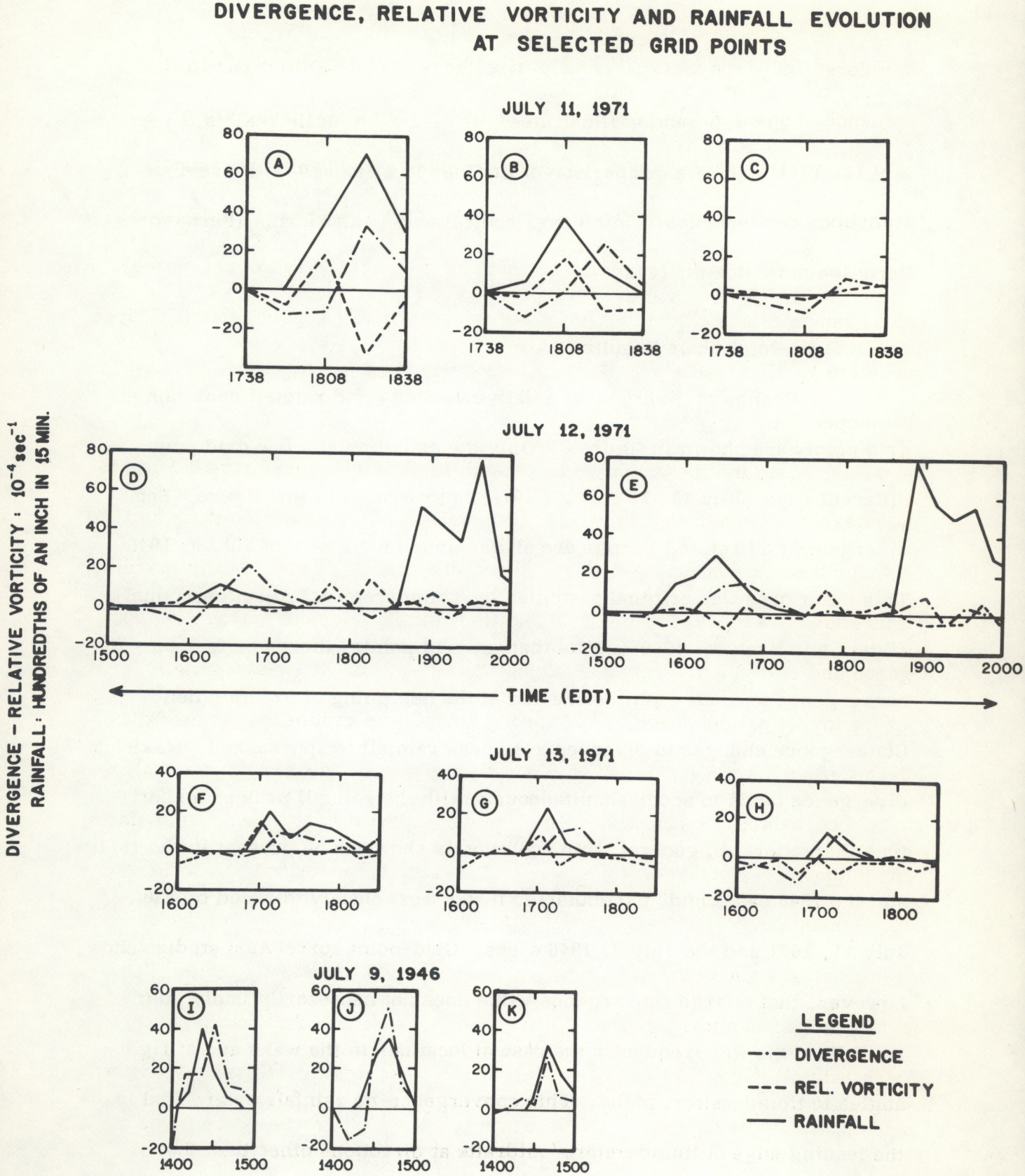

Figure 6. Graphs of divergence, relative vorticity and rainfall evolution at selected grid points.

thunderstorm propagation. Occasionally, heavy rainfall did occur in the presence of small values of convergence and divergence (particularly on July 12, 1971). These two cases of poor convergence-rainfall correlations probably have to be explained in terms of events which occured at levels above the earth's surface. Relative vorticity and rainfall relationships were also examined on a grid-point basis but no definite relation was found. Large negative vorticity values were found, however, in a few instances of fully developed thunderstorms.

Grid points which reached peak precipitation rate above 0.1 in/ 15 minutes were examined for the beginning and ending times of rainfall, and also for times of extreme convergence and divergence. Peak 15-minute rainfalls above 0.1 in were related, in addition, to the values of extreme convergence and extreme divergence which were associated with each rainfall. These investigations made use of special cumulative graphs and scatter diagrams (fig. 7 and 8). The special cumulative graphs in figure 7 confirm convergence-rainfall relationships which were previously discussed. In general, the following sequence can be stated: 1) maximum convergence occurs, 2) rain starts and a divergence pattern establishes, 3) maximum divergence occurs at the time of, or shortly after, peak rainfall and 4) rain ends. The scatter diagrams in figure 8 fail to show any consistent relationship among peak rainfall values and maximum convergence, or among peak rainfall values and maximum divergence. In fact, some large rainfall values were found to

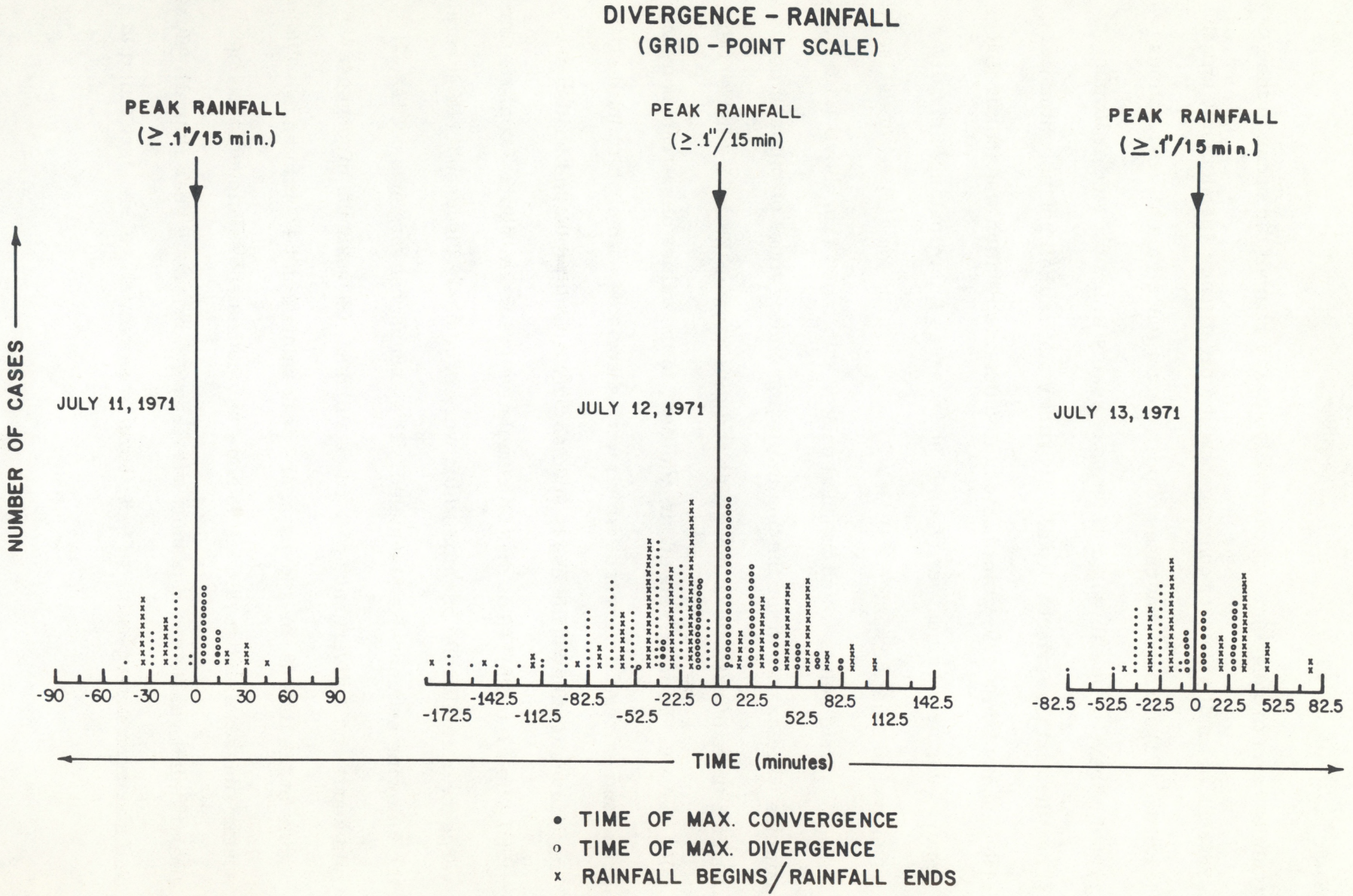

Figure 7. Special cumulative graphs which were used for convergence-rainfall studies at the grid-point scale.

correlate with relatively small convergence and divergence values, and vice versa. The scatter diagrams denote, however, that the values of extreme divergence were, in general, greater in magnitude than the extreme convergence values. This finding was in agreement with results of Thunderstorm Project (Byers and Braham, 1949). Presumably, this indicates a dominant effect of the downdraft-related divergence over the convergence at the grid-point scale.

Data in figures 7 and 8 served as the basis for a model of the more representative and more frequently observed convergence-rainfall relationship at the grid-point scale (cloud-scale). The model is presented in figure 9 and it is valid only for rainfalls equal to or greater than 0.1 in/15 minutes. The time of peak rainfall is chosen as zero-time reference. The model shows that maximum convergence tends to occur about 25 minutes before peak rainfall and that rain starts about 15 minutes before its peak occurs. Maximum divergence is observed about seven minutes after peak rainfall and rain ends about 30 minutes after peak rainfall. Extreme convergence in the model is -7×10^{-4} sec^{-1}, whereas maximum divergence is 1×10^{-3} sec^{-1}. Peak rainfall in the model is 0.30 in/15 minutes. Confidence in the time choices of the model is considered to be greater than confidence in the magnitude selections. In spite of this, the values of extreme convergence, extreme divergence and peak rainfall in the model are probably the most representative that can be derived from the scatter diagrams in figure 8.

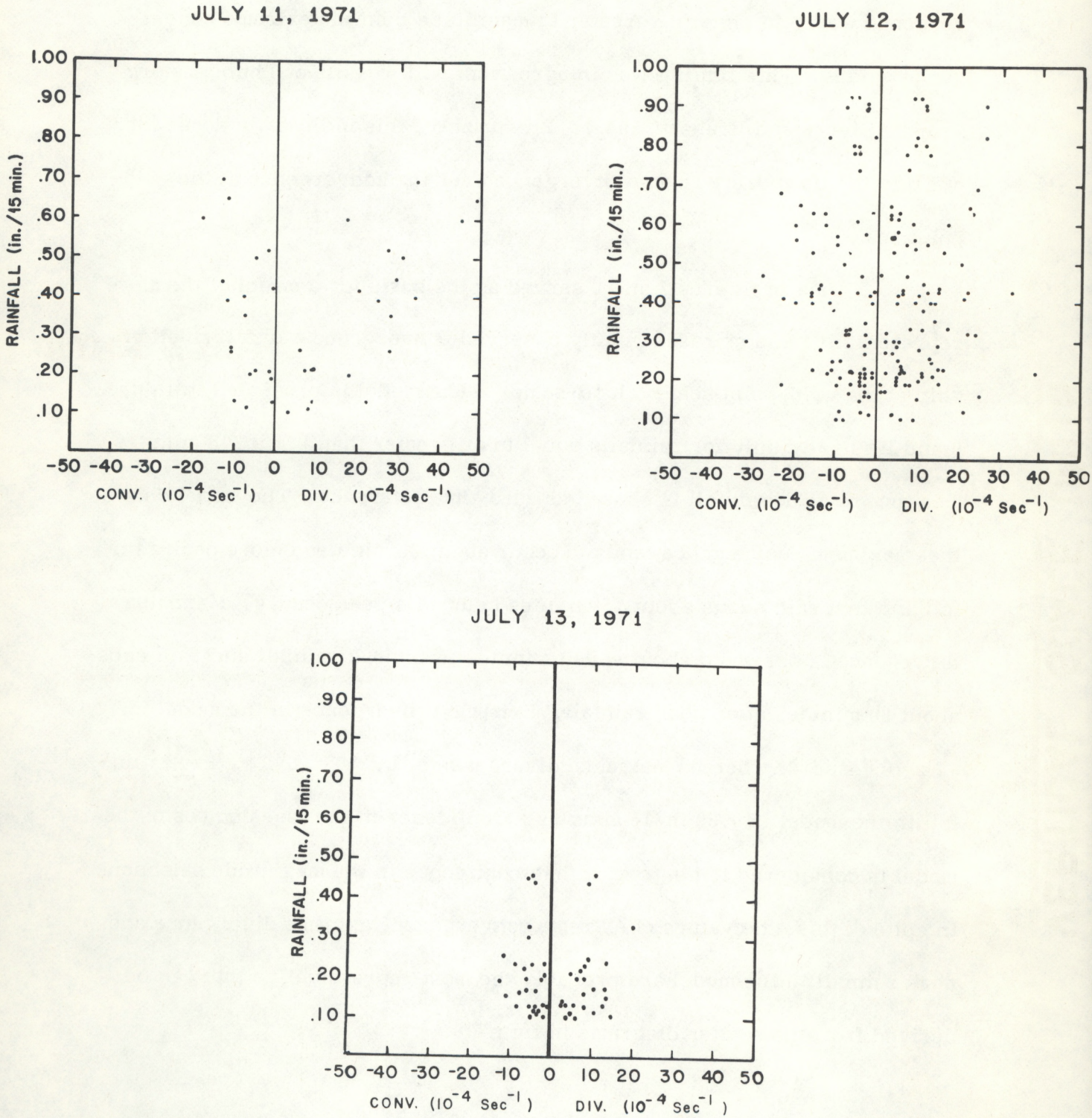

Figure 8. Scatter diagrams which were used for convergence-rainfall studies at the grid-point scale.

CONVERGENCE - RAINFALL MODEL
(GRID - POINT SCALE)

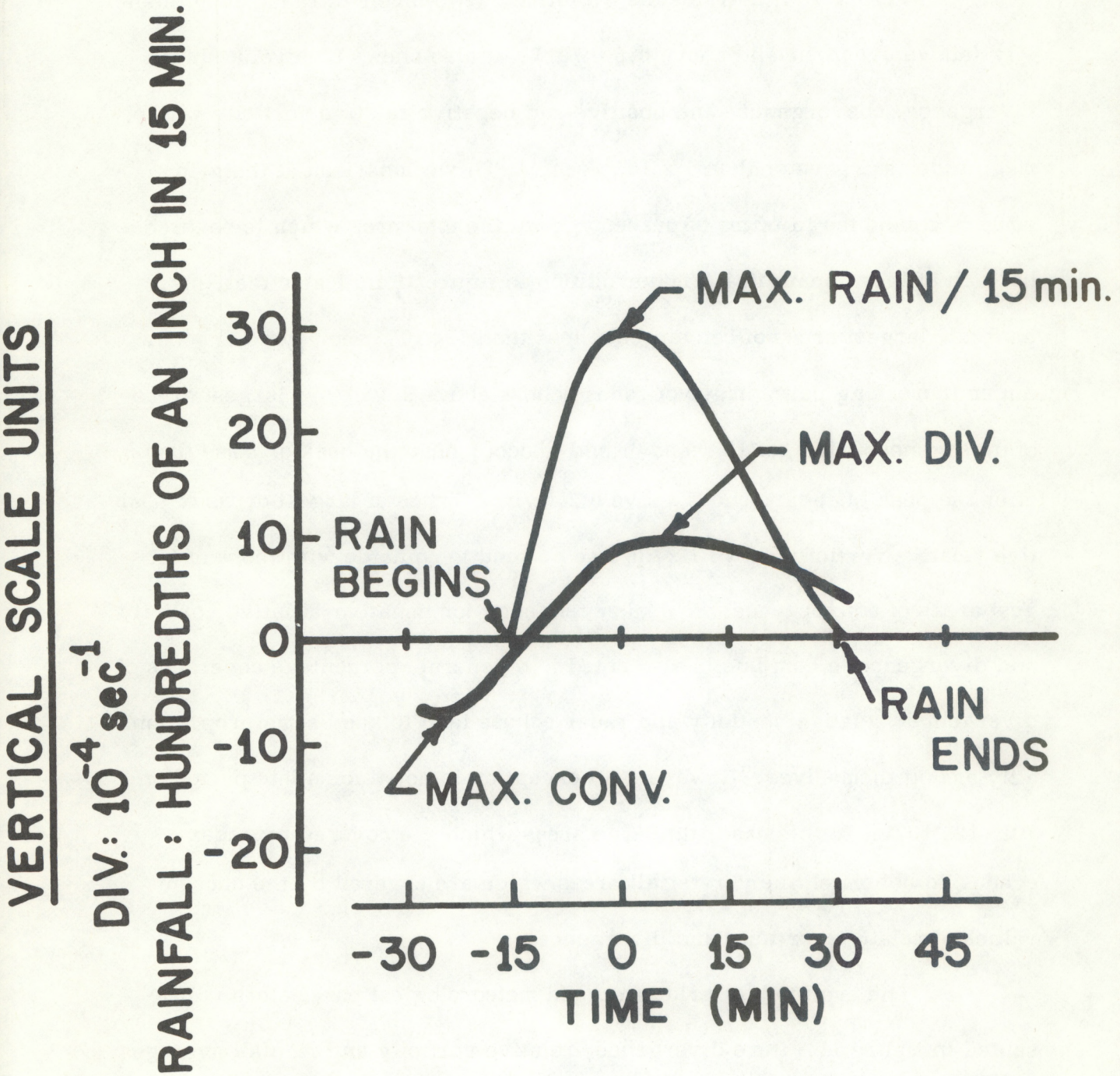

Figure 9. Convergence-rainfall model for the grid-point scale.

4.2.2 Grid-Scale Results

Convergence-rainfall relationships at the grid scale are discussed in subsequent paragraphs.

Figure 10 illustrates the evolution of two levels of radar echo intensity (above 0.1 in/hr and above 0.6 in/hr). It also shows the evolution of divergence, convergence, and positive and negative relative vorticity whose magnitudes are greater than 1×10^{-3} sec^{-1}. This comparison at the grid scale is conducted in terms of percentages of the total area which is covered by each of these quantities. The evolution in figure 10 indicates that, in general, largest areas of convergence less than 1×10^{-3} sec^{-1} tend to occur under increasing percentages of radar echoes above 0.1 in/hr; largest areas of divergence above 1×10^{-3} sec^{-1} tend to occur near the peak or some time after the peak of radar echoes above 0.1 in/hr. Times of largest areas of positive relative vorticity above 1×10^{-3} sec^{-1} tend to coincide with those of largest areas of convergence. A weaker tendency for negative relative vorticity and divergence to coincide is also noted. In general, percentage coverages of divergence, relative vorticity and radar echoes tend to keep some proportionality among themselves. However, an exception is noted for a late period on July 12, 1971. In this case, the large areas which are covered by radar echoes do not match the very small areas which are covered by the chosen values of relative vorticity and divergence.

The evolution of grid-averaged meteorological parameters is presented in figure 11. Here divergence, relative vorticity and rainfall averages

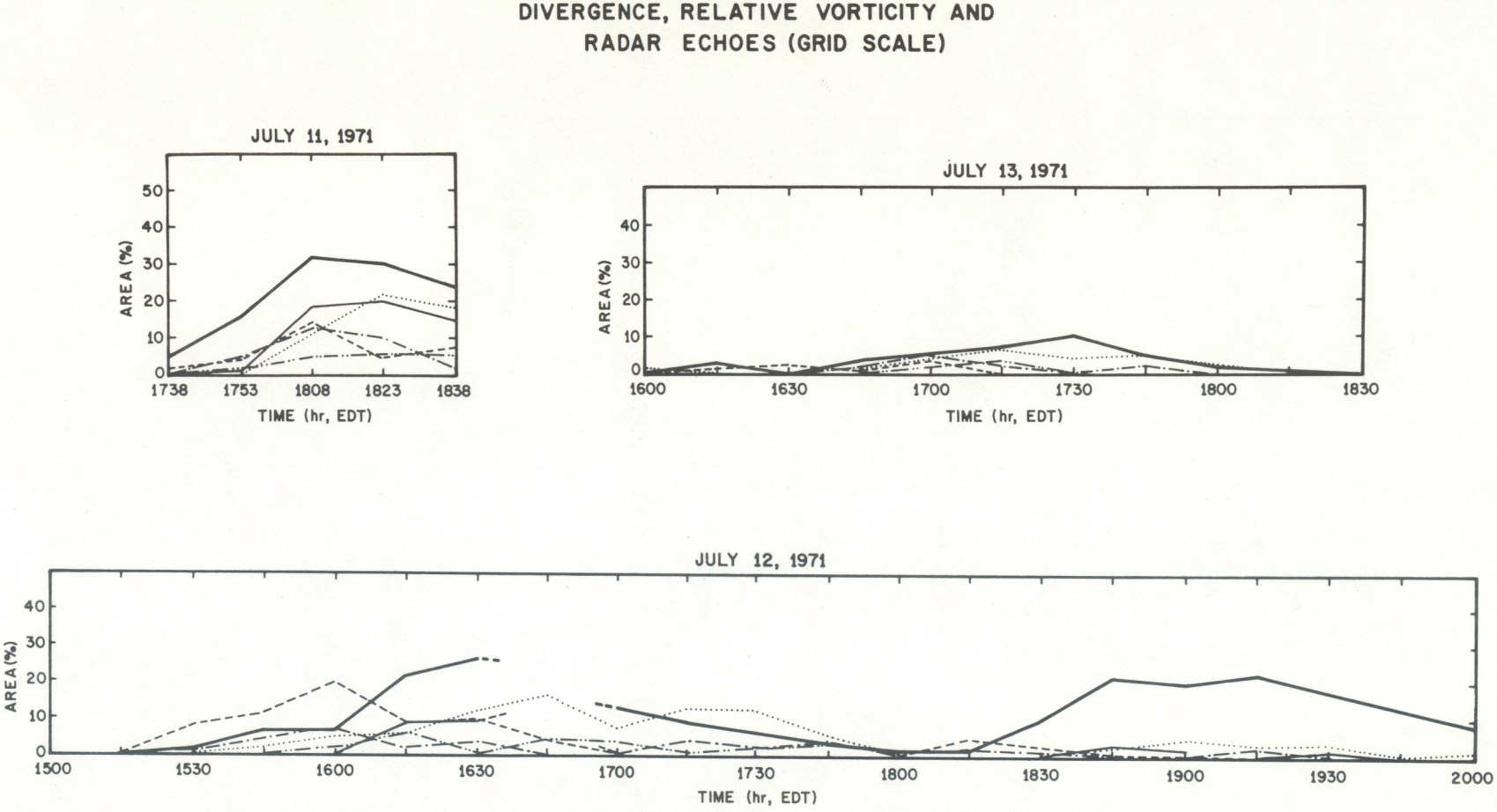

Figure 10. Evolution at the grid scale (in percent of the total area) of selected categories of divergence, relative vorticity and radar echoes.

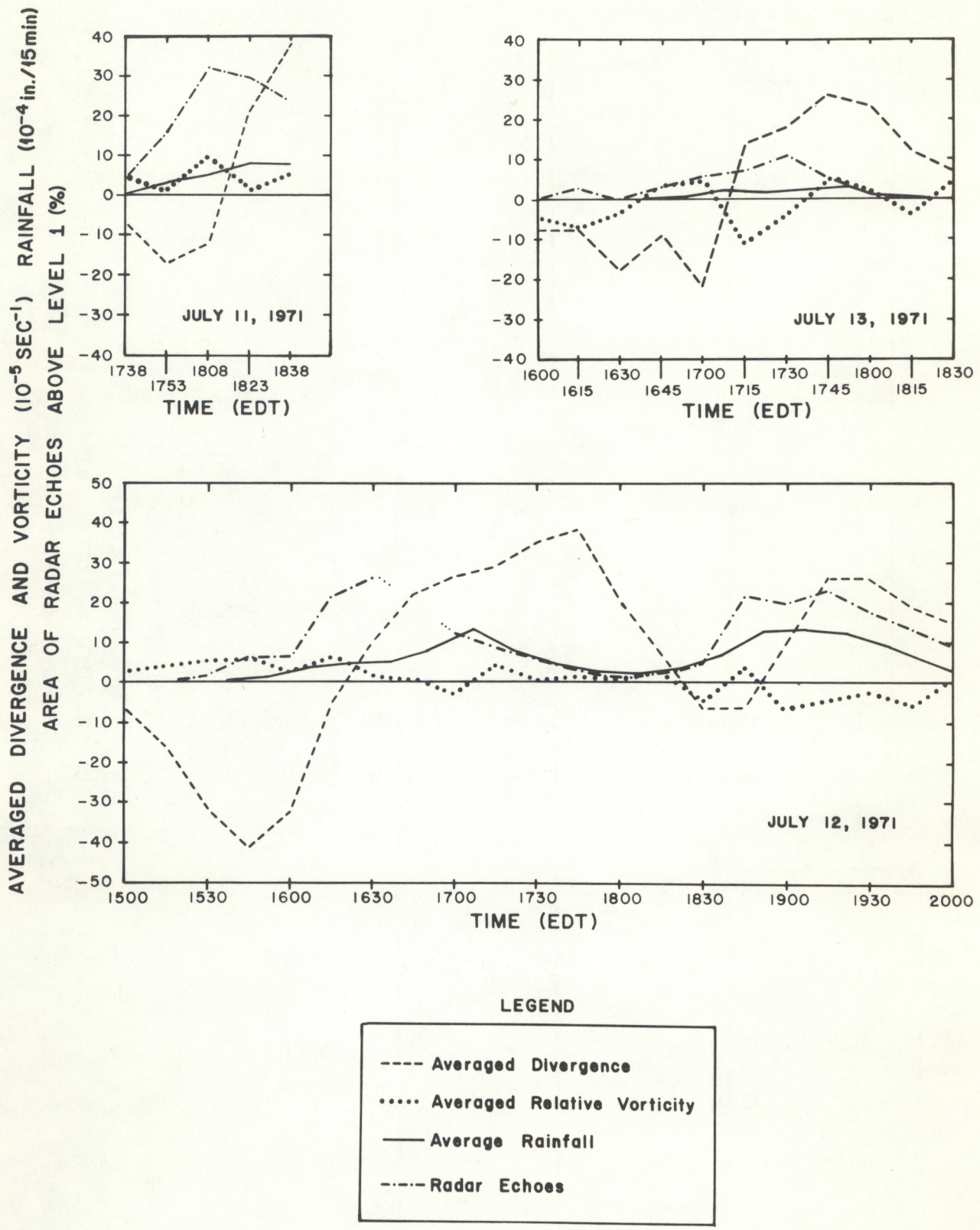

Figure 11. Evolution at the grid scale of divergence, relative vorticity and rainfall averages. The evolution of radar echoes is shown for comparison purposes.

for the grid are plotted against time; radar echo areal coverages are included for comparison. Averages have typical absolute values of 10^{-4} sec^{-1} for divergence, 10^{-5} sec^{-1} for relative vorticity and 10^{-4} in/15 minutes for rainfall. Divergence, rainfall and echoes are shown to be fairly well correlated, but with different lags. Relative vorticity is shown to behave erratically and it does not appear to be correlated to the other meteorological parameters. The sequence of convergence-rainfall events is: 1) averaged divergence minimum (convergence maximum), 2) peak of radar echo areal coverage, 3) averaged rainfall maximum, and 4) averaged divergence maximum. The lag between maximum convergence and the peak of radar echo areal coverage can be interpreted as a necessary time for vertical motion and condensation to occur, and for raindrops to reach the size capable of producing radar returns. The lag between the peak of radar echo areal coverage and maximum rainfall is due to the fact that radar measurements are taken at some elevation above the surface network (for the Miami radar, roughly 6000 ft with a 0.5° antenna elevation angle) whereas rainfall is collected at the ground. Finally, maximum divergence is due to the general cooling which accompanies and follows rainfall.

The convergence-rainfall lag which was observed at the grid scale was investigated further by making use of specially designed scatter diagrams. Separate convergence vs. rainfall diagrams were prepared by permitting the lag to vary from 15 minutes to 1 1/2 hours to determine, in a single operation,

the best correlations and lags. Scatter diagrams for best fits and lags are illustrated in figure 12. The convergence-rainfall best fit was found with a lag of one hour for the July 13, 1971 case; the best fit for July 12, 1971 was found with a lag of 1 hour and 15 minutes. However, this latter fit had to exclude a few points which were representative of a poor correlation period on July 12, 1971.

Grid-point and grid scale studies showed that a similar type of convergence-rainfall relationship exists at both scales, but with entirely different lags and magnitudes of the correlated quantities. In the grid-point scale model (fig. 9), the time elapsed from extreme convergence to rainfall peak is about 25 minutes; in the grid scale studies (fig. 12), the time elapsed from the averaged convergence peak to the averaged rainfall peak ranges from 1 hour to 1 hour and 15 minutes. This can be interpreted in terms of a forcing of the meso-scale into the cloud-scale to produce cumulus development and rain. A representative rainfall peak for the grid-point scale is 3×10^{-1} in/15 minutes, whereas a typical rainfall peak for the grid scale is 1×10^{-3} in/15 minutes. The convergence extreme is -7×10^{-4} sec^{-1} for the grid-point model and about -3 to -4×10^{-4} sec^{-1} for the grid scale studies. The divergence peak in the grid-point model is about 1×10^{-3} sec^{-1}, whereas 3×10^{-4} sec^{-1} is a representative value of the divergence peak for the grid scale. Note that, for the grid scale, extreme convergence and extreme divergence have about the same absolute value. This contrasts with a dominant divergence value in

CONVERGENCE VS. RAINFALL
(AFTER ALLOWING FOR VARYING LAGS)

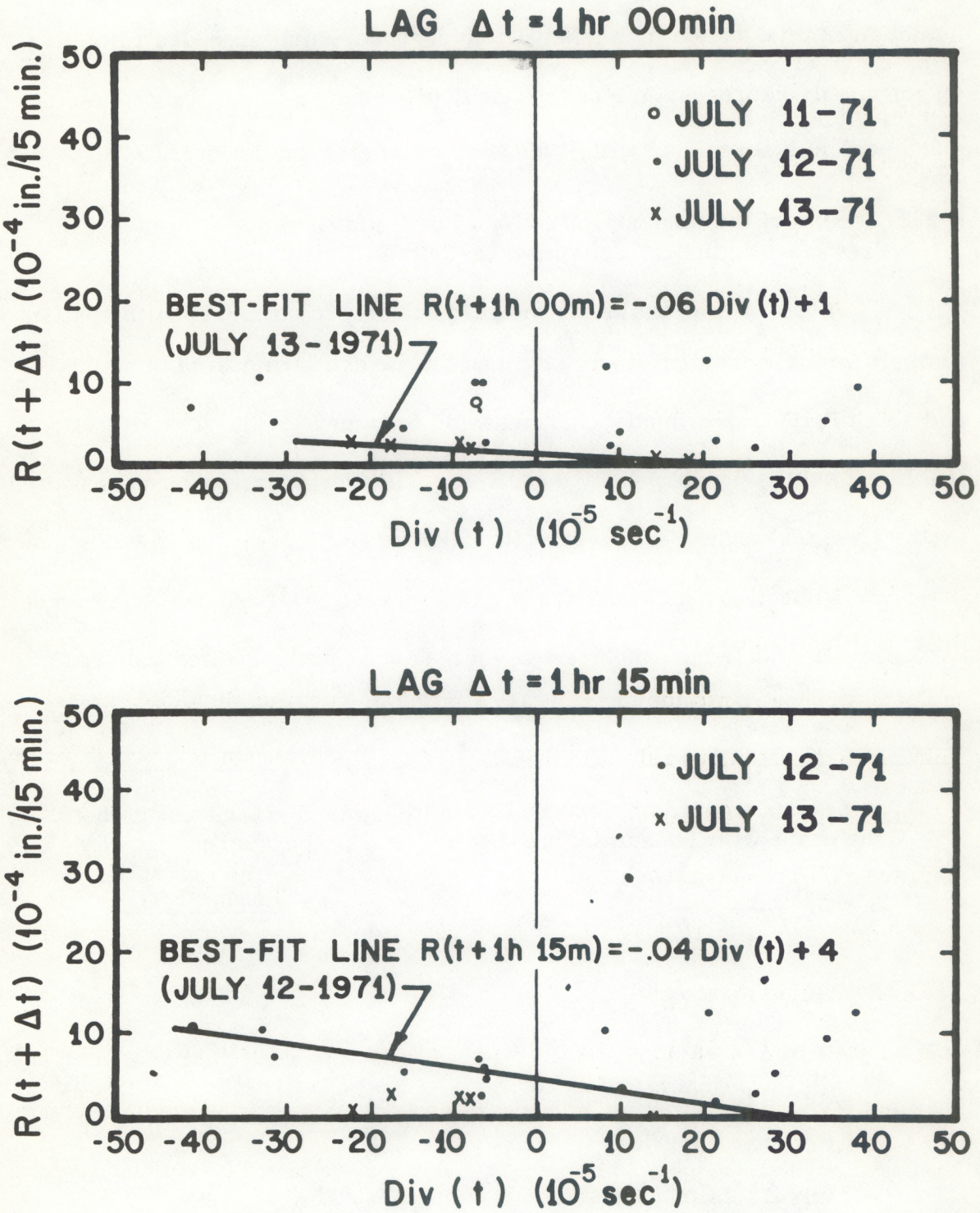

Figure 12. Convergence vs. rainfall diagrams (after allowing for varying lags). Convergence-rainfall correlations at the grid scale are shown for 1 hour, and 1 hour and 15 minute lags.

the grid- point model. The more equal values of extreme convergence and extreme divergence at the grid scale (meso-scale) are probably due to a better depiction at this scale of the general convergence which precedes rainfall. It also probably represents a less precise depiction at the mesoscale of the divergence which is associated with individual thunderstorm downdrafts.

4.2.3 Results of the Comparison of Grid Point and Grid Scale Studies with Previous Studies on Convergence-Rainfall Relationships.

Some of the results for the grid scale were compared with similar findings which were previously obtained for a much larger area of central and south Florida (Fernandez-Partagas and Estoque, 1972). The latter area will be called the "larger scale" hereafter. The "larger scale" area is limited by the polygon Tampa-Fort Myers-Miami-Palm Beach-Vero Beach-Melbourne-Orlando-Tampa (Fernandez-Partagas and Estoque, 1972). Divergence, relative vorticity and radar echo areal coverages were compared for the six times which are shown in table 2.

Table 2. Comparison Times of Meteorological Parameters at the Grid-scale with Meteorological Parameters at the "Larger Scale"

Dates	Times (EDT)
July 11, 1971	1800
July 12, 1971	1600
July 12, 1971	1800
July 12, 1971	2000
July 13, 1971	1600
July 13, 1971	1800

The times in table 2 were the only instances having simultaneous information at the grid scale and at the "larger scale." Figure 13 shows a scatter diagram of grid scale vs. "larger scale" quantities. It was surprising that the six divergence values correlated so well among themselves that a best-fit line could be easily drawn. The six relative vorticity values also correlated among themselves, and the corresponding best-fit line was drawn. Radar echo percentages did not show, however, a good correlation and no best-fit line was attempted. The equation of the best-fit line for divergence indicates an order of magnitude difference between the grid scale and the "larger scale" divergences. Grid-scale relative vorticities are found to be about one and a half times larger than relative vorticity values for the "larger scale." Because of the sample which was used is quite small, these results have to be taken with caution. Moreover, uncertainty remains about whether similar findings might have been obtained by setting the meso-network at a different location within the "larger scale" domain.

The last study of the present investigation was an attempt to link the typical evolution of divergence at various scales (grid point scale, grid scale and "larger scale") with a distinct, common feature in rainfall occurence. This attempt required a careful inspection of the evolution of divergence and rainfall. An examination of rainfall at the grid-point scale (cloud-scale) and at the grid scale (meso-scale) revealed that peak rainfall times tended to coincide. After some minor adjustments, 1800 EDT was set as a crude estimate for

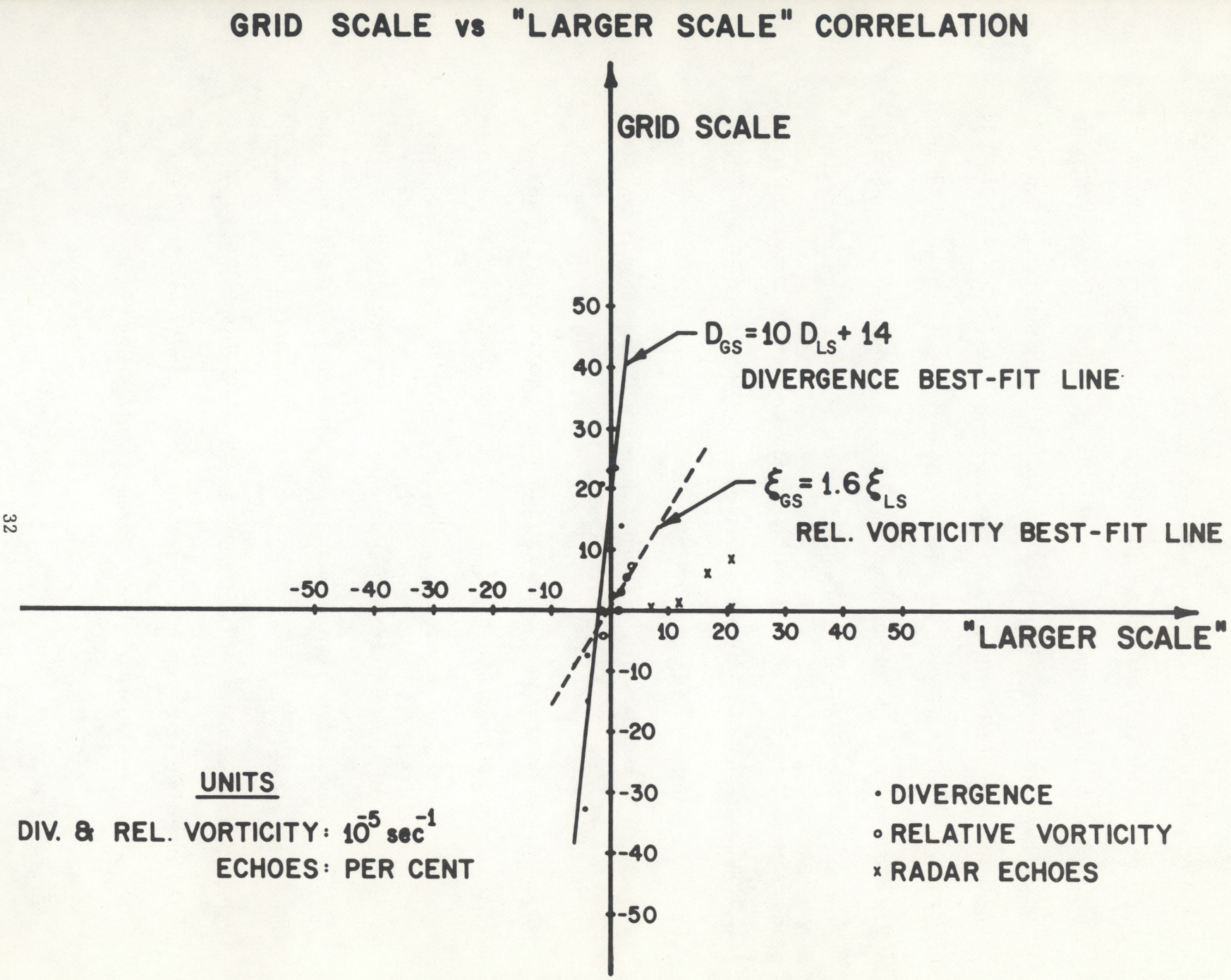

Figure 13. Scatter diagram showing grid scale vs. "larger scale" correlations for divergence, relative vorticity and radar echoes.

the time of coincidence. For the "larger scale", maximum rainfall (radar echo percentage) was also found to occur at 1800 EDT for the July 11-13, 1971 period (Fernandez-Partagas and Estoque, 1972). Thus, in view of the time coincidence of peak rainfall at the three scales, divergence vs. time curves for the cloud-scale, the meso-scale and the "larger scale" were combined on a single graph. This graph, which uses 1800 EDT as zero-time reference, is shown in figure 14.

A straightforward conclusion from figure 14 is that the smaller the scale of motion, the larger the peak divergence and peak convergence values which are encountered. Of much higher impact, however, is the transition of the convergence peak from the "larger scale" into the meso-scale and then from the meso-scale into the cloud-scale. This transition is observed to occur over a two-hour period before peak rainfall. For divergence, the opposite evolution is seen after peak rainfall. In this case, maximum divergence is observed first at the cloud-scale a few minutes after peak rainfall and it is followed by the maximum divergence at the meso-scale (about 45 minutes after peak rainfall) and by the maximum divergence at the "larger scale" (about two hours after peak rainfall).

The results of this last study are important in relation to the problems of parameterization and short-range forecasting of convective rainfall. The results are significant for the parameterization problem in two ways. First, they provide observational support for the hypothesis that larger scale

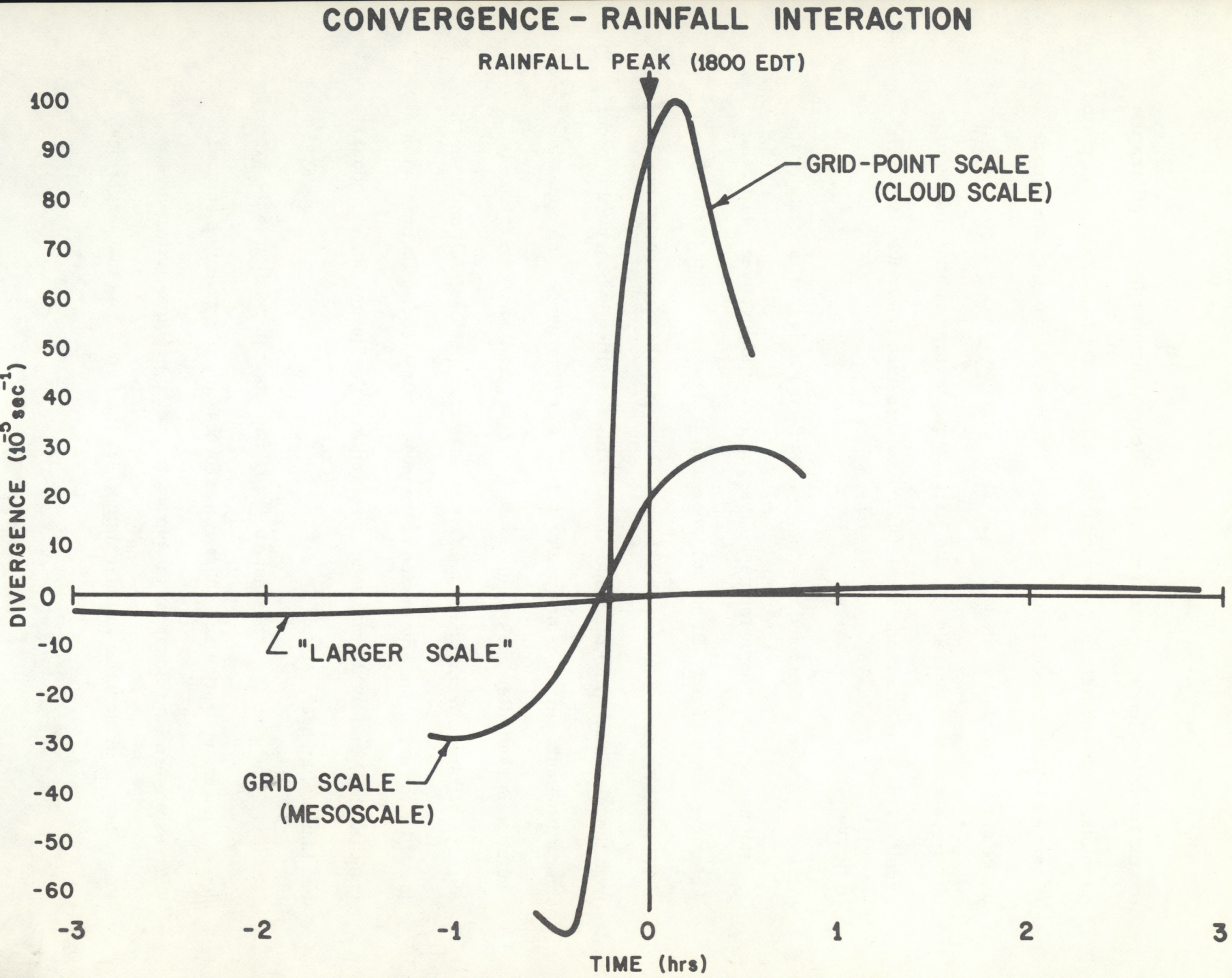

Figure 14. Convergence-rainfall interaction among three subsynoptic scales of motion. See text for explanation.

convergence induces convective rainfall. Second, they indicate an additional complication in formulating parameterizing schemes due to the lag between "larger scale" convergence and convective rainfall, and hence, condensation heating.

Although this lag is a complicating factor in parameterization, it is an advantage in short-range forecasting. Because of this lag, "larger scale" convergence can be used as a short-range predictor for convective activity.

5. CONCLUSION

Analyses of surface winds, wind-derived quantities and rainfall at subsynoptic scales formed the basis for the present convergence-rainfall investigation. These analyses permitted the determination of convergence-rainfall relationships at the cloud-scale (grid-point scale) and at the meso-scale (grid scale) in the vicinity of Florida thunderstorms. The above-mentioned relationships, together with those previously found for the Florida peninsula ("larger scale"), showed the relation which links convergences and divergences at the three scales with peak rainfall. Maximum convergence occurred first at the "larger scale" and it was followed by corresponding maxima at the meso-scale and then at the cloud-scale. After peak rainfall, maximum divergence occurred first at the cloud scale and then it was followed by meso-scale and then by "larger scale" divergences. These results are important for the parameterization of convective rainfall because they provide observational support for the hypothesis that "larger scale" convergence produces smaller scale convergence which, in turn, induces rainfall. However, the results show a complicating factor in formulating parameterizing schemes because rainfall lags behind "larger scale" convergence. This lag, on the other hand, is an advantage for short-range forecasting since "larger scale" convergence can be used as a short-range predictor for convective activity.

Caution must be exercised in generalizing the results of this study. Several limitations are present. One of these is a problem of representativeness. Are the values of convergence and rainfall for the surface network

representative of other areas within the "larger scale" domain (southern Florida peninsula)? Another limitation is the fact that the results of this study are appropriate only to the particular synoptic-scale conditions described in the Introduction. It is expected that different conditions could modify significantly these results. A third limitation is that the convergence-rainfall relationships presented in this paper are based upon three-dimensional (x, y, t) analyses. In order to incorporate the effect on convergence-rainfall relationships of meteorological events at levels above the earth's surface, analyses should be extended to the vertical (z) coordinate in future research work. For this, subsynoptic observations at various atmospheric levels (i.e. doppler radar, pilot balloon, cloud movement and research aircraft observations) would have to be taken simultaneously with surface data.

6. ACKNOWLEDGMENTS

The research work which is presented in this paper was sponsored by the NOAA Environmental Research Laboratory under Grant No. 04-3-022-2 to the Rosenstiel School of Marine and Atmospheric Science, University of Miami, Coral Gables, Florida. Facilities for this study were provided by the NOAA Experimental Meteorology Laboratory, Coral Gables, Florida.

Co-principal investigator Mariano A. Estoque contributed many imaginative ideas in the course of this research work.

Thomas Elmore, Cecilia G. Griffith, Alan Herndon, Ronald L. Holle, William Riebsame, Rosa L. Salom, Harry V. Senn and William L. Woodley contributed to the scientific and/or technical parts of this work. Richard Decker, Paul M. Hannum, Dale B. Martin, Scott J. Miller and Robert N. Powell assisted in preparing the figures. Constance Arnhols and Phyllis Olson helped in preparing the manuscript.

The author wishes to extend his sincere gratitude to the above-mentioned institutions and individuals.

7. REFERENCES

Byers, H. and R.R. Braham (1949), The Thunderstorm (Report of the Thunderstorm Project), Washington, D.C., 287 pp.

Fernandez-Partagas, J.J. and M.A. Estoque (1972), Meteorological studies in relation to cloud seeding experiments over south Florida in 1971. Final report prepared for NOAA Grant No. E-22-96-71 (G), Rosenstiel School of Marine and Atmospheric Science, Div. of Atmospheric Science, University of Miami, Coral Gables, Florida 33124, 104 pp.

Herrera Cantilo, L.M. and J.J. Fernandez-Partagas (1972), Analysis of a tropical depression based on radar data, J. Appl. Meteorol. 11: 298–303.

Operations Staff (1971), The NSSL surface network and observations of hazardous wind gusts, NOAA Technical Memorandum ERL NSSL-55, U.S. Department of Commerce, National Oceanic and Atmospheric Administration, Environmental Research Laboratories, Norman, Oklahoma, 20 pp.

Pacheco, P.P. (1972), On the sub-cloud layer structure relative to cumulonimbus systems in Venezuela, Department of Atmospheric Science, Colorado State University, Fort Collins, Colorado, 23 pp.

APPENDIX A

The July 11, 1971 case study

A single, well-developed thunderstorm occurred over the western part of the mesonetwork in the evening of July 11, 1971. This thunderstorm provided an opportunity for studying a thunderstorm evolution under the simplest possible conditions, and free of the complex interactions which are frequently associated with thunderstorm clusters.

The thunderstorm developed about 1730 EDT, moved towards the north northwest and left the network area by 1900 EDT. Pictures of the thunderstorm are shown in figure A 1.

Some aspects of the July 11, 1971 thunderstorm are presented in figure A 2. This figure illustrates the tracks of the center of outdraft, the center of heaviest rainfall and the center of radar echoes of greatest intensity. In an effort to avoid bias, these centers were determined on an entirely independent basis. Note that, at all times, distances between locations of these centers were in the range of one to two statute miles. This is believed to be an excellent agreement, especially if allowance is given for the independence of analyses. In addition, note that the outdraft showed up later than rainfall in the process of thunderstorm development. Isochrones for the leading edge of the outdraft are shown in figure A 3.

Wind fields, relative wind fields and divergence and relative vorticity fields for the July 11, 1971 case study are presented in figures A4 to A8.

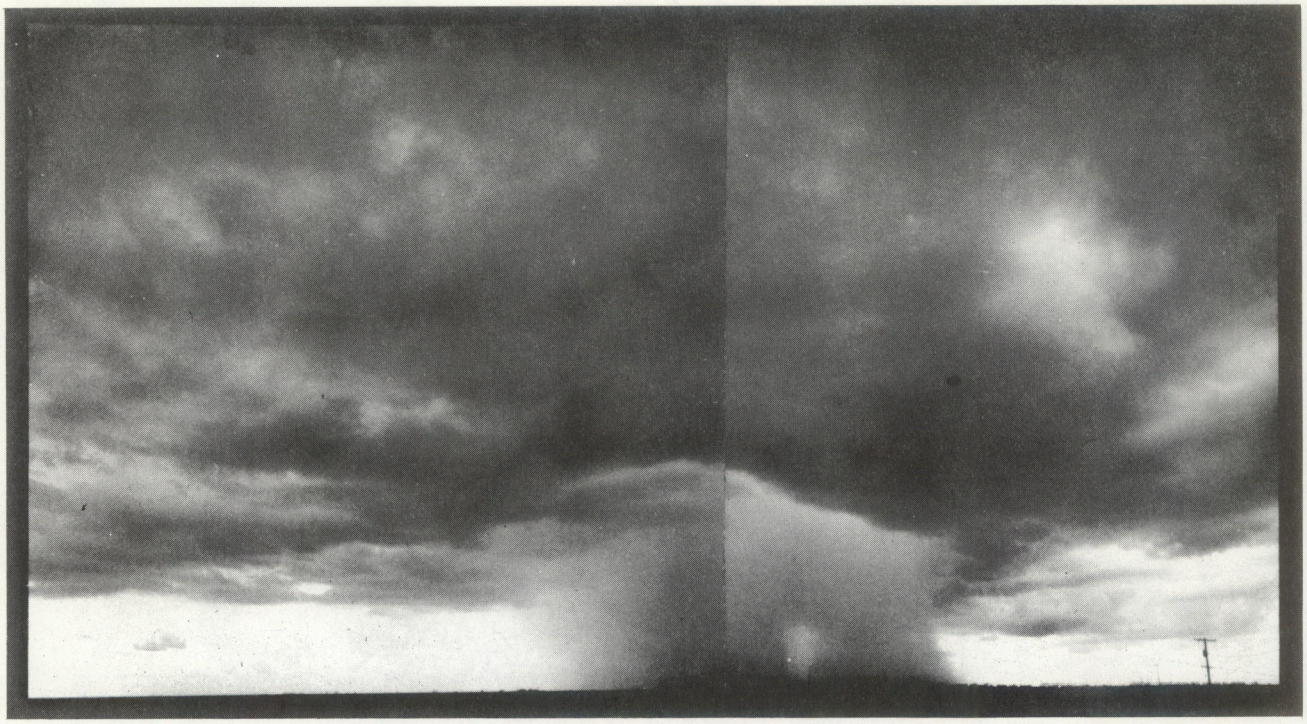

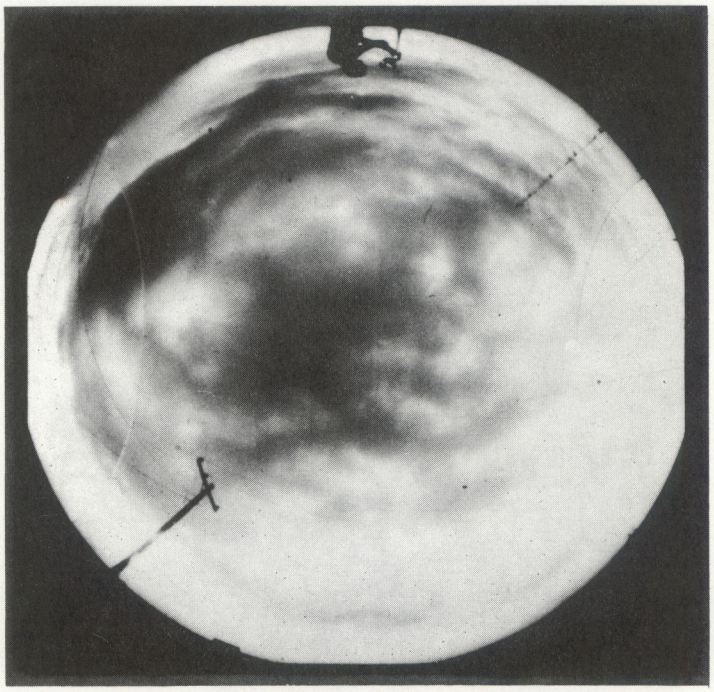

Figure A1. The July 11, 1971 thunderstorm. Top: a mosaic of two pictures taken at 1800 EDT with a Hasselblad wide-angle lens camera from location T (Central Site) in figure 1 of the main text. The center of the mosaic represents the west direction (north is on the right and south is on the left). Bottom: View taken with a Nikon whole-sky camera from location T at 1800 EDT. The July 11, 1971 thunderstorm can be seen near the upper-left corner.

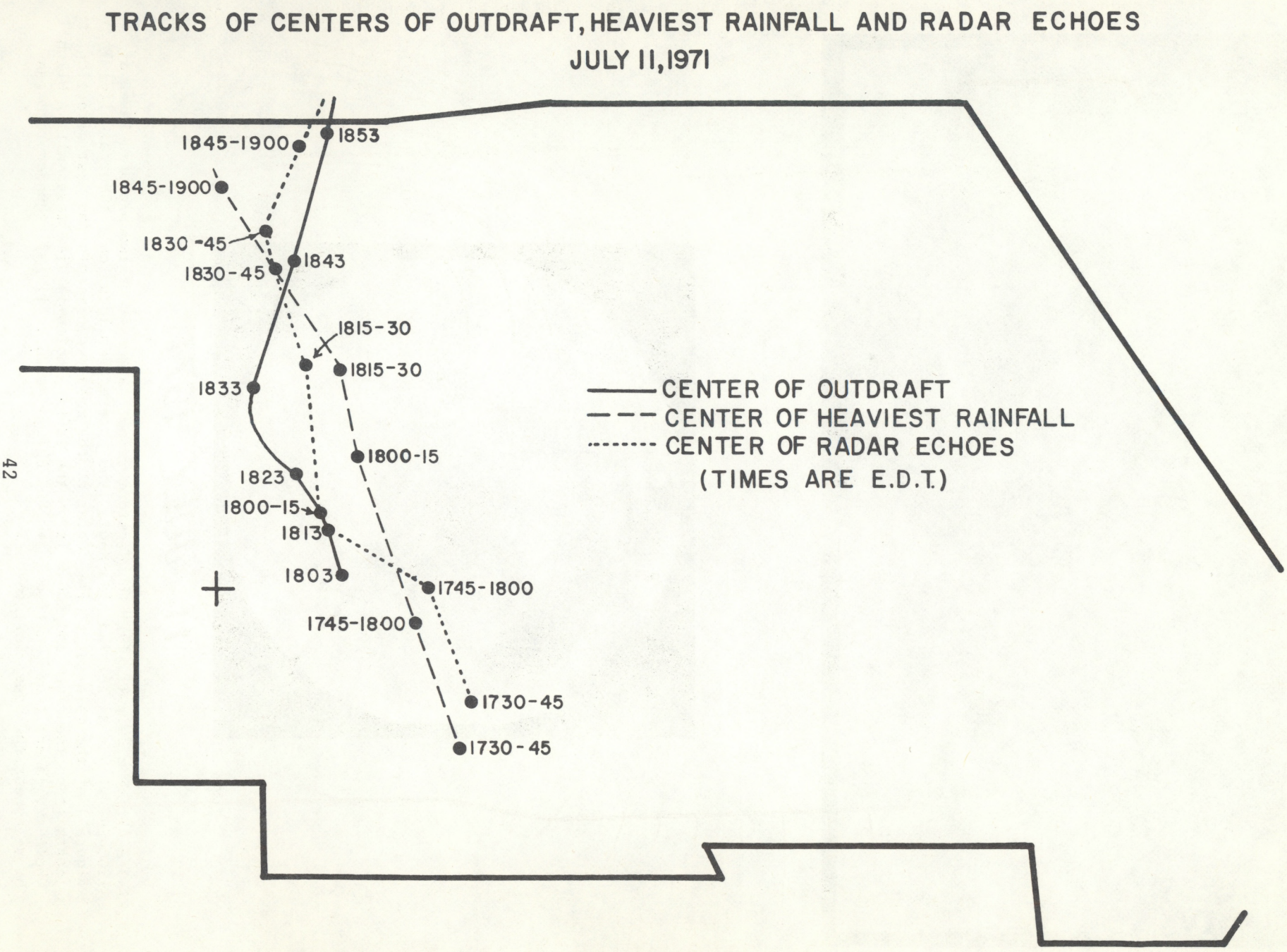

Figure A2. Graph showing some aspects of the July 11, 1971 thunderstorm.

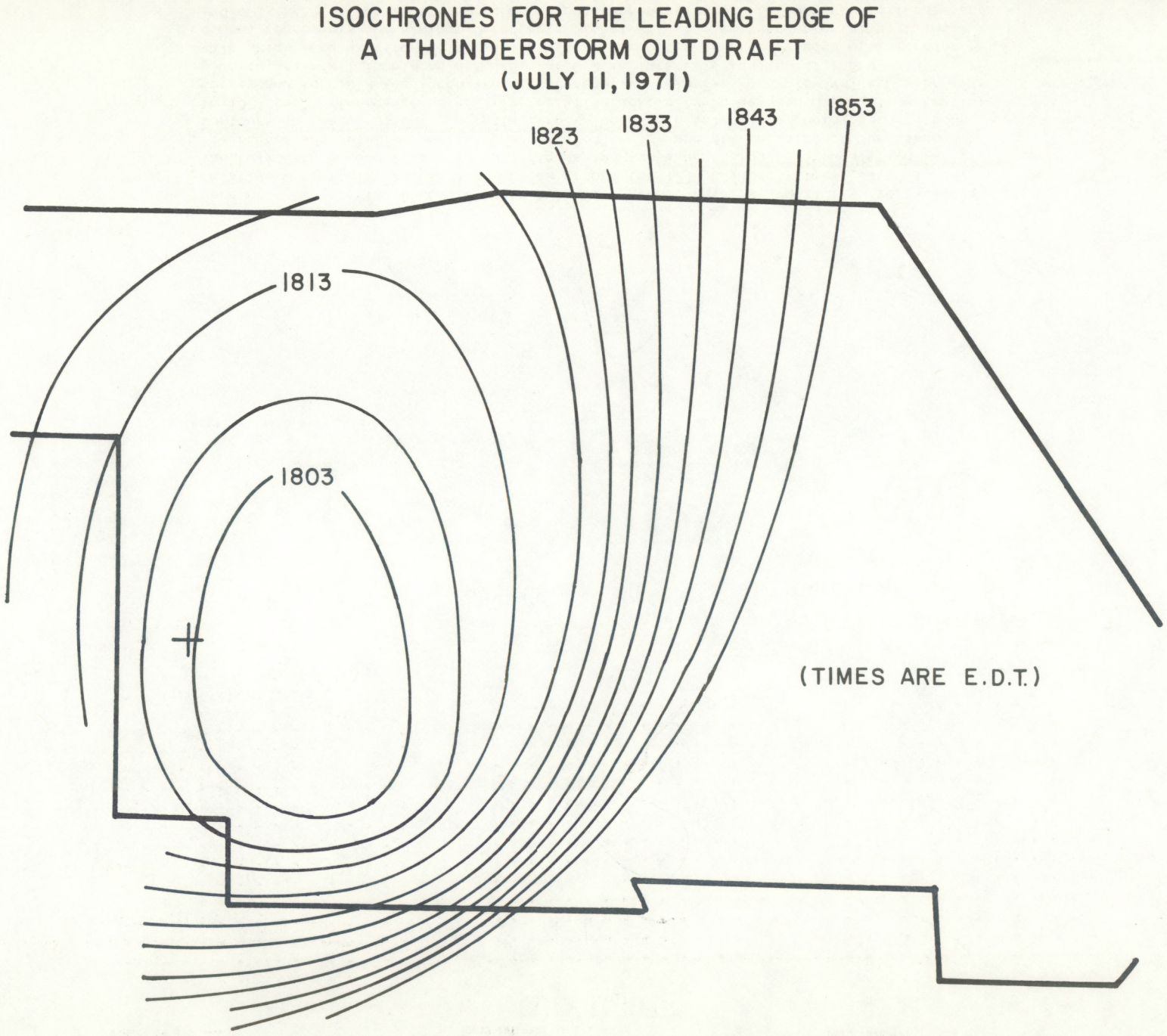

Figure A3. Graph showing the evolution of the outdraft related to the July 11, 1971 thunderstorm.

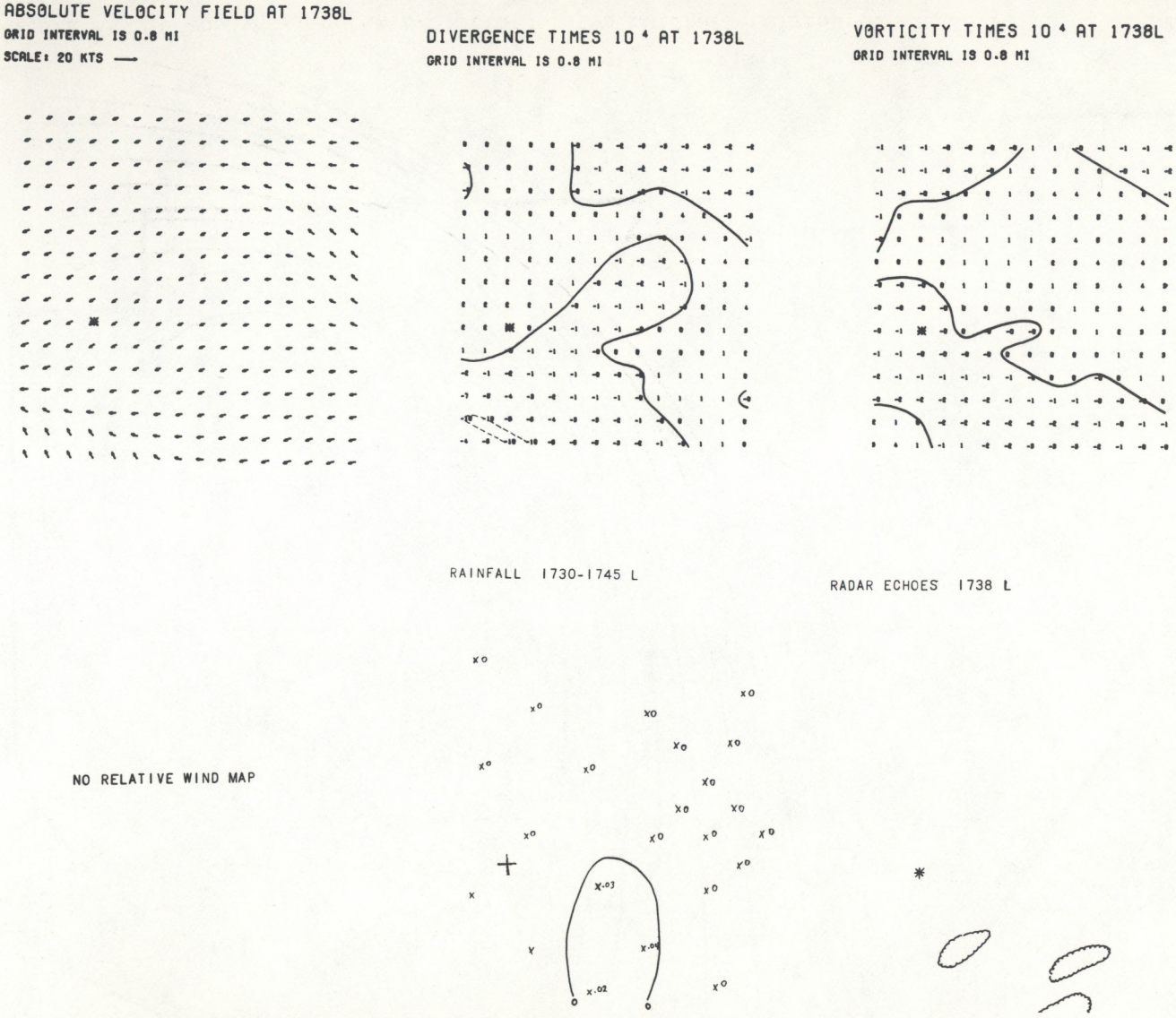

Figure A4. Wind field (absolute velocity), divergence, relative vorticity (vorticity), relative wind field, rainfall and radar echoes for 1738 L (local time), July 11, 1971. The following is applicable to this figure and subsequent figures: Local time is EDT. Divergence and relative vorticity are scaled to 10^4 and are in units of "per second." Contours in heavy solid line denote zero values; thin solid line contours correspond to 10^{-3} sec^{-1} divergence or positive relative vorticity values and dashed line contours correspond to -10^{-3} sec^{-1} convergence or negative relative vorticity values. For simplicity, rainfall isopleths are shown at 0.2 in intervals in lieu of the 0.1 in intervals which were used for original analyses. The outer (serrated) edge of the radar echoes represents the Minimum Detectable Signal (M.D.S.) as seen on original films. (~0.003 in/hr). The first iso-echo contour represents a 0.1 in/hour rainfall rate and the second iso-echo contour represents a 0.6 in/hour rainfall rate.

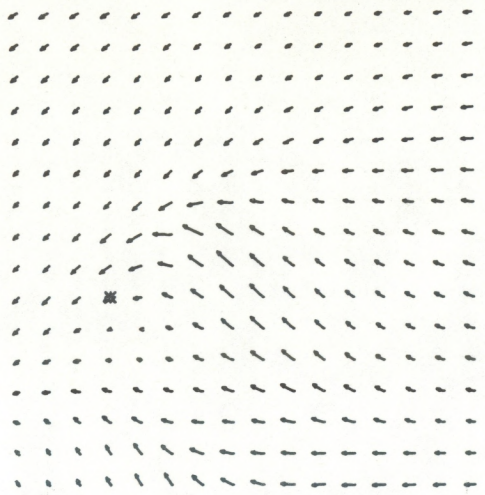

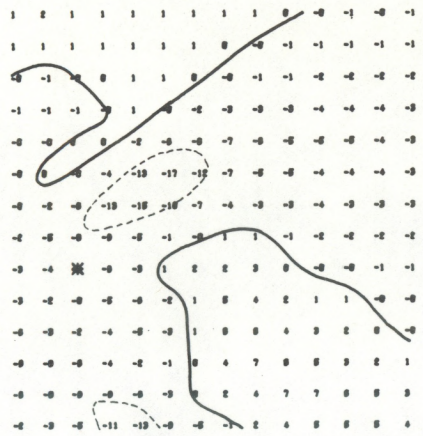

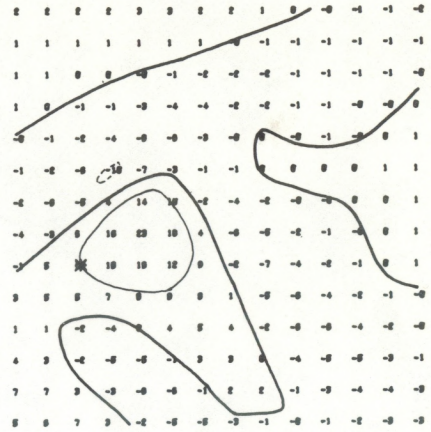

NO RELATIVE WIND MAP

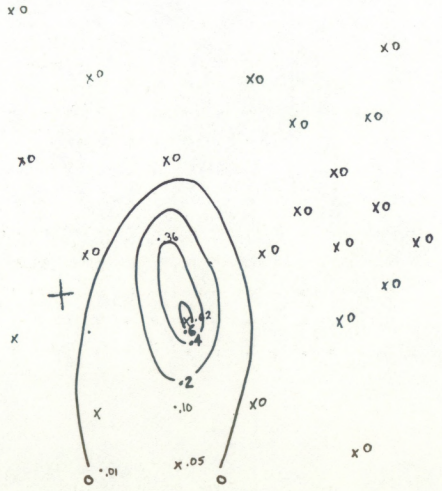

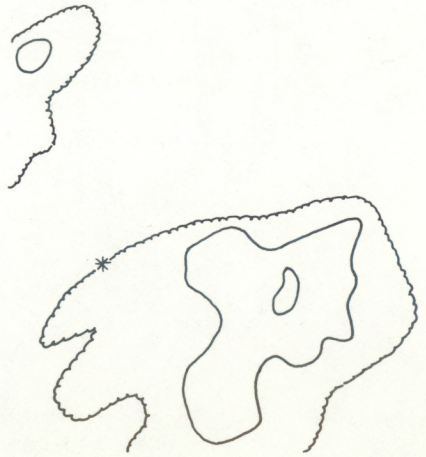

Figure A5. Same as figure A4 but for 1753 L (local time), July 11, 1971.

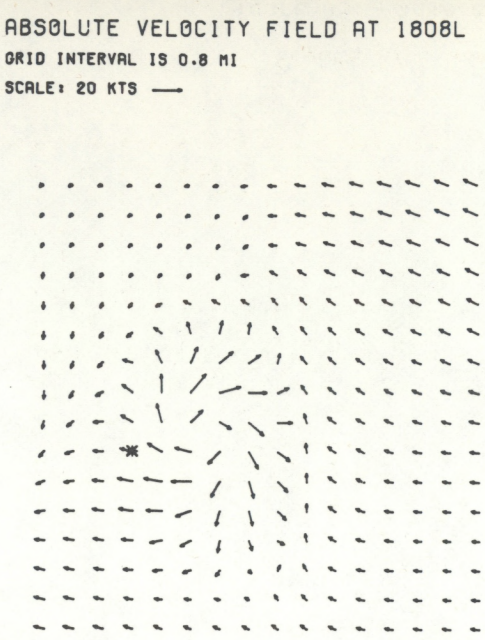

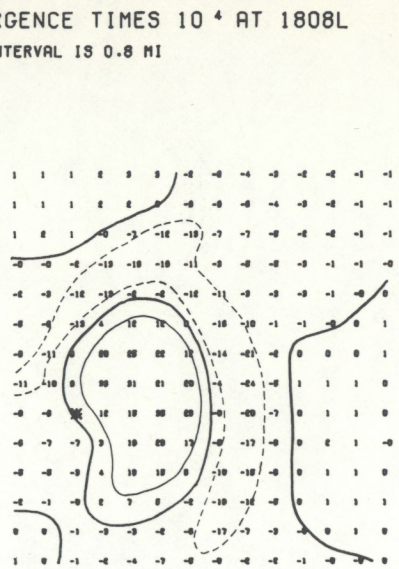

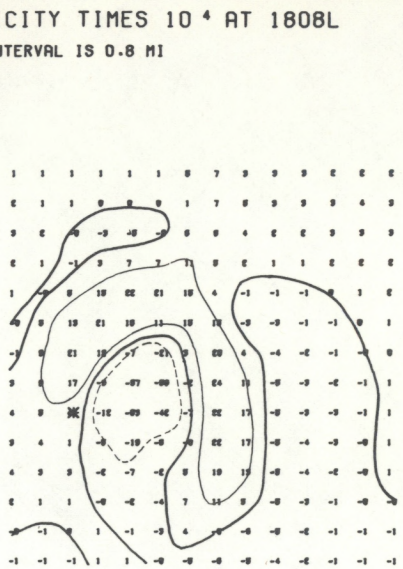

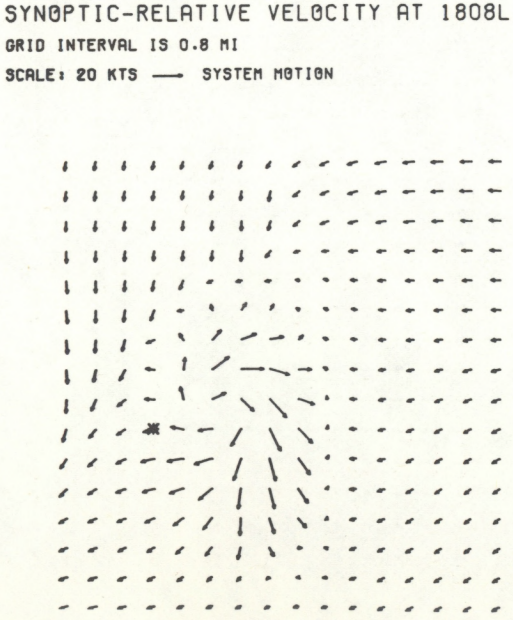

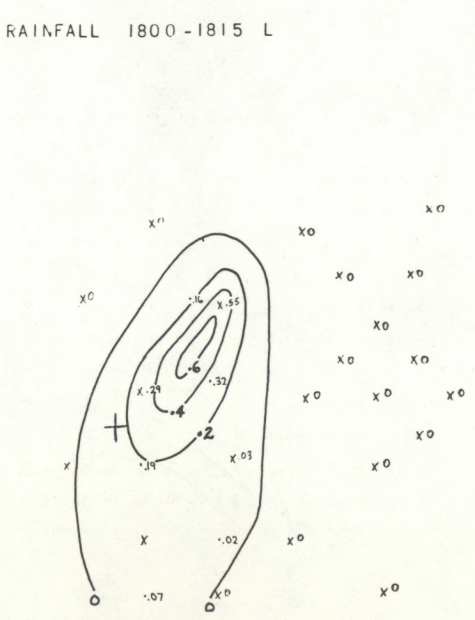

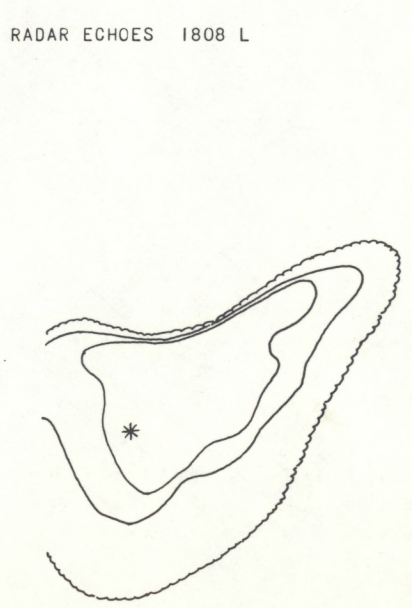

Figure A6. Same as figure A4 but for 1808 L (local time), July 11, 1971. In this figure, "synoptic-relative velocity" is equivalent to relative wind field.

ABSOLUTE VELOCITY FIELD AT 1823L
GRID INTERVAL IS 0.8 MI
SCALE: 20 KTS ——

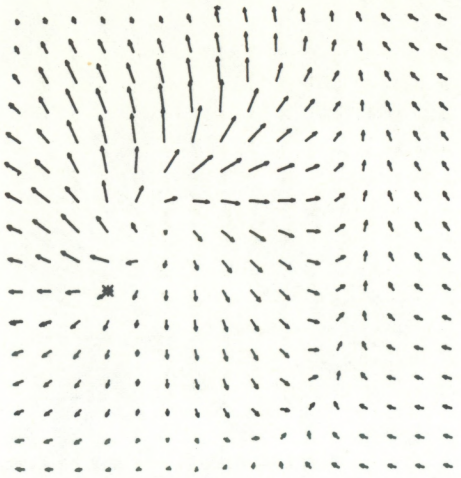

DIVERGENCE TIMES 10^4 AT 1823L
GRID INTERVAL IS 0.8 MI

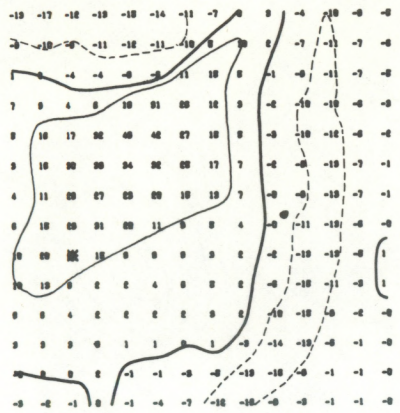

VORTICITY TIMES 10^4 AT 1823L
GRID INTERVAL IS 0.8 MI

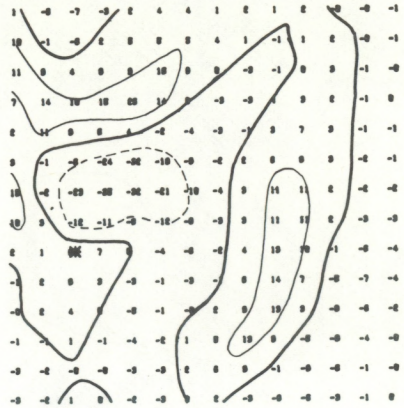

SYNOPTIC-RELATIVE VELOCITY AT 1823L
GRID INTERVAL IS 0.8 MI
SCALE: 20 KTS —— SYSTEM MOTION ↖

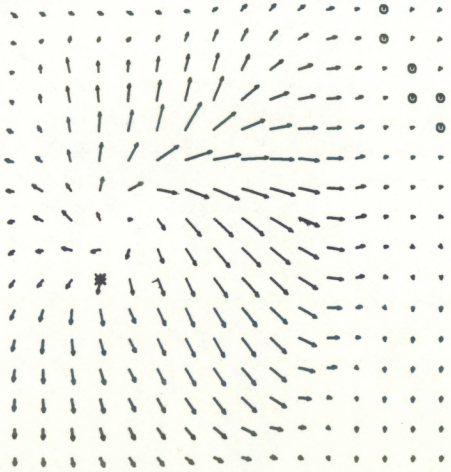

RAINFALL 1815-1830 L

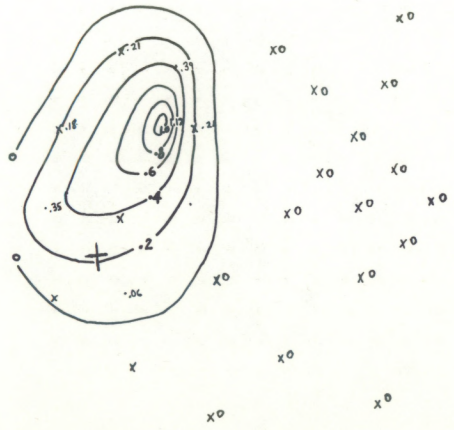

RADAR ECHOES 1823 L

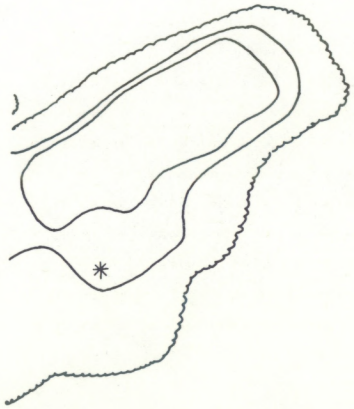

Figure A7. Same as figure A6 but for 1823 L (local time), July 11, 1971.

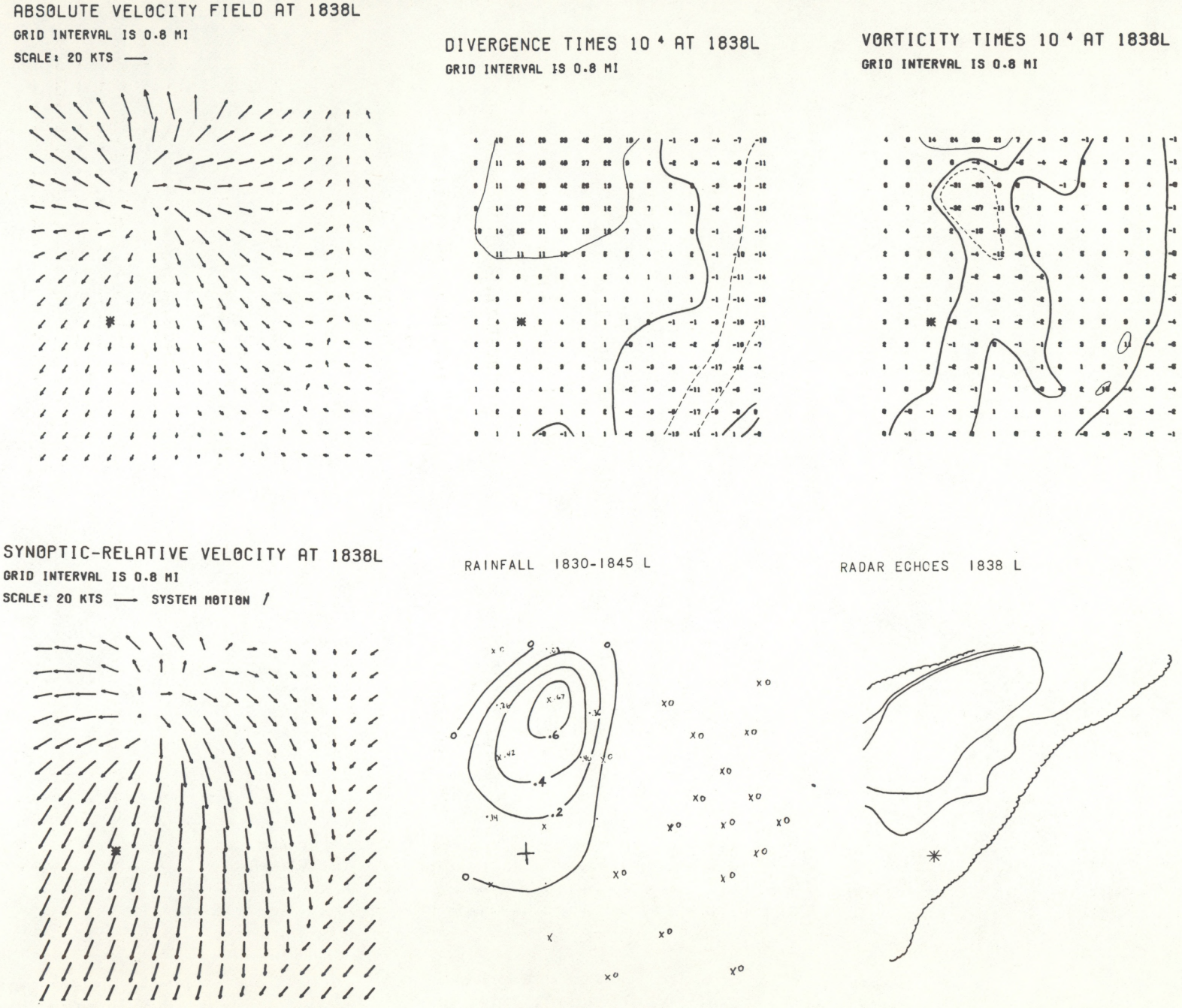

Figure A8. Same as figure A6 but for 1838 L (local time), July 11, 1971.

Rainfall analyses and radar echo depictions are also shown in these figures. These figures present sets of graphs at 15-minute intervals. Because all graphs are believed to be self explanatory, no detailed description of them will be included here. It should suffice to point out: a) the rain occurrence under a convergence pattern at the early stages, b) the asymmetry of the anticyclonic outdraft in the relative wind field, c) the convergence and divergence values which were the largest ones encountered for the July 11-13, 1971 period, d) the large values of negative vorticity which were associated with the thunderstorm surface anticyclone and e) the good agreement between intense radar echoes and heavy rainfall.

Figure A 9 shows the evolution of divergence, relative vorticity and rainfall with respect to a moving center which was chosen to be the center of the thunderstorm outdraft. The evolution near the center and at selected sectors to the front and to the rear of the moving thunderstorm is illustrated in figure A 9. The isolated character of the July 11, 1971 thunderstorm encouraged the use of this Lagrangian approach. Note that the largest absolute values of divergence, relative vorticity and rainfall are found near the center of outdraft. Values of these quantities drop significantly over short distances from the center of outdraft. As in the case of Eulerian studies, rain is observed to start under a weak to moderate convergence, and rainfall and divergence maxima are observed to coincide. Large values of negative relative vorticity are shown near the center of the moving thunderstorm. For most

EVOLUTION OF DIVERGENCE, RELATIVE VORTICITY AND RAINFALL RELATIVE TO A MOVING THUNDERSTORM

(JULY 11, 1971)

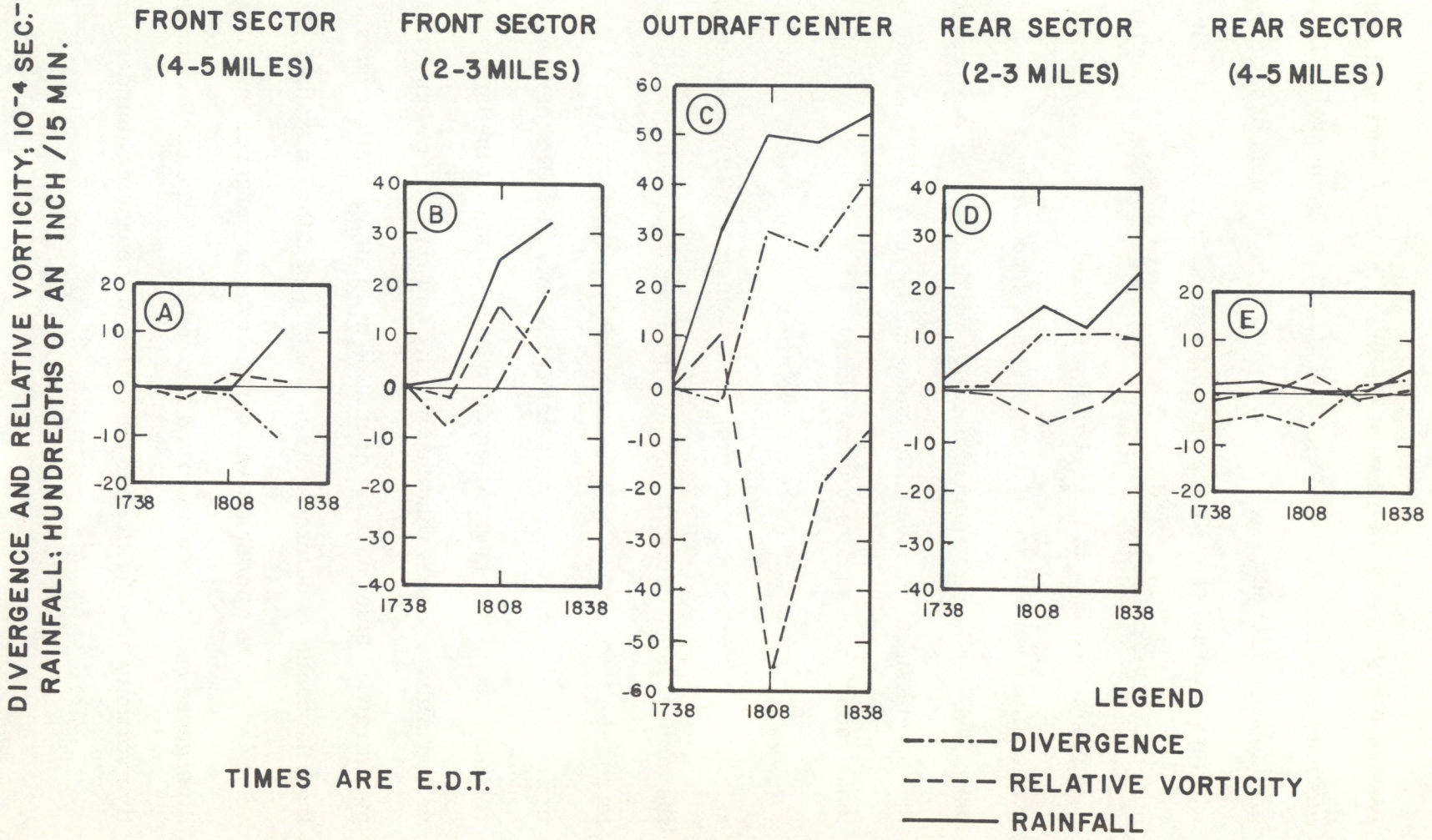

Figure A9. Evolution of divergence, relative vorticity and rainfall relative to a moving center (outdraft center) of the July 11, 1971 thunderstorm.

sectors (particularly for those at the front), convergence and positive relative vorticity are found to be related to the edge of the expanding outdraft. A later occurrence of divergence and negative relative vorticity is found to be related to the thunderstorm outdraft itself.

Convergence-rainfall relationships for July 11, 1971 both at the grid- point scale (cloud-scale) and at the grid scale (meso-scale), are included in the main text of this paper.

APPENDIX B

The July 12, 1971 case study

Analyses for the July 12, 1971 case extended for five hours (1500-2000 EDT). Wind fields, divergence and relative vorticity fields, rainfall analyses and radar echo depictions at 30-minute intervals are illustrated in figures B1 to B11. Cloud pictures for the July 12, 1971 case are shown in figure B12. Examination of figures B1 to B11 and of analyses at more frequent intervals (not reproduced) revealed a complicated thunderstorm pattern for the July 12, 1971 case study. This complicated pattern was in contrast with the simple one which was observed for July 11, 1971. However, some overall characteristics of the surface air flow evolution and of the rainfall evolution could still be inferred. Three successive features were found to occur in the surface wind field. These features were: 1) the development of a well-defined convergence line over the network, 2) a gradual change of this convergence pattern into a divergence pattern over the entire network and 3) an eastward propagation of a second line of convergence over the network. The rainfall sequence indicated: 1) precipitation to occur first near the western part of the well-defined convergence line in the wind field, 2) precipitation to occur next over the eastern and northern portions of the network and 3) precipitation to occur last over the western and central portions of the network.

An application of the July 12, 1971 wind analysis was the comparison of the surface air flow with cloud photographs taken by high-level

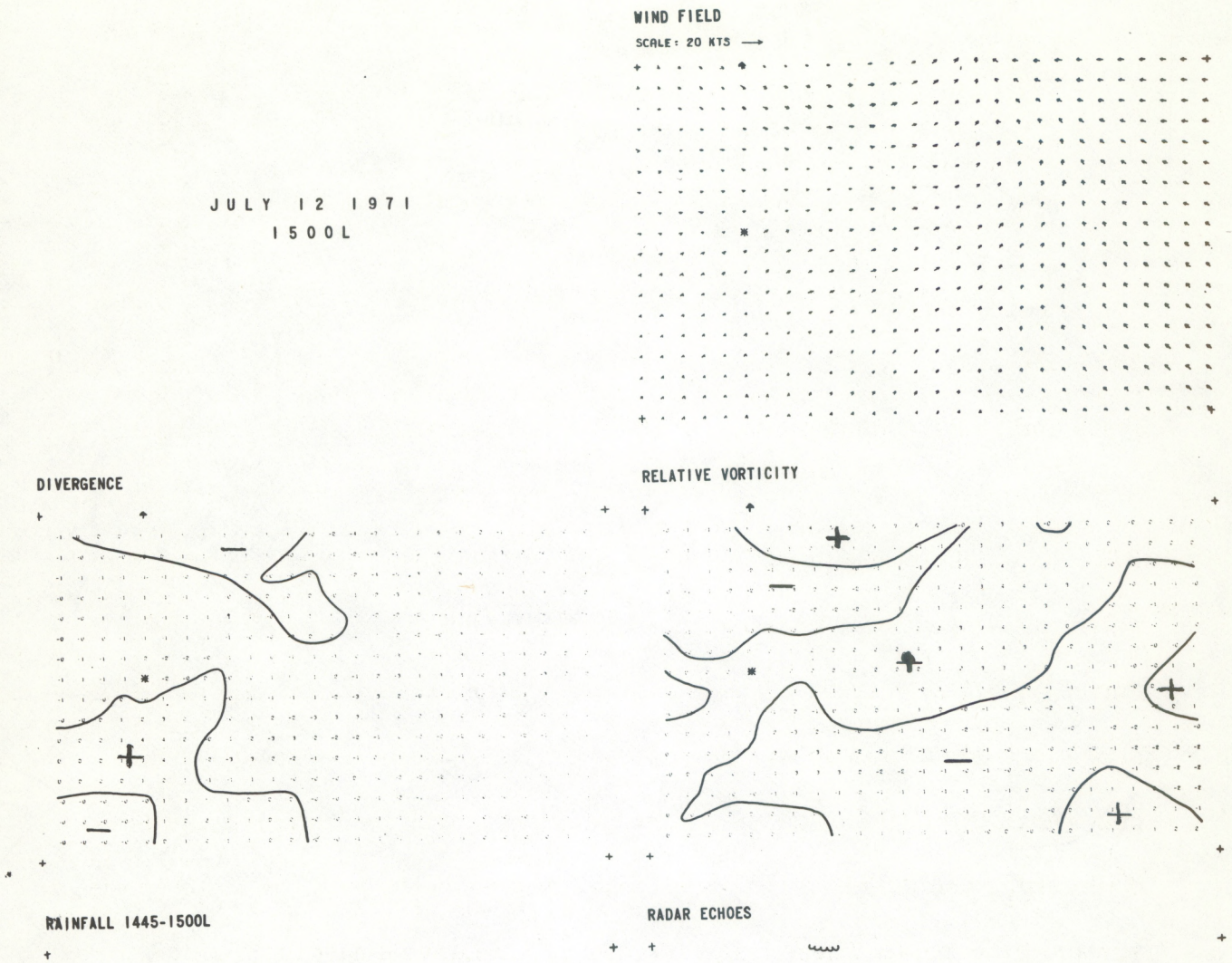

Figure B1. Wind field, divergence, relative vorticity, rainfall and radar echoes for 1500 L (local time), July 12, 1971. The following is applicable to this figure and subsequent figures: Local time is EDT. Wind field is presented in vectorial form; vectors at a few isolated grid points are in error due to mistakes on punch card information for such grid points. Divergence and relative vorticity are scaled to 10^4 and are in units of "per second." Contours in heavy solid line denote zero values; thin solid line contours correspond to 10^{-3} sec^{-1} divergence or positive relative vorticity values. Dashed line contours correspond to -10^{-3} sec^{-1} convergence or negative relative vorticity values. Positive signs indicate divergence and positive relative vorticity areas. Negative signs indicate convergence and negative relative vorticity areas. For simplicity, rainfall isopleths are drawn at 0.2 in intervals in lieu of the 0.1 in intervals which were used for original analyses. The outer (serrated) edge of the radar echoes represents the Minimum Detectable Signal (M.D.S.) as seen on original films (~0.003 in/hr). The first iso-echo contour represents a 0.1 in/hour rainfall rate and the second iso-echo contour represents a 0.6 in/hour rainfall rate.

JULY 12 1971
1530L

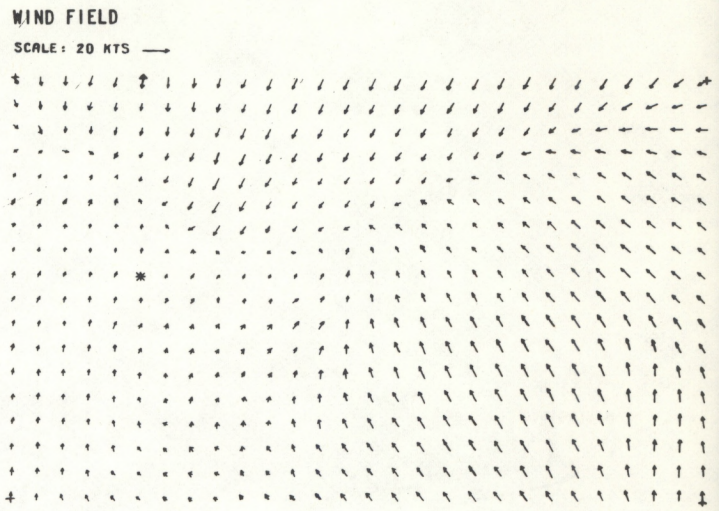

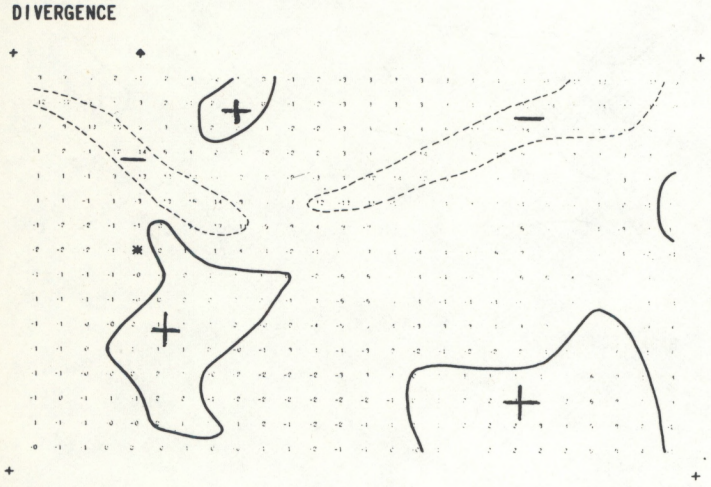

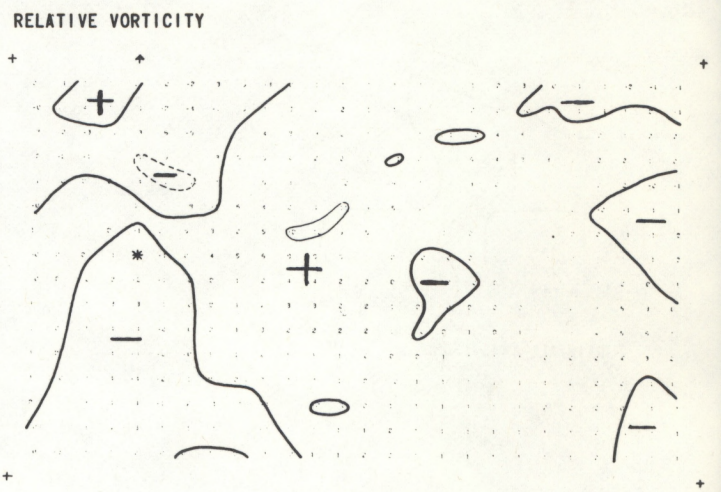

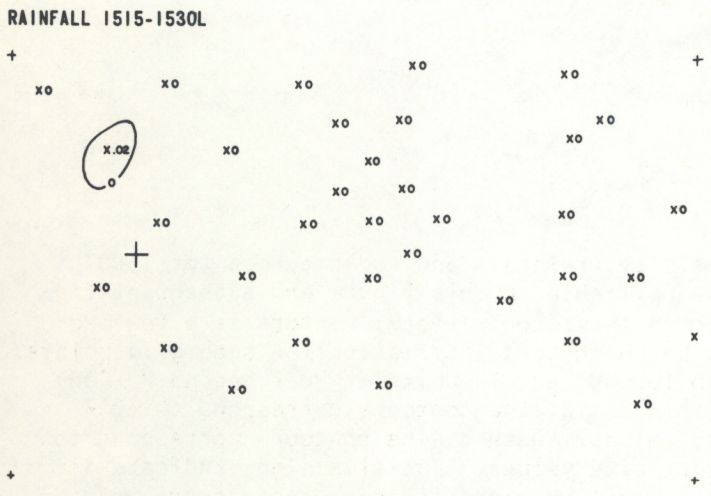

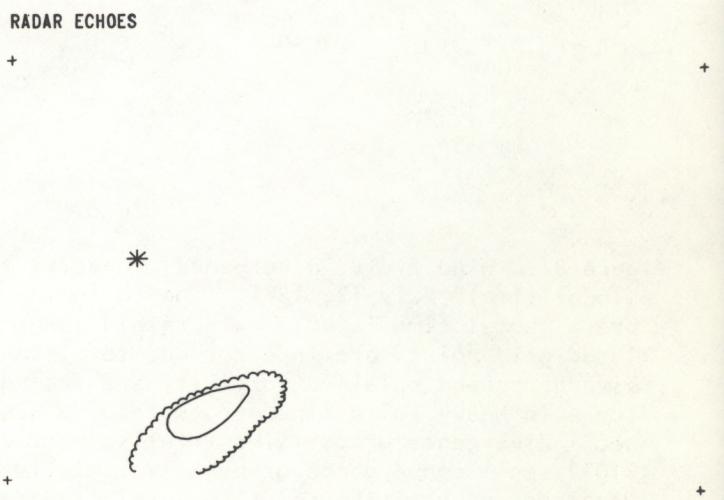

Figure B2. Same as figure B1, but for 1530 L (local time), July 12, 1971.

JULY 12 1971
1600L

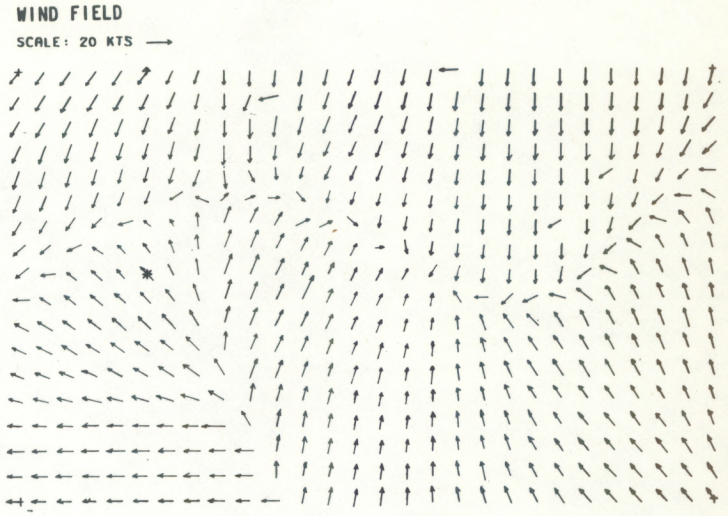

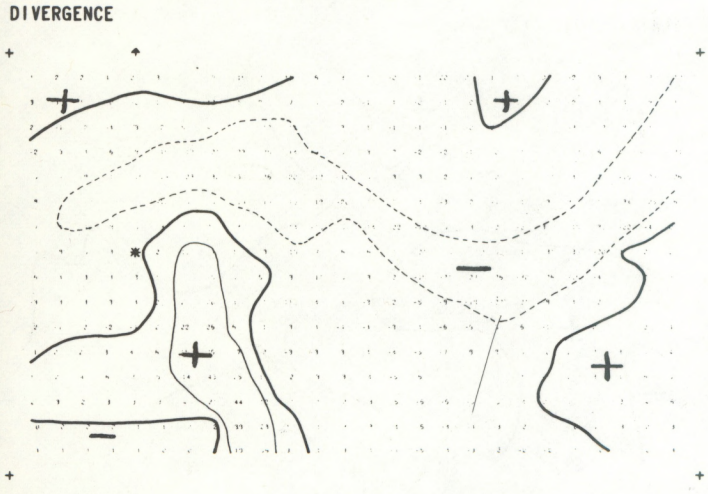

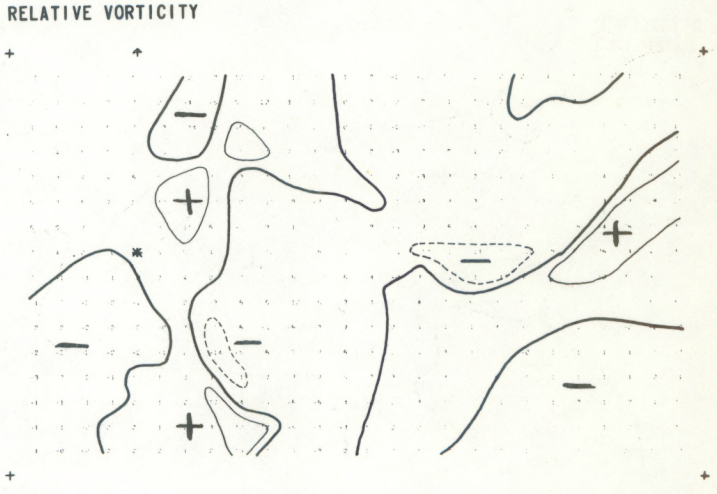

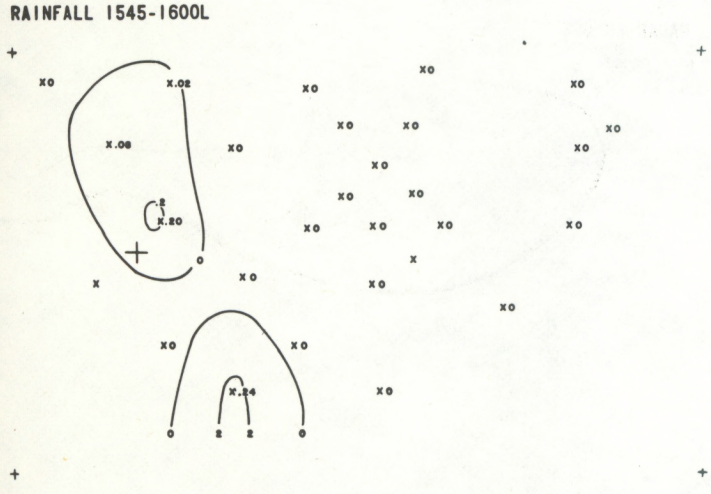

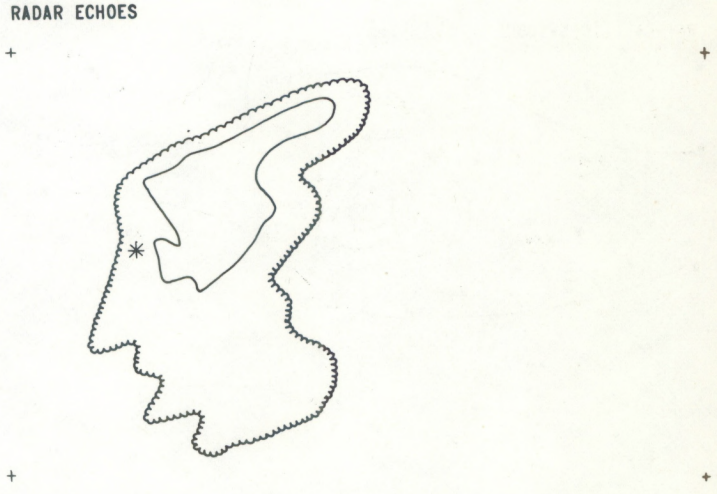

Figure B3. Same as figure B1 but for 1600 L (local time), July 12, 1971.

JULY 12 1971
1630L

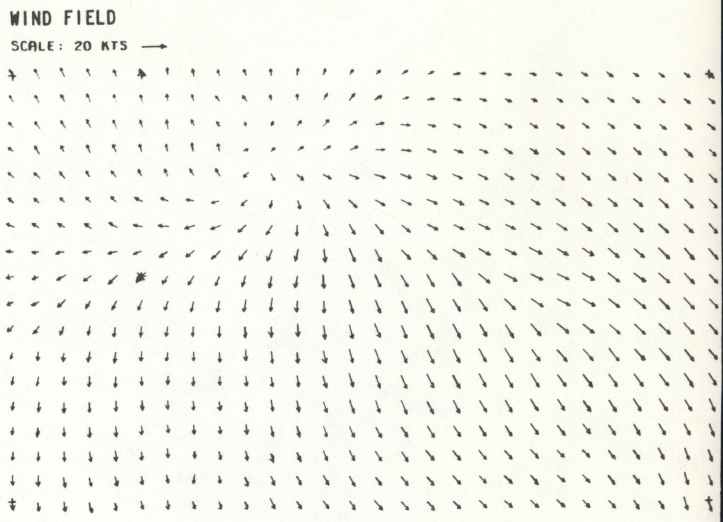

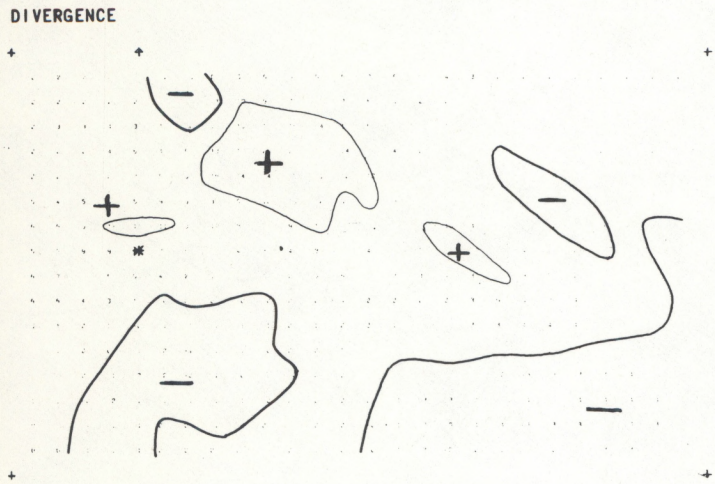

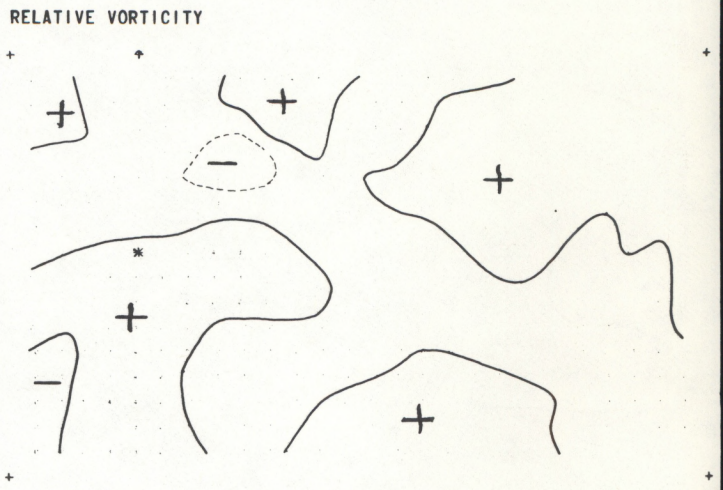

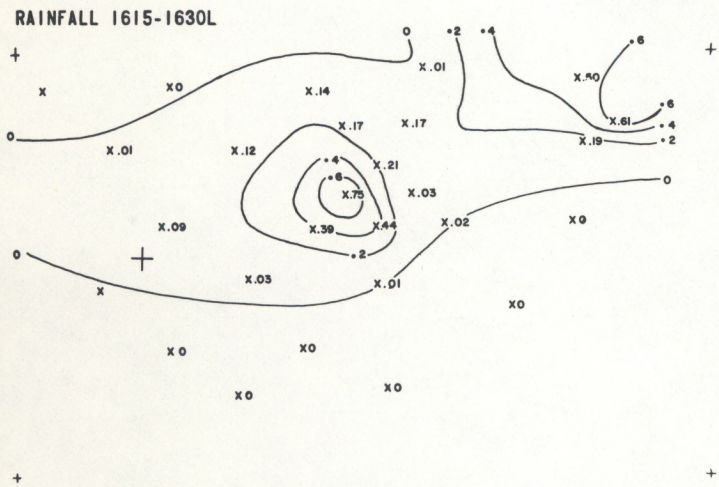

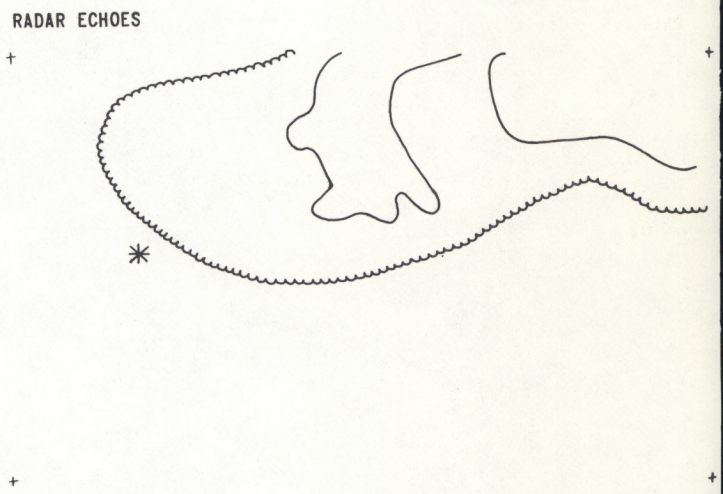

Figure B4. Same as figure B1 but for 1630 L (local time), July 12, 1971.

JULY 12 1971
1700L

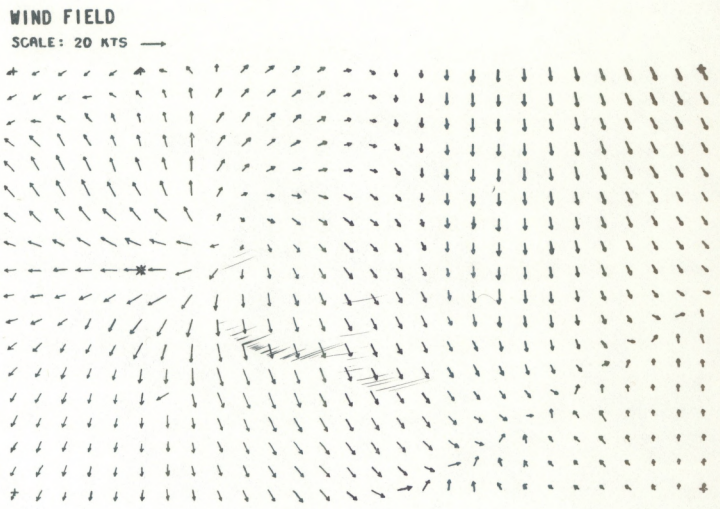

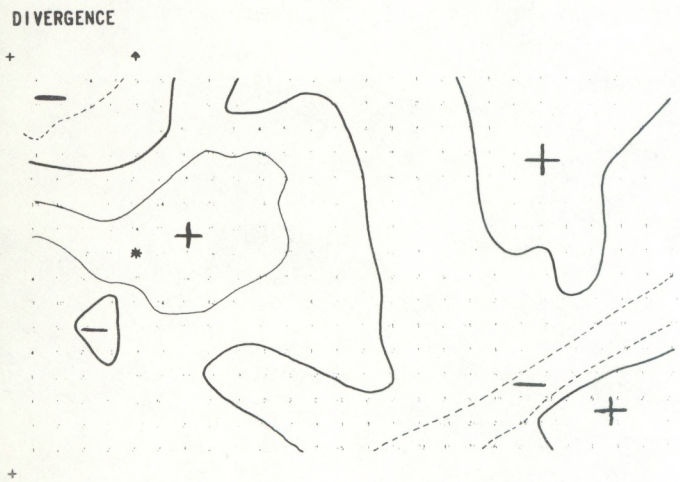

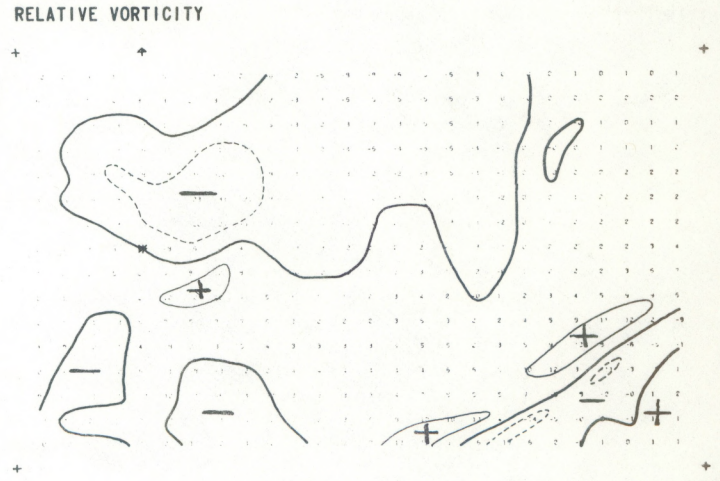

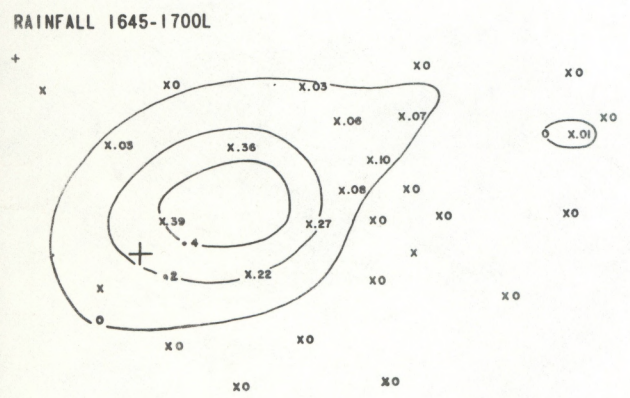

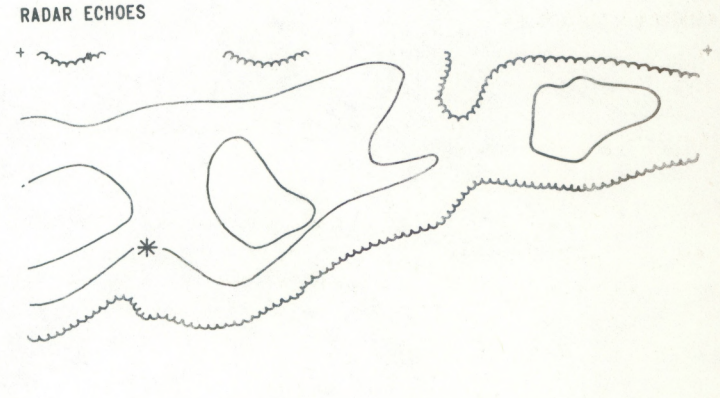

Figure B5. Same as figure B1 but for 1700 L (local time), July 12, 1971.

JULY 12 1971
1730L

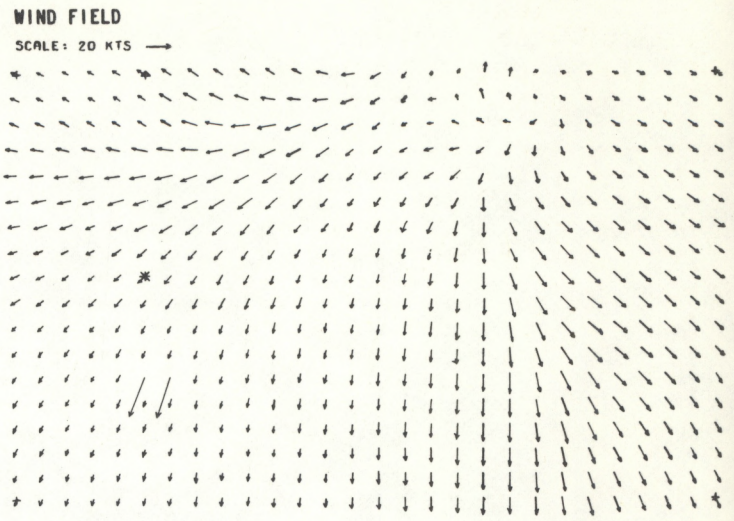

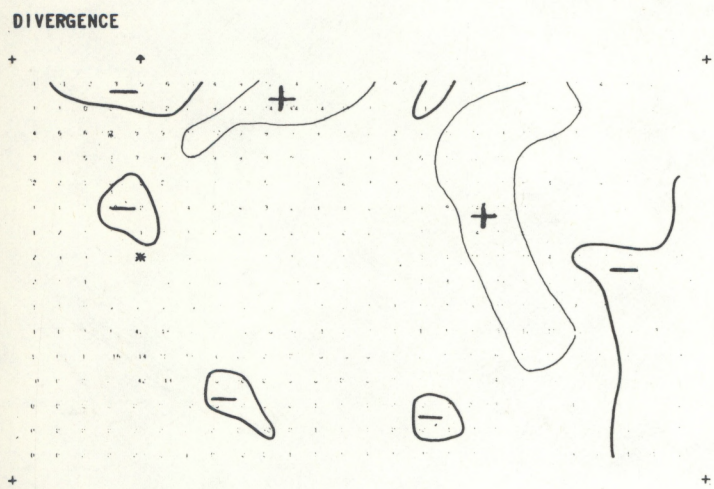

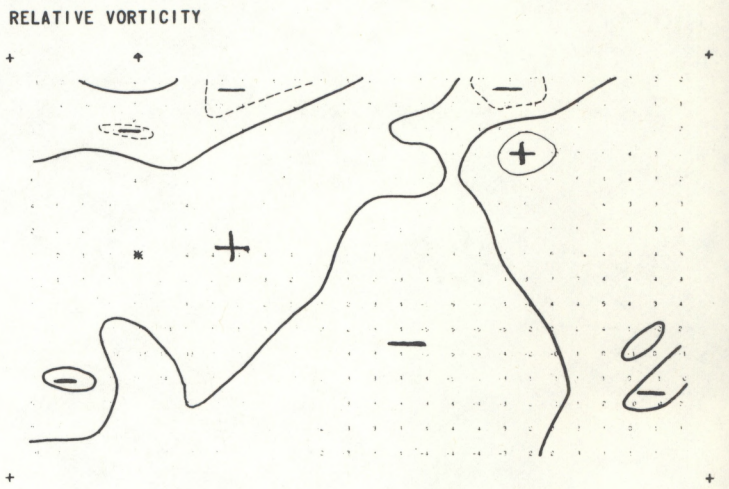

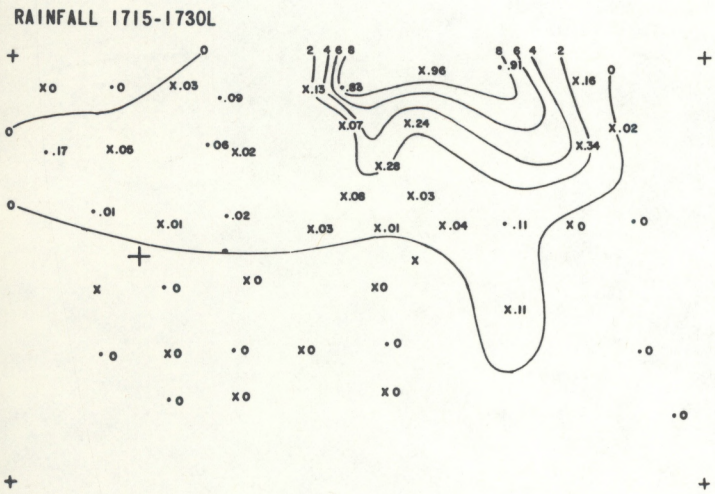

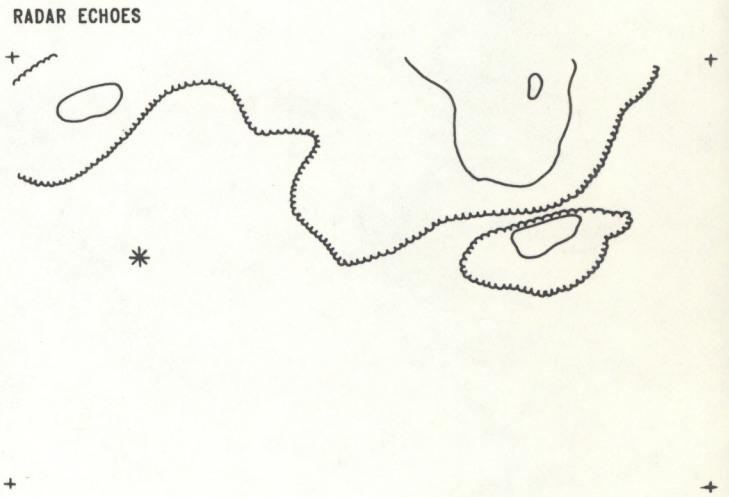

Figure B6. Same as figure B1 but for 1730 L (local time), July 12, 1971.

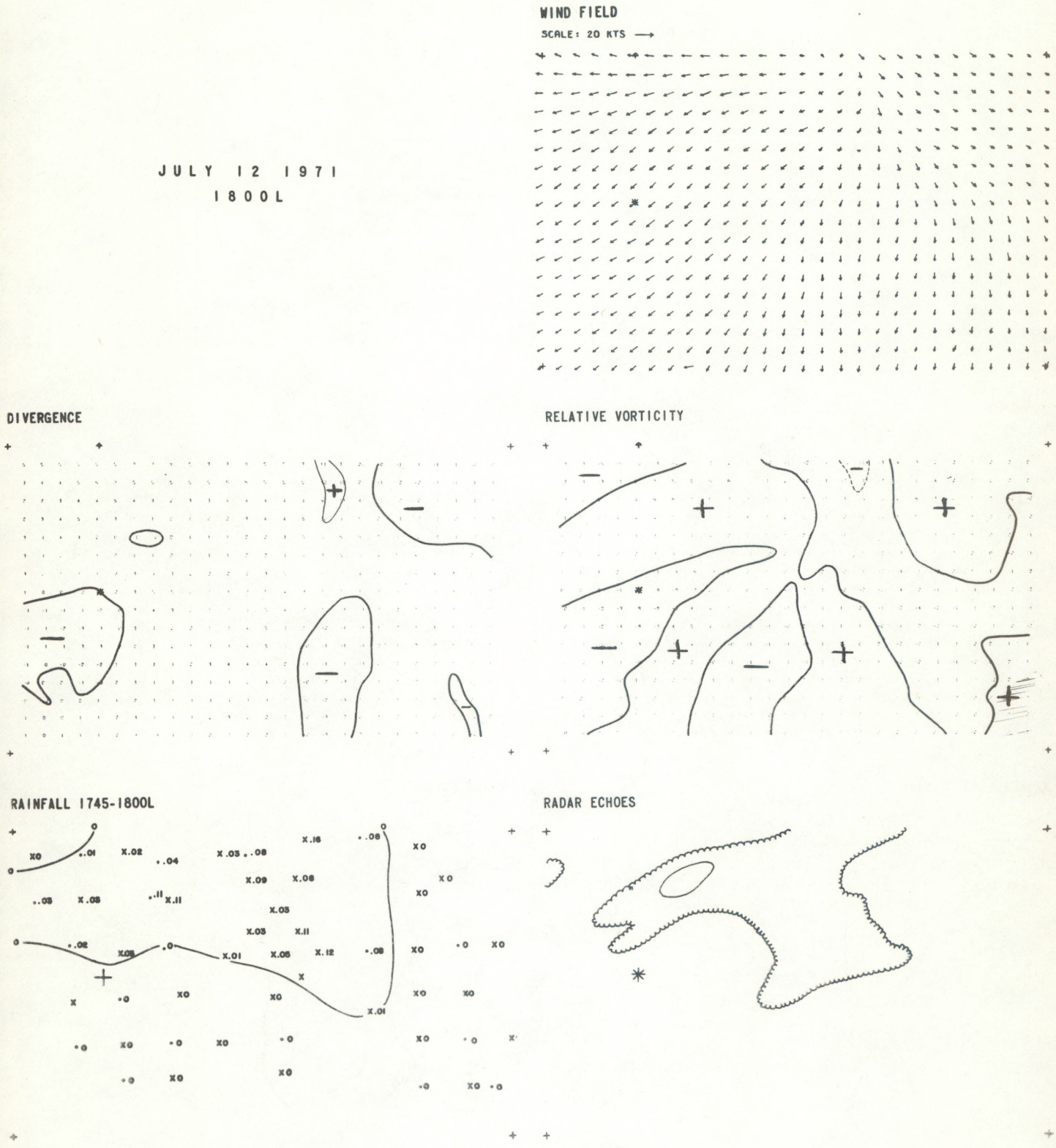

Figure B7. Same as figure B1 but for 1800 L (local time), July 12, 1971.

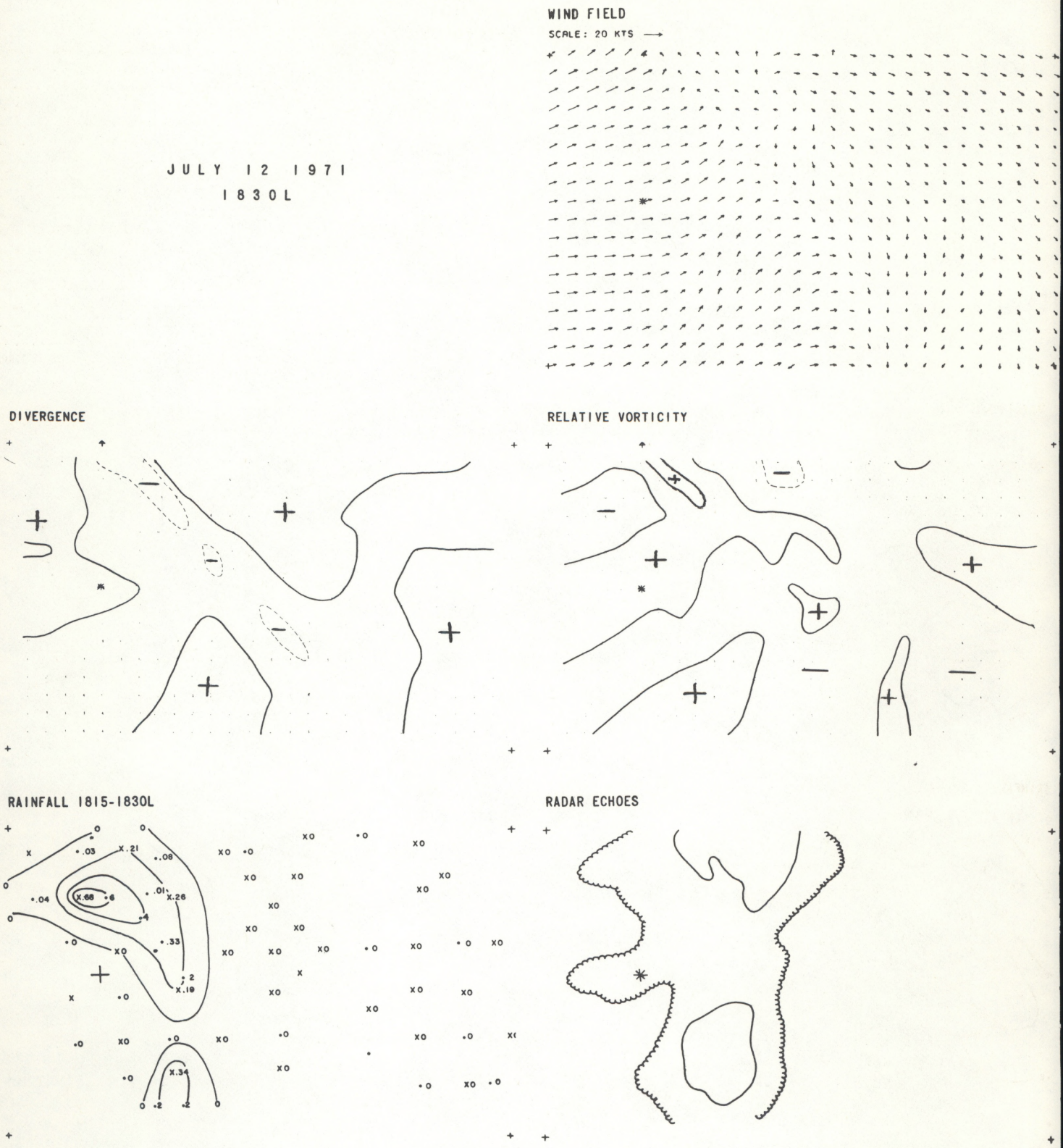

Figure B8. Same as figure B1 but for 1830 L (local time), July 12, 1971.

JULY 12 1971
1900L

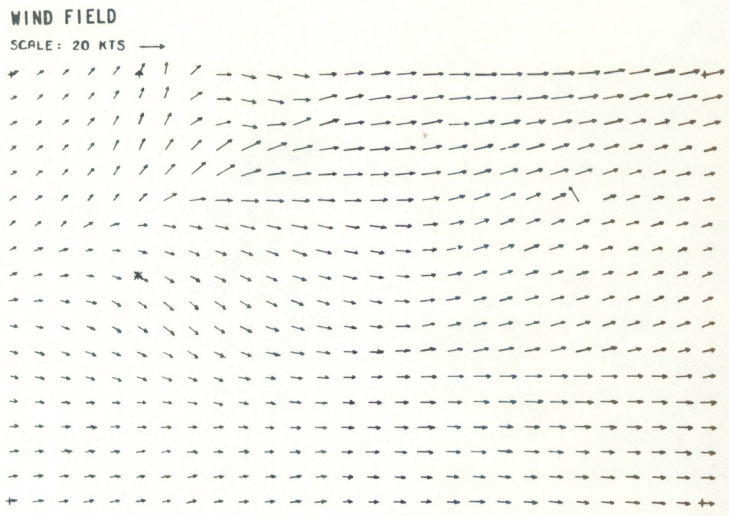

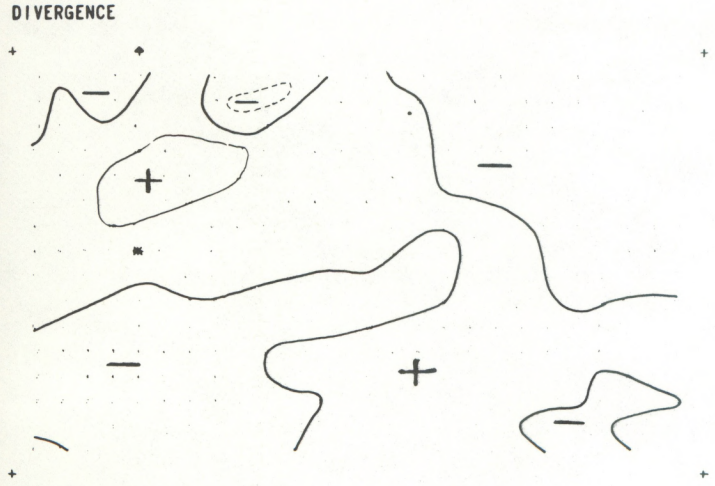

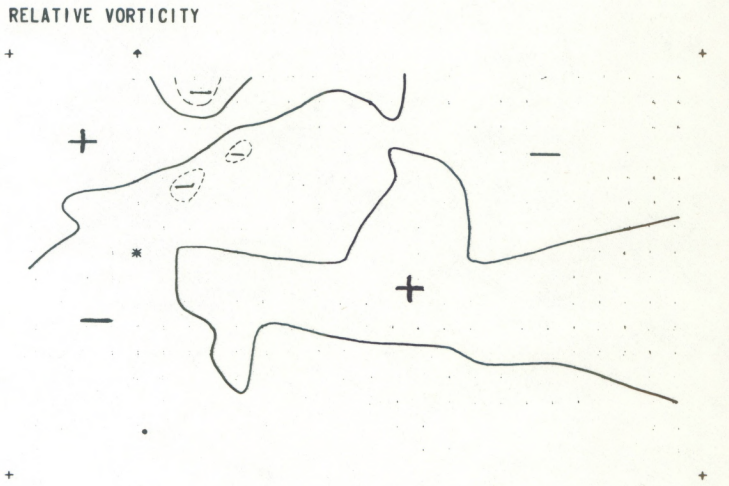

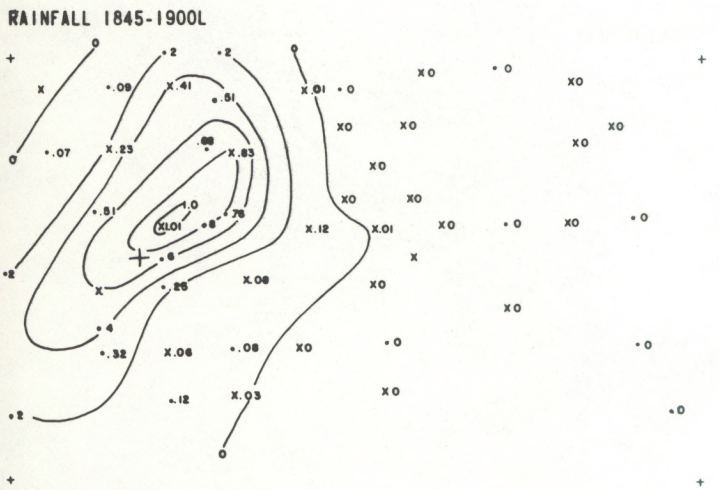

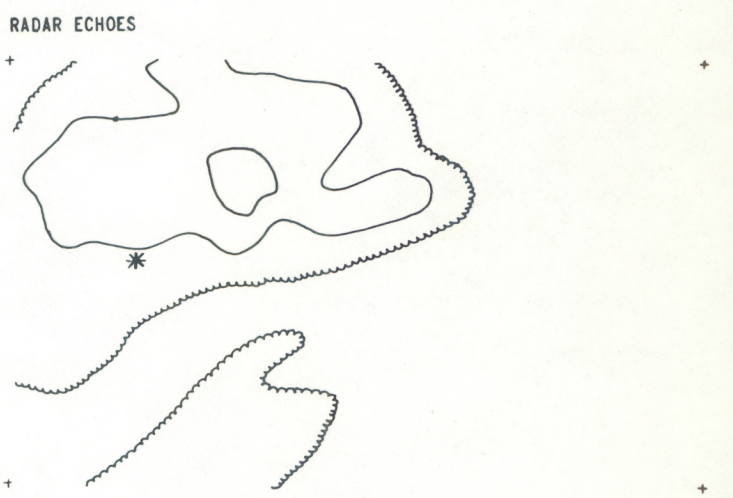

Figure B9. Same as figure B1 but for 1900 L (local time), July 12, 1971.

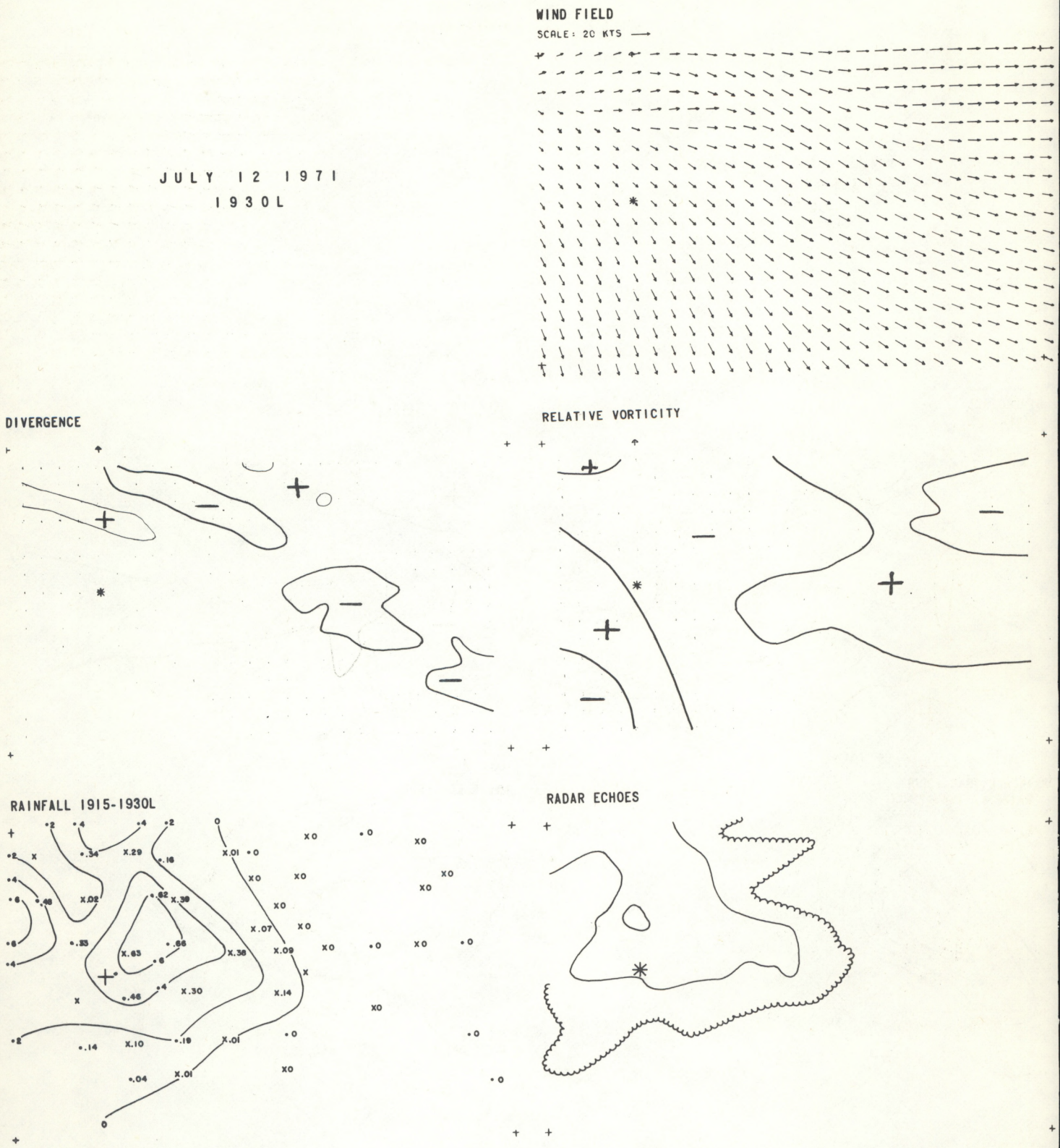

Figure B10. Same as figure B1 but for 1930 L (local time), July 12, 1971.

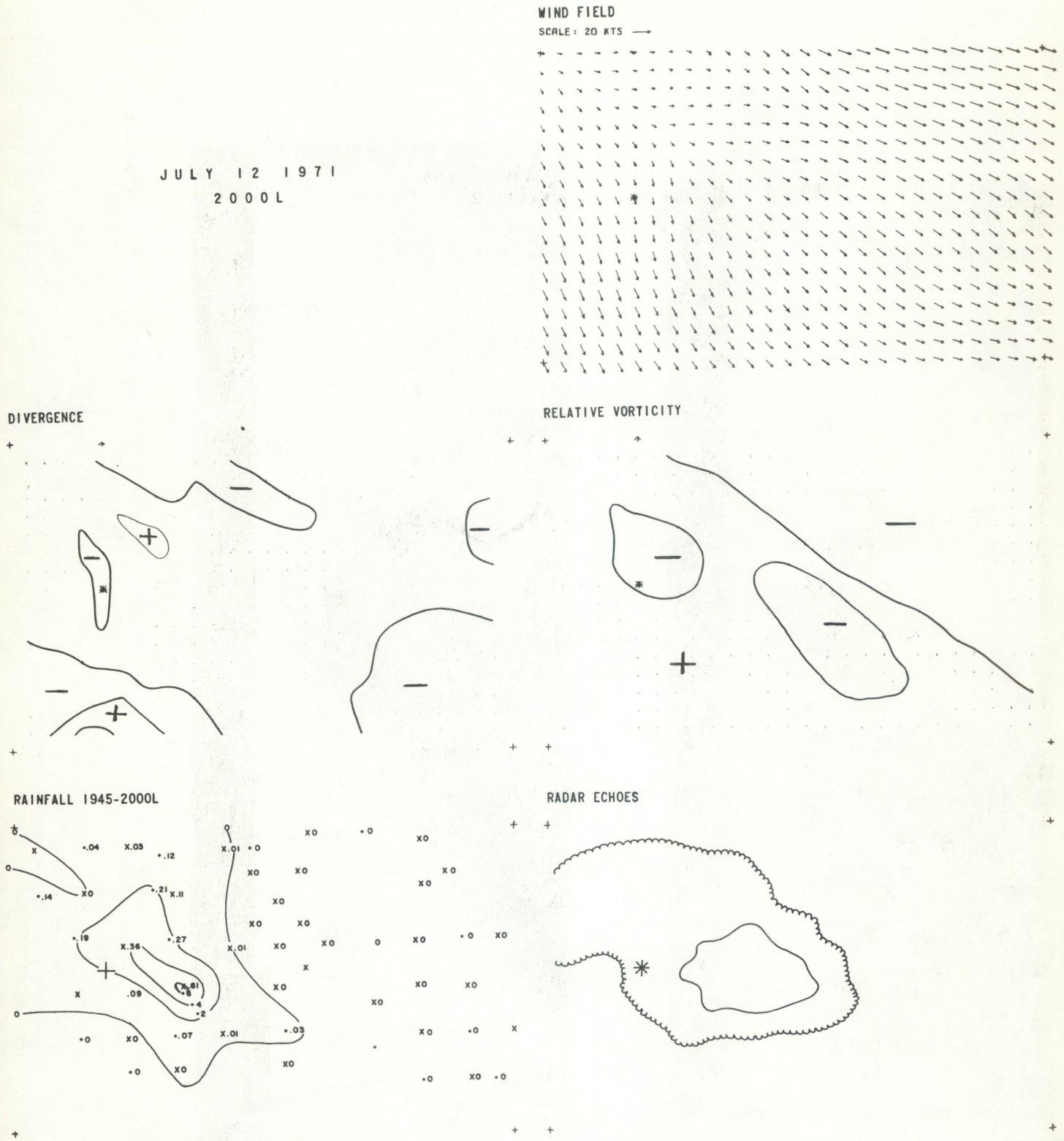

Figure B11. Same as figure B1 but for 2000 L (local time), July 12, 1971.

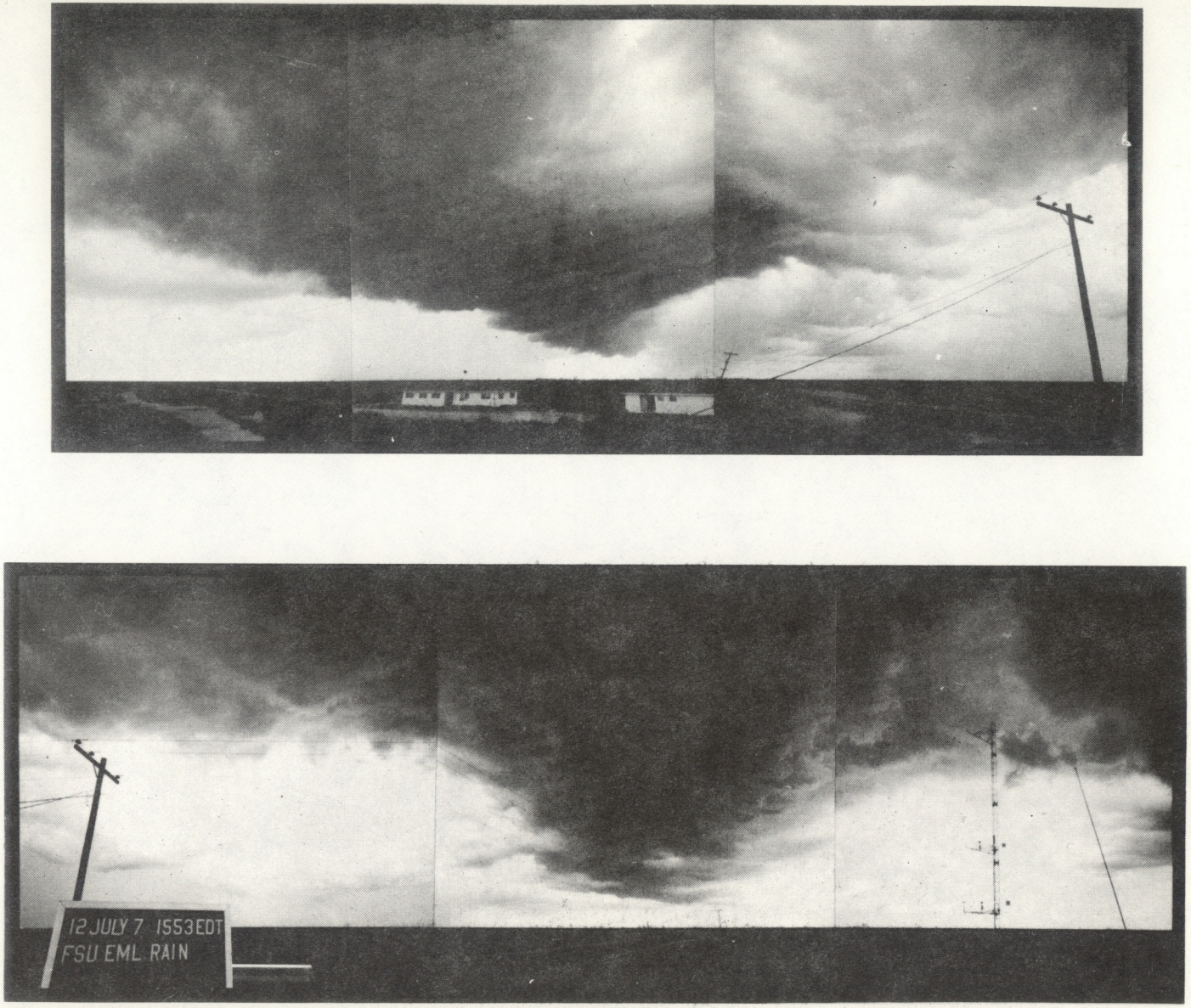

Figure B12. Mosaics of several pictures taken with a Hasselblad wide-lens camera from location T (Central Site) in figure 1 of the main text. These pictures were taken at 1553 EDT, July 12, 1971. Top: a mosaic of pictures of the western half of the sky (north is on the extreme right and south is on the extreme left). Bottom: the eastern half of the sky (north is on the extreme left and south is on the extreme right). Note the cloud line which extends along an east-west direction and passes overhead of location T. This cloud line roughly coincides with the position of the asymptote of confluence in the wind field which is shown in figure B3.

reconnaissance aircraft. Times of cloud pictures (about 1355, 1435, and 1450 EDT) were prior to the main analysis period (1500-2000 EDT). So, additional wind charts were prepared for the period 1345-1500 EDT. Figure B13, B14 and B15 illustrate cloud fields as seen from a U. S. Air Force B-57 aircraft flying at approximately 60,000 ft. Corresponding surface wind fields (streamlines) were superposed over the cloud fields. Surface wind fields underwent a point-to-point mapping from a Cartesian coordinate system into the panoramic coordinate system of the aerial photography. The comparison of the surface wind fields (streamlines) with the cloud fields showed a tendency for more clouds to be present in the vicinity of confluence zones than in the vicinity of other streamline features.

Convergence-rainfall relationships for July 12, 1971, both at the grid-point scale (cloud-scale) and at the grid scale (meso-scale), are included in the main text of this paper.

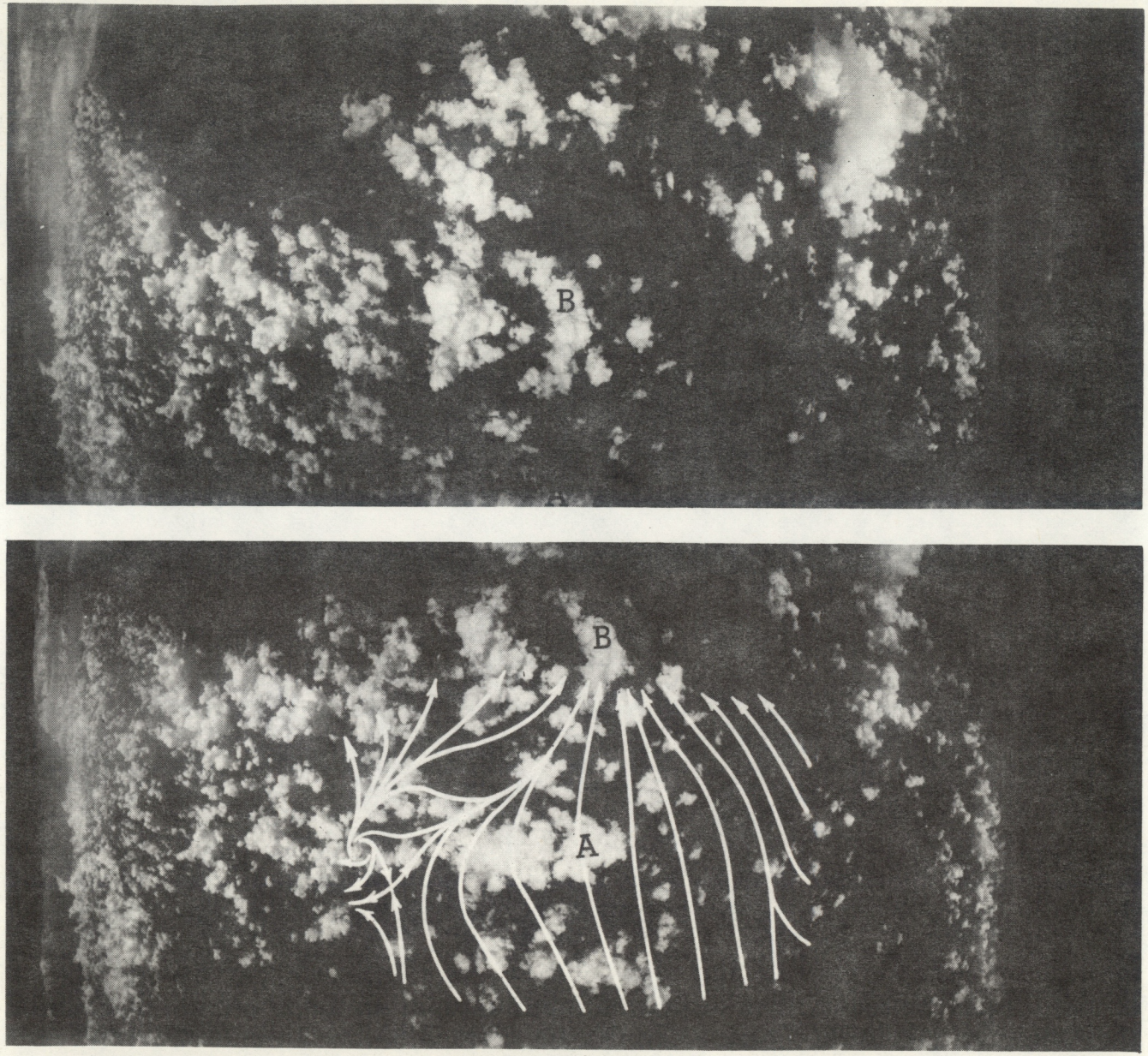

Figure B13. Cloud pictures taken from about 60,000 ft by high level reconnaissance B-57 aircraft at 1355 EDT (1755 GMT), July 12, 1971. A streamline analysis of simultaneous wind data from the surface network is superposed over the cloud field shown by the bottom figure. The picture at the top helps in positioning the cloud field with respect to Lake Okeechobee. For this individual case, Lake Okeechobee is located near the upper-left corner of the top picture. Letters identify identical clouds in the two different views.

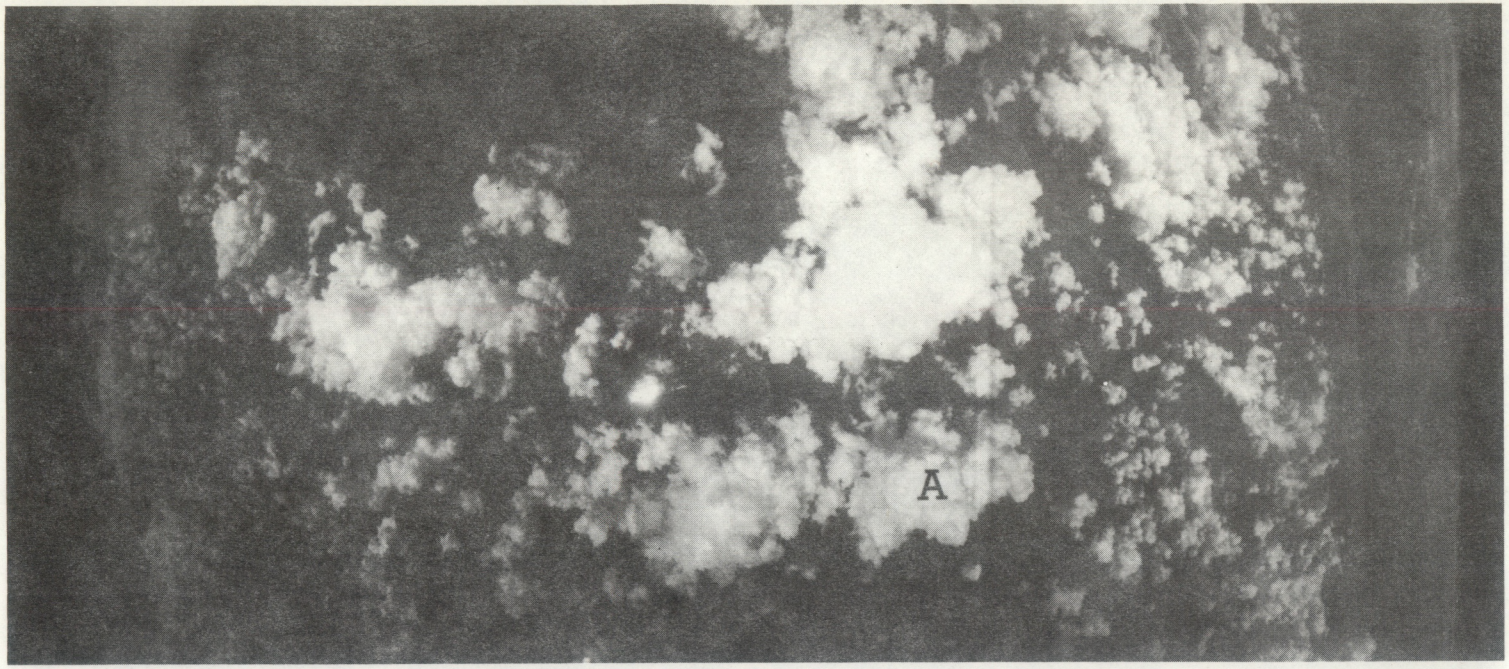

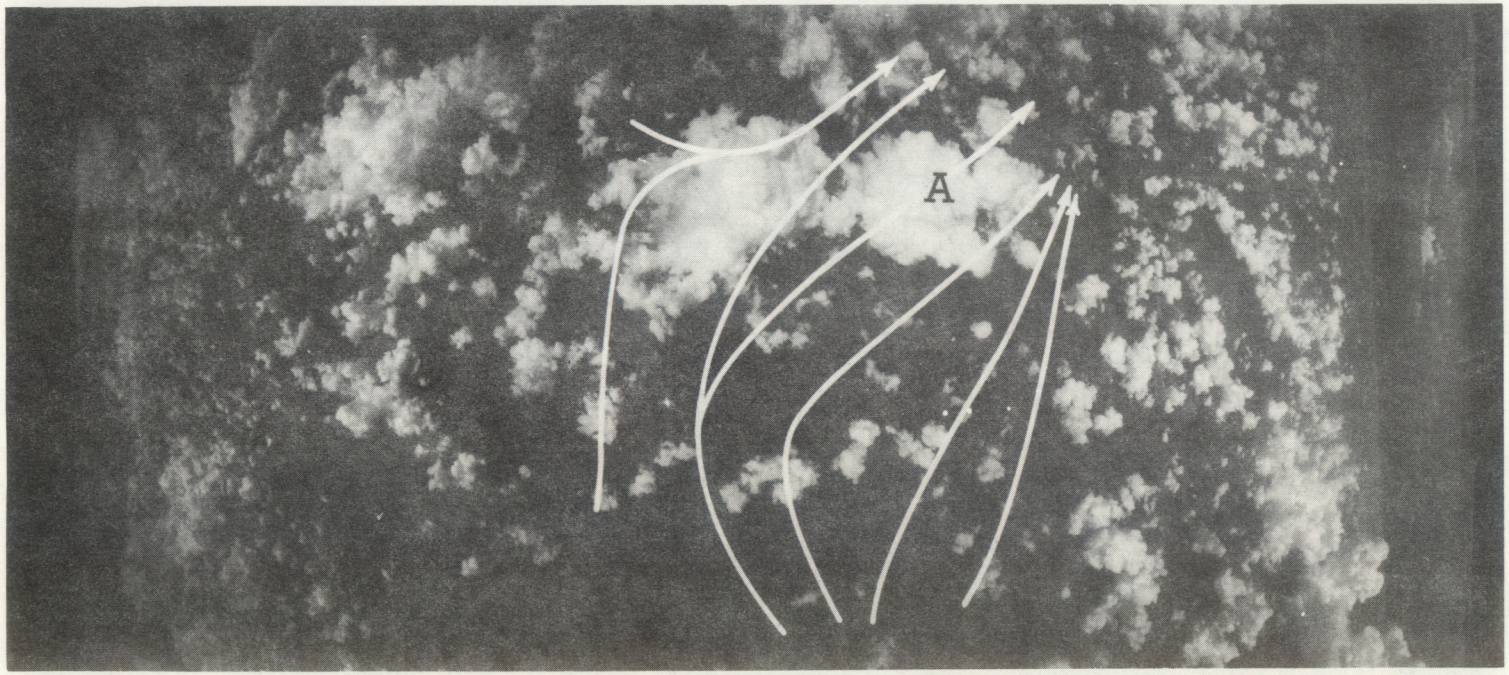

Figure B14. Same as figure B13 but for 1435 EDT (1835 GMT), July 12, 1971.

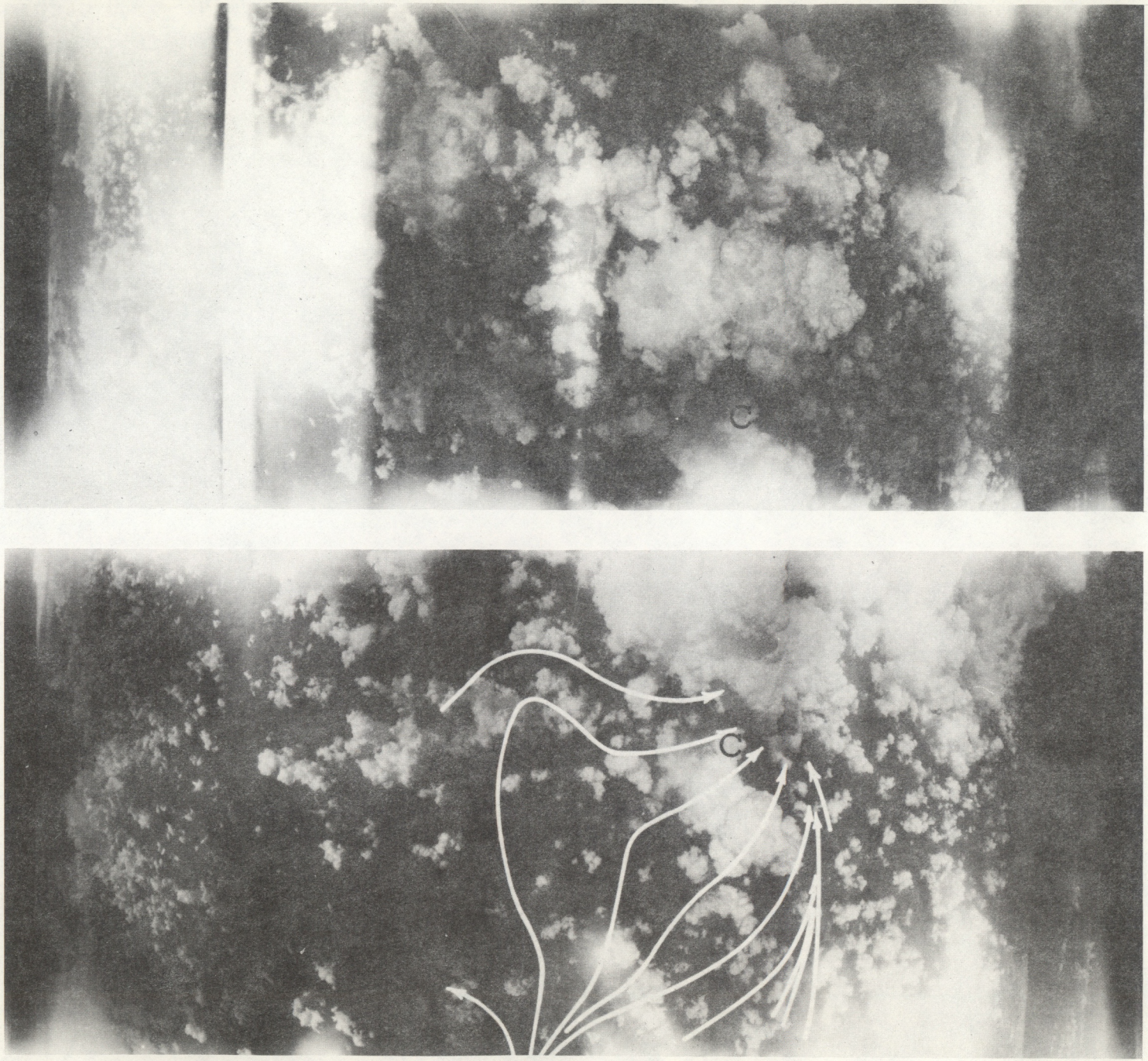

Figure B15. Same as figure B13 but for 1450 EDT (1850 GMT), July 12, 1971. For this individual case, Lake Okeechobee is located near the upper-center of the top picture.

APPENDIX C

The July 13, 1971 case study

The case study of July 13, 1971 is considered to be the least interesting one in the July 11-13, 1971 period.

Analyses for July 13, 1971 extended over two and a half hours (1600-1830 EDT). Figures C1 to C6 illustrate wind fields, divergence and relative vorticity fields, rainfall analyses and radar echo depictions at 30-minute intervals. Cloud pictures for the July 13, 1971 case are shown in figure C7. The wind fields showed a convergence line to move slowly westward during the first half of the period. Some anticyclonic meso-circulations were present at various times. The rainfall analyses and radar echo depictions exhibited some precipitation first over the eastern and central parts of the network. Heavier precipitation occurred later over the western part of the network.

Extensive cloud seeding operations took place on July 13, 1971. However, seeded clouds - with the exception of one or two - were located outside the network limits. Thus, the effect of multiple cloud modification on naturally observed convergence-rainfall relationships could not be assessed.

Convergence-rainfall relationships for July 13, 1971, both at the grid-point scale (cloud-scale) and at the grid scale (meso-scale), are included in the main text of this paper.

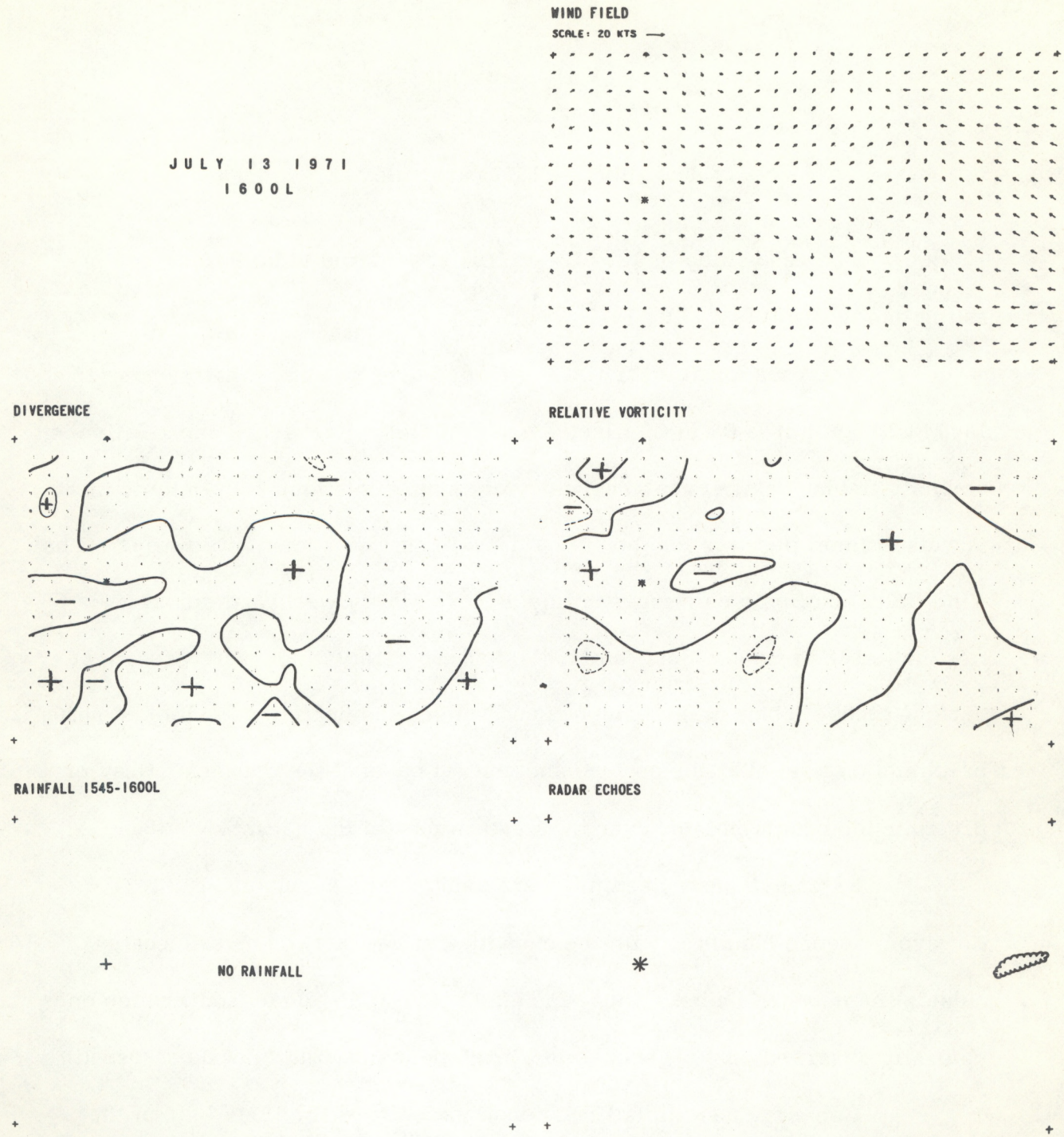

Figure C1. Wind field, divergence, relative vorticity, rainfall and radar echoes for 1600 L (local time), July 13, 1971. The following is applicable to this figure and subsequent figures; Local time is EDT. Wind field is presented in vectorial form; vectors at a few isolated grid points are in error due to mistakes on punched card information for such grid points. Divergence and relative vorticity are scaled to 10^4 and are in units of "per second." Contours in heavy solid line denote zero values; thin line contours correspond to 10^{-3} sec^{-1} divergence or positive relative vorticity values. Dashed line contours correspond to -10^{-3} sec^{-1} convergence or negative relative vorticity values. Positive signs indicate divergence and positive relative vorticity areas; negative signs indicate convergence and negative relative vorticity areas. For simplicity, rainfall isopleths are shown at 0.2 in. intervals in lieu of the 0.1 in. intervals which were used for the original analyses. The outer (serrated) edge of the radar echoes represents the Minimum Detectable Signal (M.D.S.) as seen on original films. (~0.003 in/hr). The first iso-echo contour represents a 0.1 in/hour rainfall rate and the second iso-echo contour represents a 0.6 in/hour rainfall rate.

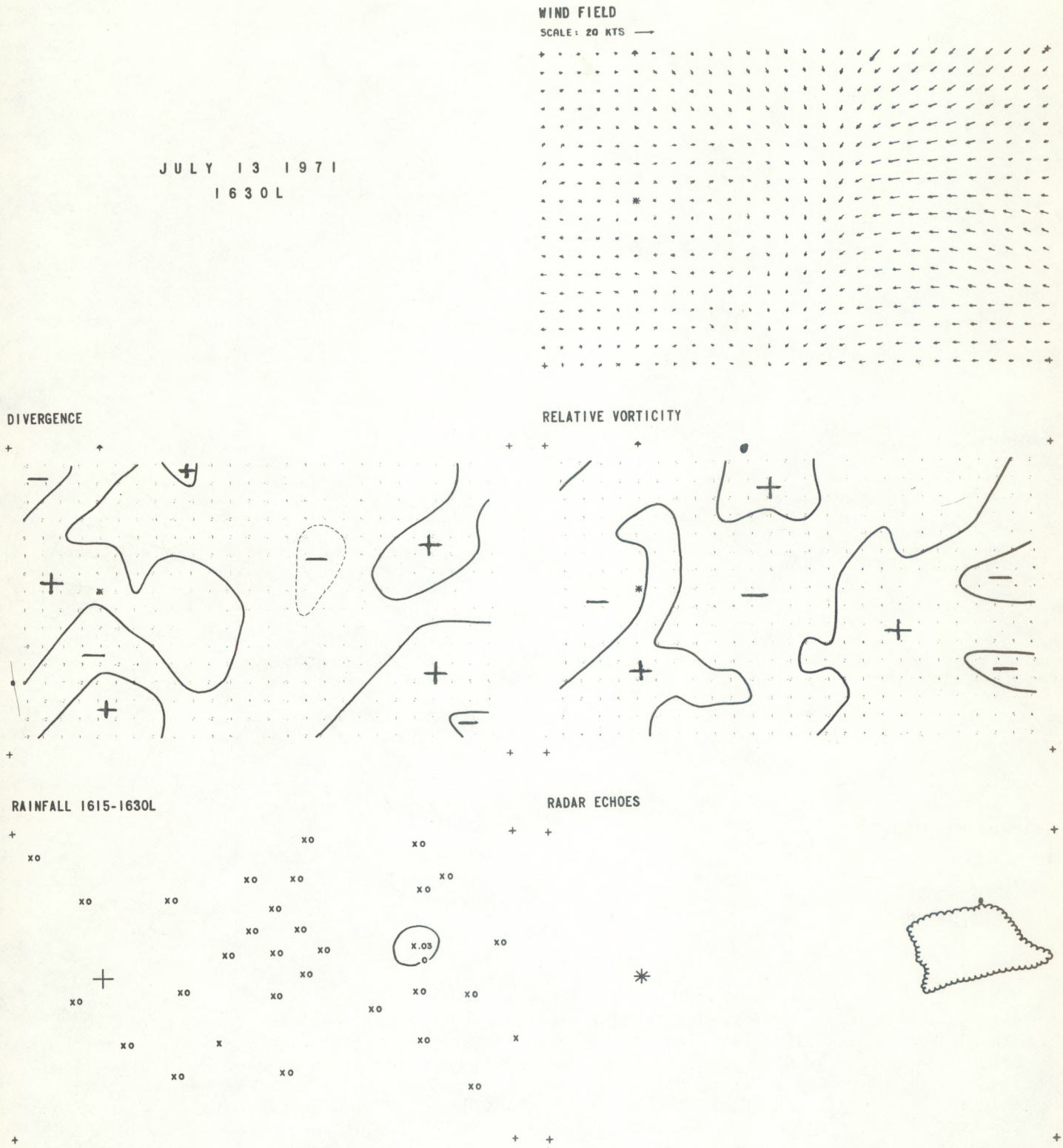

Figure C2. Same as figure C1 but for 1630 L (local time), July 13, 1971.

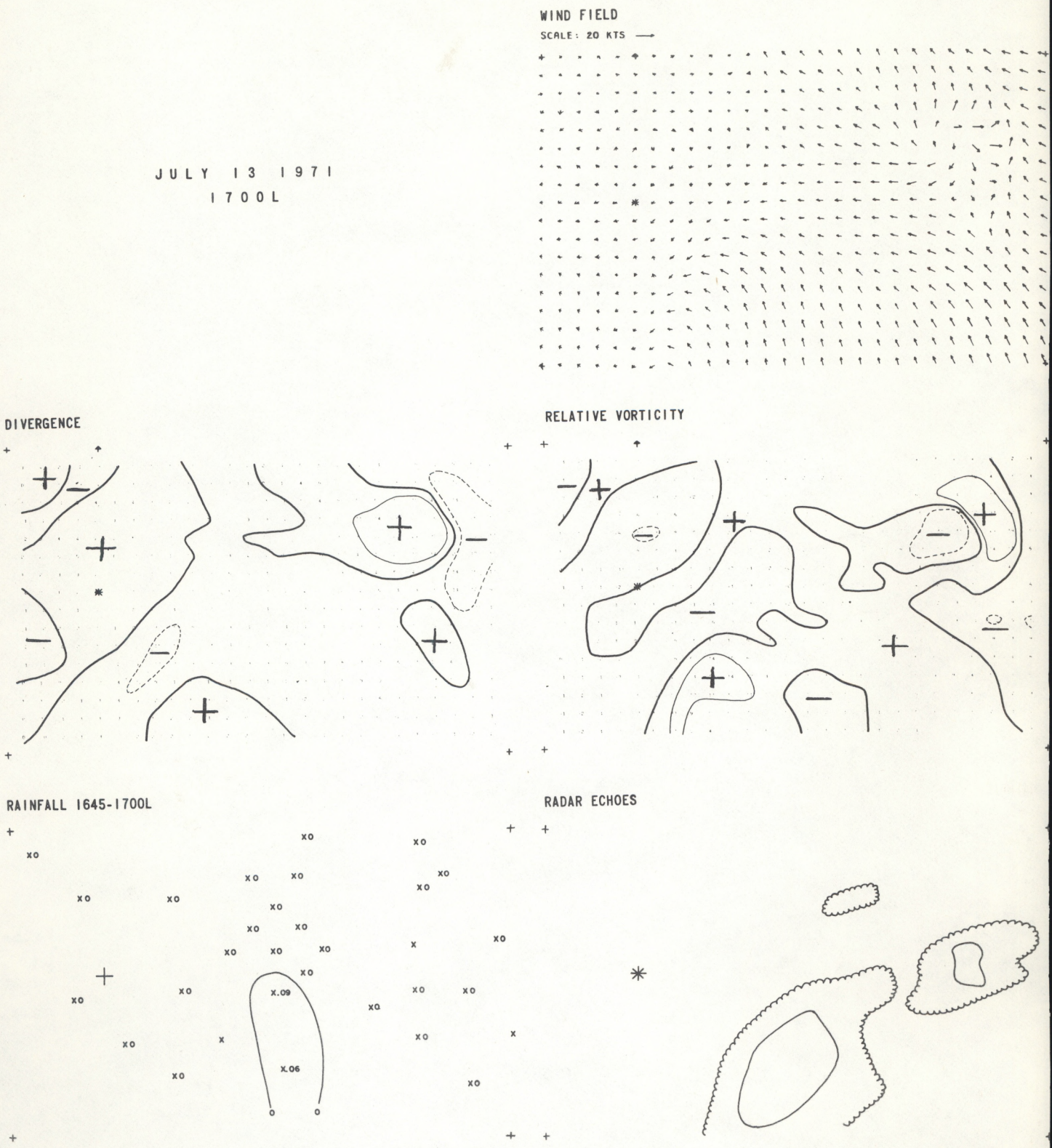

Figure C3. Same as figure C1 but for 1700 L (local time), July 13, 1971.

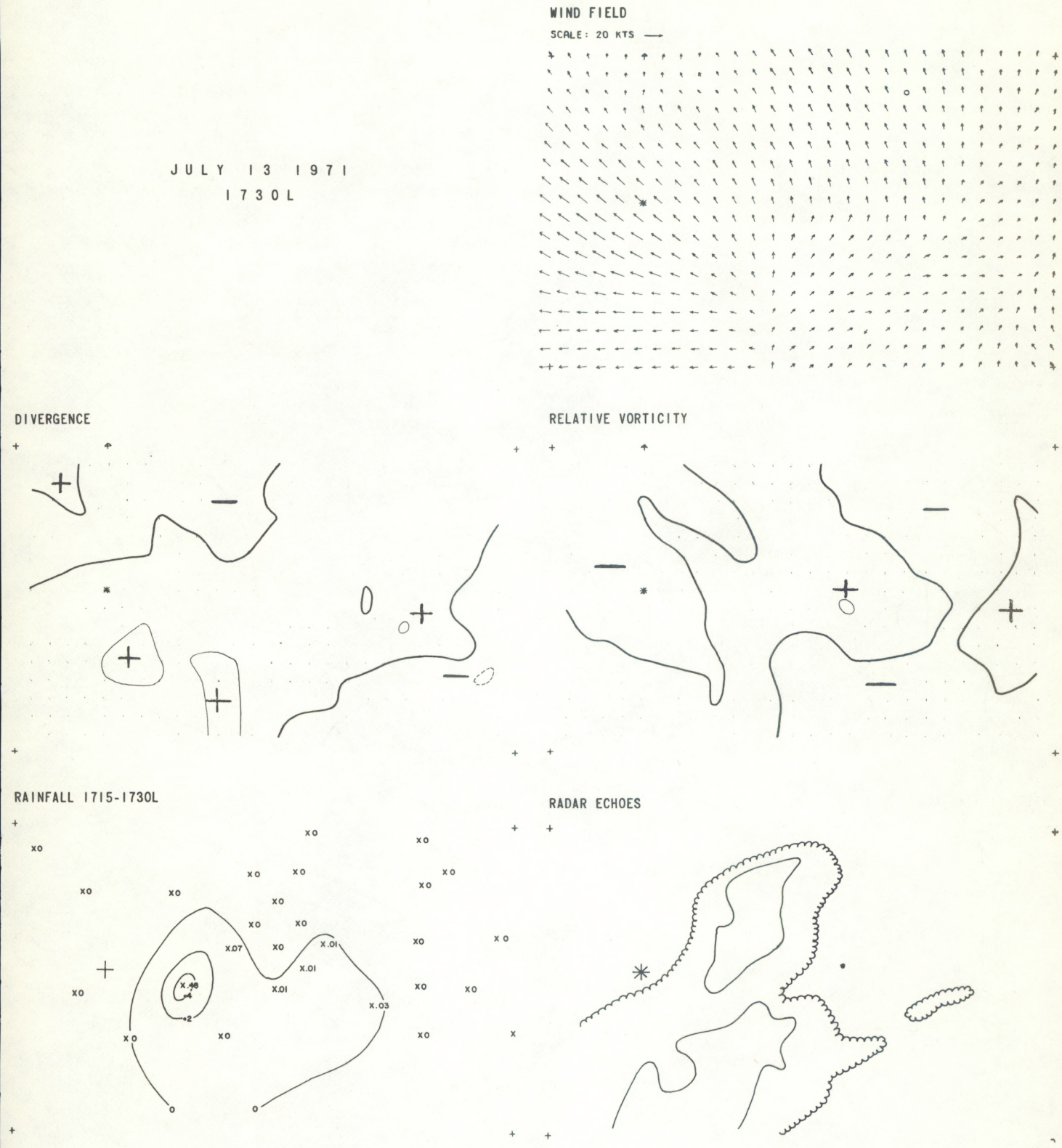

Figure C4. Same as figure C1, but for 1730 L (local time), July 13, 1971.

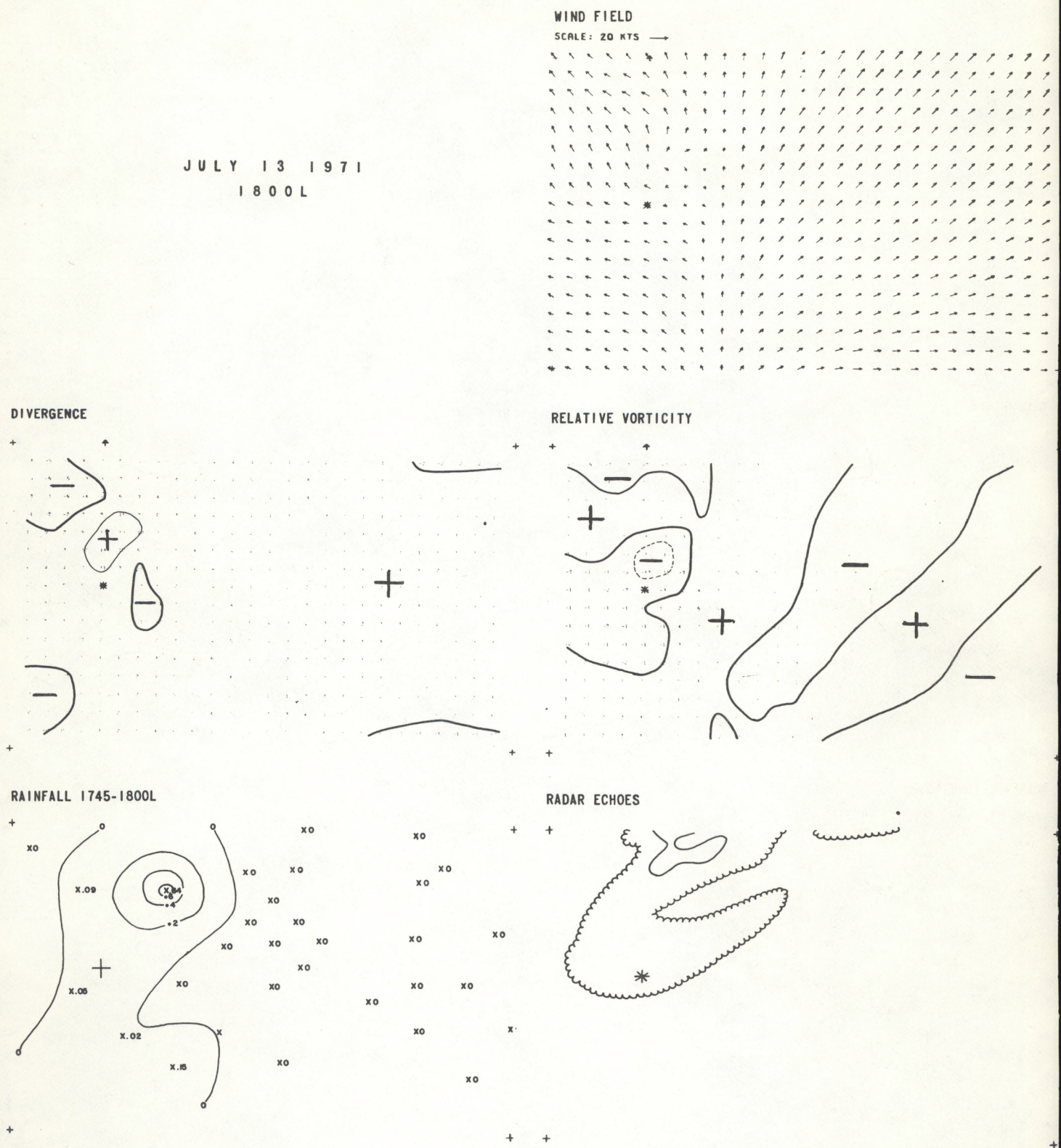

Figure C5. Same as figure C1, but for 1800 L (local time), July 13, 1971.

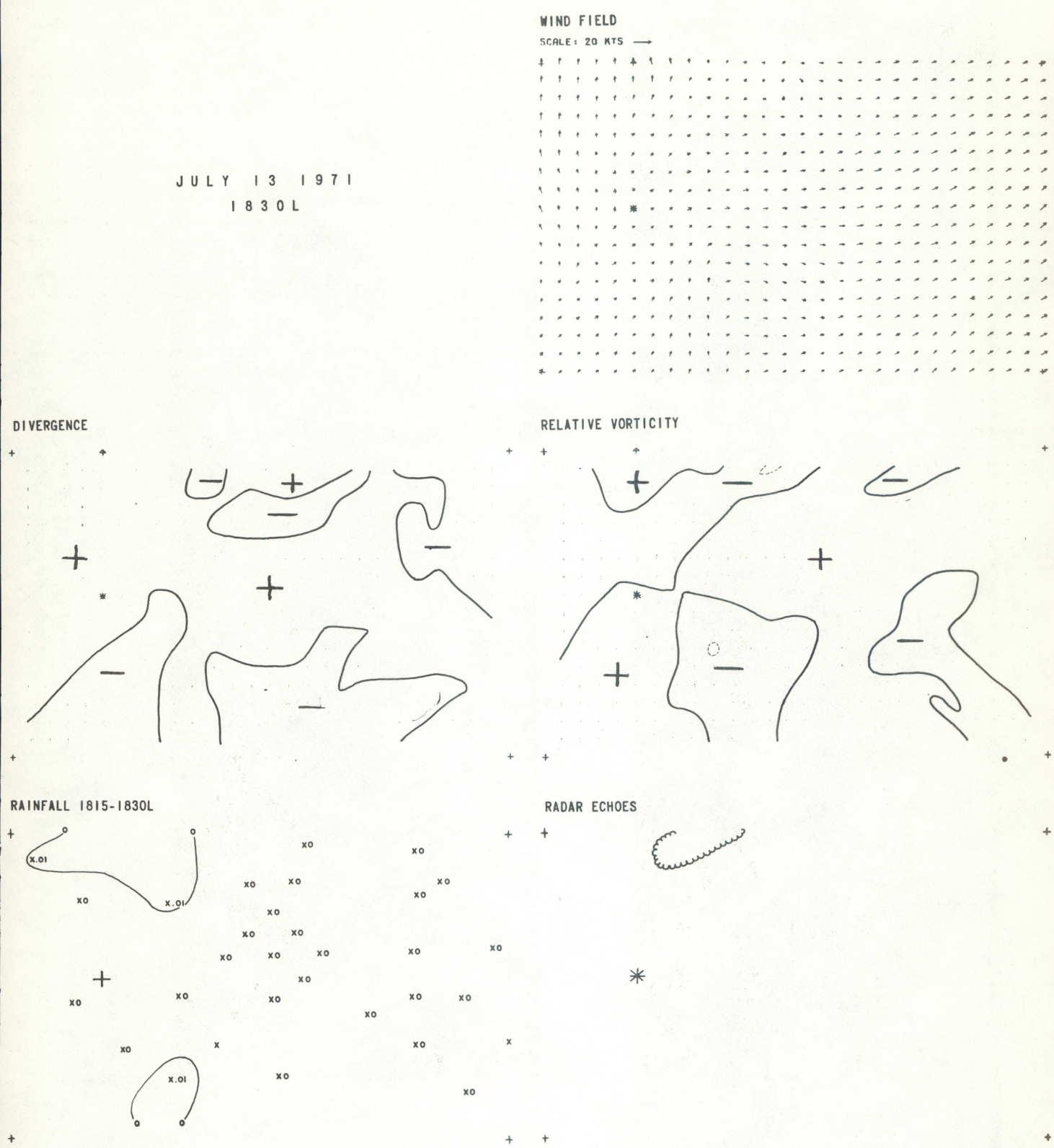

Figure C6. Same as figure C1, but for 1830 L (local time), July 13, 1971.

Figure C7. Mosaic of several pictures taken with a Hasselblad wide-lens camera from location T (Central Site) in figure 1 of the main text. Top: eastern half of the sky (north is on the extreme left and south is on the extreme right) at 1700 EDT, July 13, 1971. Bottom: western sector of the sky (north is on the right and south is on the left) at 1800 EDT, July 13, 1971.

☆GPO 1973—784-572/1235 REGION NO. 8